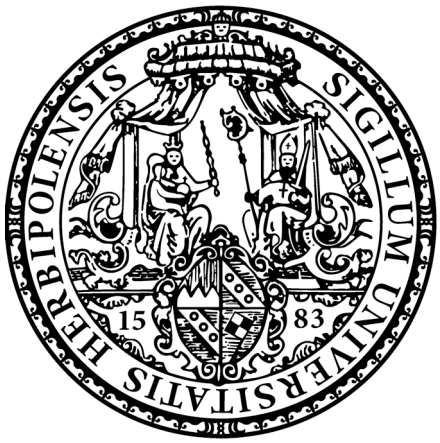


# Functional characterization of the role of ZFAND1 in stress granule turnover

# Funktionelle Charakterisierung der Rolle von ZFAND1 im Umsatz von Stressgranula

Doctoral thesis for a doctoral degree
at the Graduate School of Life Sciences,
Julius-Maximilians-Universität Würzburg,
Section: Biomedicine

submitted by

**Ankit Turakhiya**

from

**Ahmedabad, India**

**Würzburg, 2018**

**Submitted on:**

## Members of the *Promotionskomitee*:

**Chairperson: Prof. Utz Fischer**

**Primary Supervisor: Prof. Alexander Buchberger**

**Supervisor (Second): Prof. Hermann Schindelin**

**Supervisor (Third): Dr. Nikita Popov**

**Supervisor (Fourth): Prof. Dieter Wolf**

**Date of Public Defence:**

**Date of Receipt of Certificates:**

## Affidavit

I hereby confirm that my thesis entitled **'Functional characterization of the role of ZFAND1 in stress granule turnover'** is the result of my own work. I did not receive any help or support from commercial consultants. All sources and/or materials applied are listed and specified in the thesis.

Furthermore, I confirm that this thesis has not yet been submitted as part of another examination process neither in identical nor in similar form.

Place, Date:
Signature:

## Eidesstattliche Erklärung

Hiermit erkläre ich an Eides statt, die Dissertation **'Funktionelle Charakterisierung der Rolle von ZFAND1 im Umsatz von Stressgranula'** eigenständig, d.h. insbesondere selbständig und ohne Hilfe eines kommerziellen Promotionsberaters, angefertigt und keine anderen als die von mir angegebenen Quellen und Hilfsmittel verwendet zu haben.

Ich erkläre außerdem, dass die Dissertation weder in gleicher noch in ähnlicher Form bereits in einem anderen Prüfungsverfahren vorgelegen hat.

Ort, Datum:
Unterschrift:

**Acknowledgements**

I would like to extend my heartfelt gratitude to the many people I have had the pleasure of working with during my doctoral studies. Foremost, I would like to express my gratitude to my advisor, Prof. Alexander Buchberger, for giving me the opportunity to pursue my PhD in his group. His enthusiasm and passion for excellent science is unrivaled and has been a source of inspiration. His supportive guidance coupled with the freedom to explore new ideas helped me not only in successfully completing my project but also in developing myself as a scientist.

I would like to thank the members of my thesis committee, Prof. Hermann Schindelin, Dr. Nikita Popov and Prof. Dieter Wolf. Their guidance and suggestions have been instrumental in the development of this project. I am grateful to Prof. Utz Fischer for his advice.

I would like to extend my thanks to Susanne Meyer for her contribution with valuable technical support. The data and experimental support from collaborators, Prof. Kay Hofmann for the bioinformatics analysis and Jens Vanselow and Prof. Andreas Schlosser for the mass spectrometry analysis, has been critical to the completion of this project. I thank Louis and Esraa for putting effort into this project. I am grateful to the core imaging facility at Biocenter, University of Würzburg, without which this project would not have been possible. In addition, the Graduate School of Life sciences (GSLS) has partly funded my studies, and their support and administrative assistance has been invaluable to me through the last years.

Importantly, I would like to thank all past and current members of Buchberger group, including Susanne, Mona, Beynech, Maria, Andy, Gabriella, Christopher, Claudia and Sven, for scientific discussions and a wonderful working environment. Members of ‘Espresso bar’ and ‘Peanuts coffee bar’ group - thank you for providing enough caffeine to power my PhD, and for plenty of sessions filled with cakes and ice-creams that created sweet and unforgettable memories. Without you all, the lab wouldn’t be such as positive and vibrant place to work in. I also thank members of Fischer group for fruitful discussion during department seminars and for sharing laboratory reagents.

Lastly, I would like to thank the most important people of my life. None of this was possible without the love and support of my family - my father, for being a constant source of motivation and the encouragement to pursue my dreams, and my mother for being strong and supportive throughout. Thank you for everything. Last but not least, my wife Uma, for being patient and caring through difficult times. Thank you for your unconditional support and encouragement that made this journey smoother and enjoyable.

**To my parents**

**Table of contents**

**Abbreviations**

**AAA -** ATPases- ATPases associated with diverse cellular activities

**AD -** gal4 activation domain

**Ade -** adenine

**ADH1 -** alcohol dehydrogenase

**AIP-1 -** arsenite inducible protein 1

**AIRAP -** arsenite-inducible RNA-associated protein

**AIRAPL -** arsenite-inducible RNA-associated protein-like

**ALS -** amyotrophic lateral sclerosis

**Amp -** ampicillin

**APL -** acute promyelocytic leukaemia

**APS -** ammonium-peroxo-disulfate

**ATP -** adenosine 5'-triphosphate

**BD -** gal4 binding domain

**BP -** band pass

**BS1 -** binding site 1

**CAD -** chromatin associated degradation

**CDC48 -** cell division cycle 48

**CHX -** cycloheximide

**CMA -** chaperone-mediated autophagy

**Co-IP -** co-immunoprecipitation

**CP -** core particle

**CRISPR -** clustered regularly interspaced short palindromic repeats

**CuAAC -** copper(I)-catalyzed azide-alkyne cycloaddition

**Cuz1 -** cdc48-associated UBL/zinc-finger-1

**DAPI -** 4',6-diamidino-2-phenylindole

**dd$H_2O$ -** double distilled water

**DMSO -** dimethyl sulfoxide

**DNA -** deoxyribonucleic acid

**dNTP -** deoxy nucleoside triphosphate

**DRiPs -** defective ribosomal products

**DSP -** dithiobis[succinimidyl propionate]

**DTT -** 1,4-dithiothreitol

**DUB -** deubiquitinating enzyme

***E. coli* -** *Escherichia coli*

**ECL -** enhanced chemiluminescence

**EDTA -** ethylene diamine tetra-acetic acid

**eIF -** eukaryotic initiation factor

**ER -** endoplasmatic reticulum

**ERAD -** endoplasmatic reticulum associated degradation

**FITC -** fluorescein isothiocyanate

**FMRP -** fragile X mental retardation protein

**FTLD -** frontotemporal lobar degeneration

**g -** gravitational constant 9.81m/$s^2$

**G3BP1 -** ras-GTPase-activating protein SH3-domain-binding protein 1

**G418 -** geneticine disulfate

**GAL -** galactosidase

**GFP -** green fluorescent protein

**GST -** glutathione S-transferase

**GTP -** guanosine-5‘-triphosphate

**HA -** hemagglutinin

**HEPES -** 2-[4-(2-hydroxyethyl)piperazin-1-yl]ethanesulfonic acid

**His -** histidine

**HRP -** horseradish peroxidase

**HU -** hydroxyurea

**IBMPFD -** inclusion body myopathy associated with Paget’s disease of bone and frontotemporal dementia

**IgG -** immunoglobulin G

**IP -** immunoprecipitation

**Kb -** kilo basepairs

**kD -** kilo dalton

**KO -** knockout

**LB -** luria-bertani

**LC3 -** microtubule-associated protein 1A/1B-light chain 3

**Leu -** leucine

**LIR -** LC3-interacting region

**LLPS -** liquid liquid phase separation

**MEF -** mouse embryo fibroblast

**MMS -** methyl methanesulfonate

**$M_r$(K) -** molecular weight (kilo dalton)

**mRNP -** messenger ribonucleoprotein

**NAT -** nourseothricin

**NP-40** - nonidet P-40

**NPL4 -** nuclear pore localization protein 4

**OD -** optical density

**OMMAD -** outer mitochondrial membrane associated degradation

**OP-puro -** O-propargyl-puromycin

**Pbp1 -** PAB1-binding protein 1

**PBS -** phosphate buffered saline

**PCR -** polymerase chain reaction

**PDB -** protein data bank

**PEG -** polyethylene glycol

**PMSF -** phenylmethylsulfonyl fluoride

**PQC -** protein quality control

**PUB -** peptide:N-lycanase/UBA- or UBX- containing proteins

**PUL -** PLAP, Ufd3, Lub1

**PVDF -** polyvinylidene fluoride

**RBP -** RNA-binding protein

**RNA -** ribonucleic acid

**RNase A -** ribonuclease A

**ROS -** reactive oxygen species

**RP -** regulatory particle

**rpm -** rounds per minute

**RPN -** regulatory particle non-ATPase

**RPT -** regulatory particle triple A

**RQC -** ribosomal quality control

**RT -** room temperature

***S. cerevisiae* -** *Saccharomyces cerevisiae*

**SC -** synthetic complete

**SDS -** sodium dodecyl sulfate

**SDS-PAGE -** sodium dodecyl sulfate polyacrylamide gel electrophoresis

**SG -** stress granule

**siRNA -** small-interfering RNA

**SQSTM1 -** sequestosome 1

**SUMO -** small ubiquitin-like modifier

**TBE -** tris-borate-EDTA

**TBS -** tris-buffered saline

**TBST -** Tris-buffered saline with Tween

**TCA -** trichloroacetic acid

**TIA-1 -** T-cell intracytoplasmic antigen

**Tris -** tris (hydroxymethyl)aminomethane

**Trp -** tryptophan

**UB -** ubiquitin

**UBA -** ubiquitin-associated

**UBL -** ubiquitin-like

**UBX -** ubiquitin regulatory X

**UFD1 -** ubiquitin-fusion degradation protein 1

**UIM -** ubiquitin-interacting motif

**UPS -** ubiquitin-proteasome system

**Ura -** uracil

**VCP -** valosin-containg protein

**VIM -** VCP-interacting motif

**w/v -** weight per volume

**WT -** wild-type

**Y2H -** yeast two hybrid

**YPD -** yeast peptone dextrose

**Zf -** zinc-finger

**ZFAND1/2A/2B -** zinc finger AN1 type domain containing protein 1/2A/2B

# 1 Summary

Protein quality control systems are critical for cellular proteostasis and survival under stress conditions. The ubiquitin proteasome system (UPS) plays a pivotal role in proteostasis by eliminating misfolded and damaged proteins. However, exposure to the environmental toxin arsenite results in the accumulation of polyubiquitylated proteins, indicating an overload of the UPS. Arsenite stress induces the rapid formation of stress granules (SGs), which are cytoplasmic assemblies of mRNPs stalled in translation initiation. The mammalian proteins ZFAND2A/B (also known as AIRAP and AIRAPL, respectively) bind to the 26S proteasome, and ZFAND2A has been shown to adapt proteasome activity to arsenite stress. They belong to a small subfamily of AN1-type zinc finger containing proteins that also comprises the unexplored mammalian member ZFAND1 and its yeast homolog Cuz1.

In this thesis, the cellular function of Cuz1 and ZFAND1 was investigated. Cuz1/ZFAND1 was found to interact with the ubiquitin-selective, chaperone-like ATPase Cdc48/p97 and with the 26S proteasome. The interaction between Cuz1/ZFAND1 and Cdc48/p97 requires a predicted ubiquitin-like domain of Cuz1/ZFAND1. *In vivo*, this interaction was strongly dependent on acute arsenite stress, suggesting that it is a part of the cellular arsenite stress response. Lack of Cuz1/ZFAND1 caused a defect in the clearance of arsenite-induced SG clearance. ZFAND1 recruits both, the 26S proteasome and p97, to arsenite-induced SGs for their normal clearance. In the absence of ZFAND1, SGs lack the 26S proteasome and p97, accumulate defective ribosomal products and become aberrant. These aberrant SGs persist after arsenite removal and undergo degradation *via* autophagy. ZFAND1 depletion is epistatic to the expression of pathogenic mutant p97 with respect to SG clearance, suggesting that ZFAND1 function is relevant to the multisystem degenerative disorder, inclusion body myopathy associated with Paget's disease of bone and frontotemporal dementia and amyotrophic lateral sclerosis (IBMPFD/ALS).

**Zusammenfassung**

Systeme zur Sicherung der Proteinqualität sind von essentieller Bedeutung für die zelluläre Proteostase und das Überleben unter Stressbedingungen. Dabei spielt das Ubiquitin-Proteasom-System (UPS) eine entscheidende Rolle: Es beseitigt fehlgefaltete und beschädigte Proteine. Sind Zellen dem Umweltgift Arsenit ausgesetzt, kommt es zu einer Akkumulation von polyubiquitinierten Proteinen, was auf eine Überlastung des UPS hinweist. Dieser durch Arsenit verursachte Stress bewirkt eine schnelle Bildung von Stressgranula (SGs), einer cytoplasmatischen Ansammlung von mRNPs, die in der Initiation der Translation blockiert sind. Die Säuger Proteine ZFAND2A/B (auch bekannt als AIRAP und AIRAPL) binden an das 26S Proteasom. Zusätzlich wurde gezeigt, dass ZFAND2A die Aktivität des Proteasoms an durch Arsenit verursachten Stress, anpasst. Diese Proteine gehören zu einer kleinen Unterfamilie von Zinkfinger von AN1-type enthaltenden Proteinen, zu der auch das bislang nicht erforschte Säuge Protein ZFAND1 und sein Hefehomolog Cuz1 gehören.

In dieser Arbeit wurde die zelluläre Funktion von Cuz1 und ZFAND1 untersucht. Es zeigte sich, dass Cuz1/ZFAND1 mit dem 26S Proteasom und der Ubiquitin-selektiven, Chaperon-ähnlichen ATPase Cdc48/p97 interagiert. Die Interaktion zwischen Cuz1/ZFAND1 und Cdc48/p97 benötigt eine vorhergesagte Ubiquitin-ähnliche Domäne von Cuz1/ZFAND1. Diese Interaktion ist *in vivo* stark von akutem Arsenitstress abhängig, was darauf hindeutet, dass sie Teil der zellulären Stressantwort gegen Arsenit ist. Fehlt Cuz1/ZFAND1, so kommt es zu einer Störung bei der Beseitigung der von Arsenit verursachten SGs. Normalerweise rekrutiert ZFAND1 sowohl das 26S Proteasom als auch p97 zu diesen SGs, um sie zu entfernen. Wenn ZFAND1 jedoch fehlt, sind auch p97 und das 26S Proteasom nicht an den SGs lokalisiert. Dadurch sammeln sich dort defekte ribosomale Produkte an, und die SGs werden abnormal. Auch nach Entfernung des Arsenitstresses bestehen diese abnormalen SGs fort und werden schließlich über Autophagie abgebaut. Bei der Beseitigung der SGs ist das Fehlen von ZFAND1 epistatisch zu der Expression einer pathogenen p97-Mutante, was darauf hinweirt, dass ZFAND1 bei der degenerativen Multisystemerkrankung Einschlusskörper-Myopathie assoziiert mit Pagets Erkrankung der Knochen und frontotemporaler Demenz und Amyotrophe Lateralsklerose (IBMPFD/ALS) eine Rolle spielt.

# 2 Introduction

## 2.1 Protein quality control

Proteins are the major structural and functional component of all cell types in the body and perform a variety of functions. Protein synthesis is therefore vital for the growth and development of cells. In a cell, thousands of proteins, with half-lives ranging from minutes to days, are produced every day. For optimal functioning, the cell continuously needs to rid itself of damaged, misfolded and aggregated proteins, toxic conformers and defective ribosomal products (DRiPs) (Balchin et al., 2016; Buchberger et al., 2010; Yewdell, 2011). A balance between protein synthesis and degradation, termed protein homeostasis, is critical in order to maintain the physiological protein concentration in cells (Balchin et al., 2016; Labbadia and Morimoto, 2015).

For each protein to carry out its defined function, a correct protein conformation and hence optimal folding mechanisms are crucial. Protein folding begins at the ribosome itself, while amino acids are being added to the nascent polypeptide chain. Molecular chaperones play a major role in maintaining each protein in its native state (Hendrick and Hartl, 1995). Proteins face a constant threat of misfolding and aggregation during stress conditions such as heat, osmotic stress, reactive oxygen species (ROS) production, or heavy metals, leading to a perturbed protein homeostasis (Balchin et al., 2016; Buchberger et al., 2010; Dobson, 2003). In order to cope with this, cells possess three different highly efficient protein quality control (PQC) strategies. This includes refolding assisted by molecular chaperones, degradation pathways and adaptive responses (Fig. 1) (Balchin et al., 2016; Buchberger et al., 2010).

Chaperones assist the folding of unfolded or misfolded proteins into a native protein, failure of which leads to formation of terminally misfolded proteins that are then targeted for degradation (Hendrick and Hartl, 1995). Degradation of misfolded or aggregated proteins occurs with the help of protein degradation machineries including the ubiquitin proteasome system (UPS) and autophagy. The UPS plays a major role in recognizing and degrading soluble proteins, whereas autophagy is responsible for degrading insoluble protein aggregates and damaged organelles (Collins and Goldberg, 2017; Mizushima et al., 2011). Apart from these mechanisms, cells have evolved different adaptive responses including the upregulation of chaperones and folding helpers (e.g., UPR [unfolded protein response]) or the reduction of bulk translation, accompanied by formation of stress granules (SGs) (Rutkowski and Kaufman, 2003; Yamasaki and Anderson, 2008).

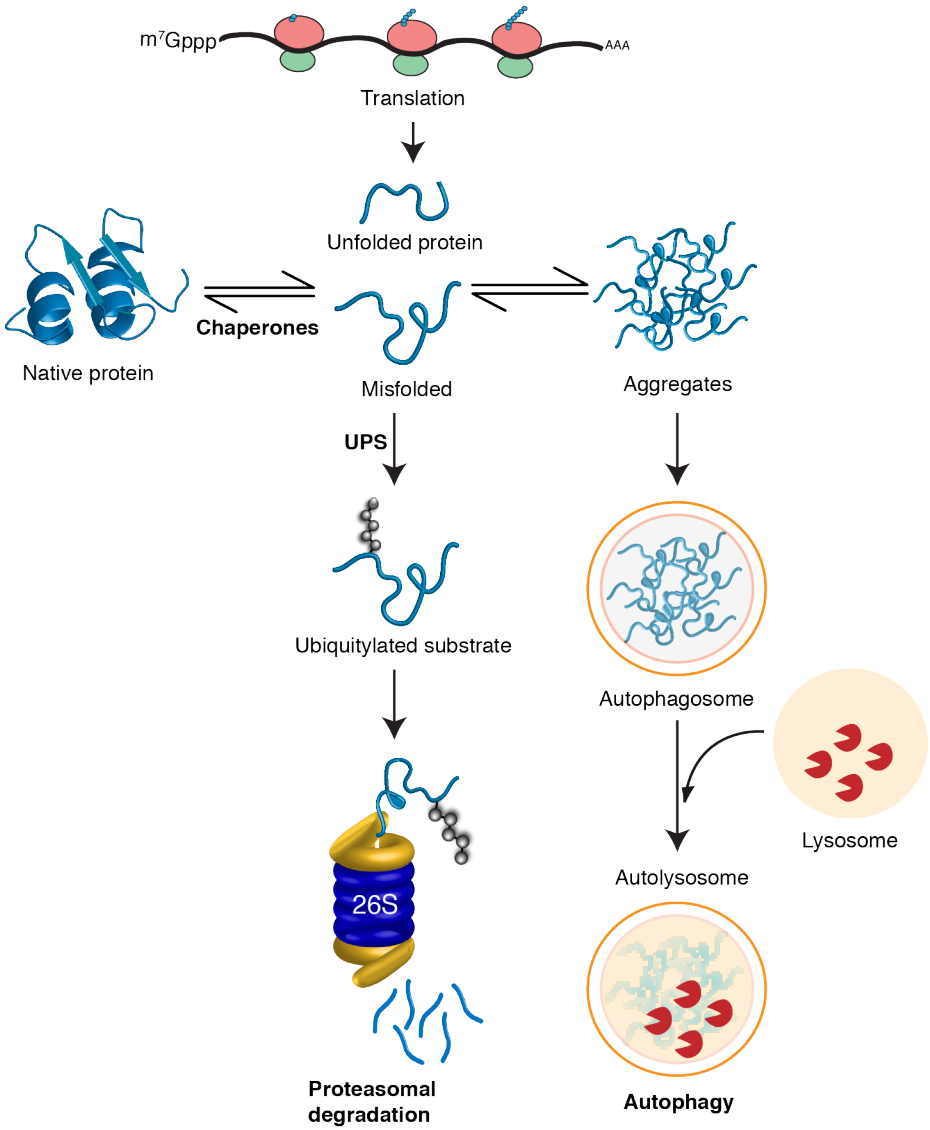


**Figure 1. Protein quality control systems.** Schematic depicting the three major quality control systems of cell – chaperones, ubiquitin proteasome system (UPS), and autophagy.

## 2.2 The ubiquitin proteasome system

### 2.2.1 Ubiquitin

About 80% of intracellular protein degradation occurs *via* the UPS. In this process, soluble proteins destined for degradation are first marked with ubiquitin moieties in a process called ubiquitylation (Hershko and Ciechanover, 1998; Komander and Rape, 2012). Ubiquitin is a small, 76 amino acid protein, and is highly conserved among all eukaryotes. Ubiquitylation is a posttranslational modification where the C-terminus of ubiquitin is covalently bound to the ε-amino groups of target protein lysine residues *via* an (iso)peptide bond (Hershko and Ciechanover, 1998).

### 2.2.2 Ubiquitin conjugation

The process of ubiquitylation requires the catalytic cascade of three enzymatic activities, carried out by the enzymes E1-E3 (Fig. 2). E1 (ubiquitin activating enzyme) activates ubiquitin in an ATP-dependent reaction by C-terminal adenylation and formation of thioester intermediate proteins (Ciechanover et al., 1981; Hass et al., 1982). The activated ubiquitin is then transferred in a trans-esterification reaction to the active site cysteine of E2 (ubiquitin conjugating enzyme). This is followed by E3 (ubiquitin protein ligase)-mediated conjugation to target lysine residues (Pickart, 2001; Pickart and Eddins, 2004).

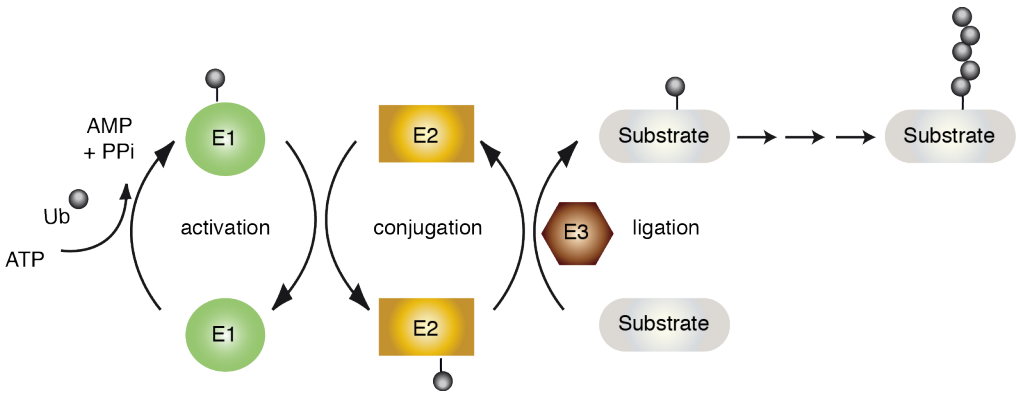


**Figure 2. Ubiquitin conjugation.** Schematic depicting the enzymatic cascade leading to substrate ubiquitylation. See text for details.

The process of ubiquitylation can modulate protein-protein interactions and can regulate the degradation of proteins *via* the proteasome and autophagy. Apart from this, it can also regulate activity and localization of proteins (Wang et al., 2018; Gregory et al., 2003). Importantly, ubiquitylation is a reversible post-translational modification. Ubiquitin-linked chains bound to substrate proteins can undergo removal by deubiquitinating enzymes (DUBs) (Komander and Rape, 2012).

### 2.2.3 Diversity of ubiquitin chains

Substrate proteins can be ubiquitylated either at a single or at multiple lysine residues in the same protein molecule leading to either mono-/multi-monoubiquitylation or poly-ubiquitylation (Komander and Rape, 2012). Morever, ubiquitin itself has seven lysine residues (K6, K11, K27, K29, K33, K48, and K63) and the N-terminal amino group (M1) that can be ubiquitylated (Fig. 3) (Akutsu et al., 2016). This increases the permutations and combinations of the types and length of ubiquitin chains that can be added to the substrate (Komander, 2009).

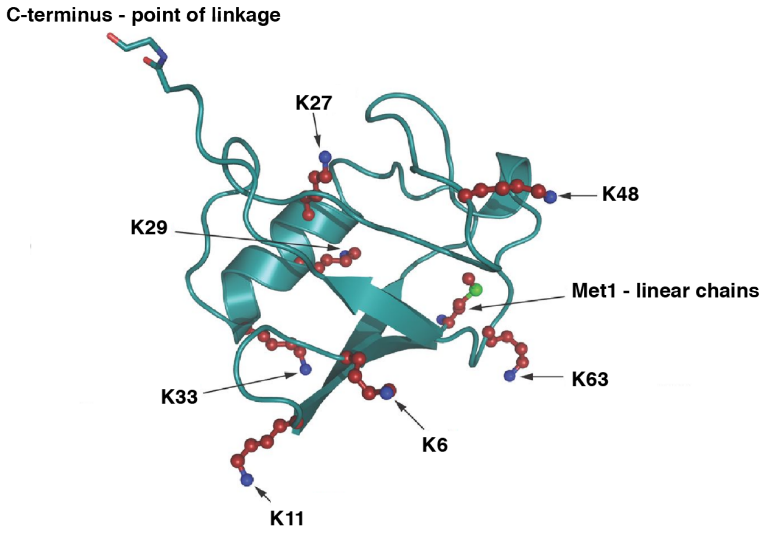


**Figure 3. Ubiquitin and its lysine residues.** The structure of ubiquitin (green, PDB code 1UBQ) and its seven lysine residues (red, with blue nitrogen atoms). All seven lysine residues (K6, K11, K27, K29, K33, K48, and K63) and the N-terminus amino group (M1) residing on different surfaces of the molecule are labeled (From Komander, 2009).

Depending on the lysine residue of ubiquitin that is linked to the substrate protein, ubiquitin chains can be classified into eight different categories: K6, K11, K27, K29, K33, K48, K63, and M1 chains. The type of ubiquitin chain decides the fate of the substrate protein, and thereby not only increases the complexity, but also provides more specificity to the process of substrate turnover (Fig. 4). K48-linked chains, which occur most frequently, target the substrates to the 26S proteasome for degradation (Thrower et al., 2000). By contrast, mono-ubiquitin or K63-linked chains target the substrate protein to non-proteasomal pathways of protein turnover, including selective autophagy, endocytocis, innate immunity, NF-κB signaling, and DNA repair (Spence et al., 1995; Pickart and Fushman, 2004; Xu et al., 2009). K11-linked chains are mainly involved in cell cycle quality control, while K6-linked chains are being studied for their role in DNA damage and parkin-mediated mitophagy (Xu et al., 2009). M1-linked chains play a major role in inflammatory and immune responses by regulating the activation of the transcription factor NF-κB (Akutsu et al., 2016).

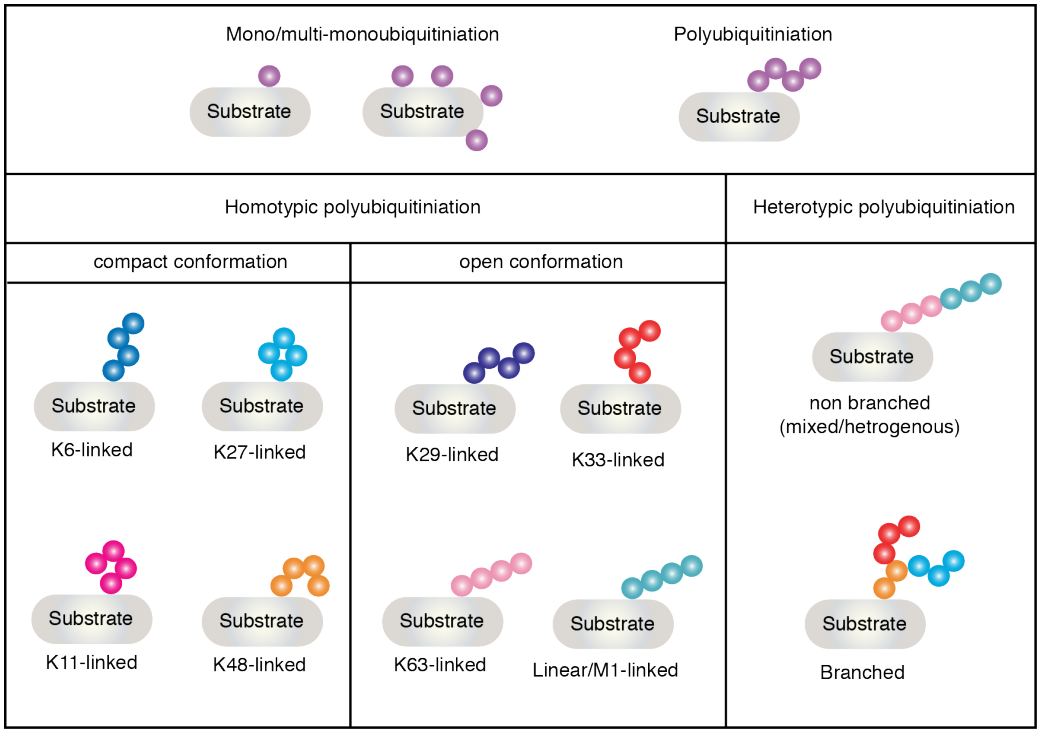


**Figure 4. Diversity of ubiquitin modification.** The substrate protein can be ubiquitylated in three different ways: monoubiquitylation, multi-monoubiquitylation, and polyubiquitylation. Polyubiquitin chains are further subdivided into homotypic or heterotypic. Heterotypic chains can also be branched where single ubiquitin can get ubiquitylated at two different lysine residues (Adapted from Komander, 2009).

### 2.2.4 The 26S proteasome

In the eukaryotic cell, the 26S proteasome is responsible for the vast majority of protein degradation. Given the critical role of the UPS in maintaining protein homeostasis in the cell, the functionality of the 26S proteasome is of high importance.

The eukaryotic 26S proteasome is a 2.5 MDa large, highly evolutionarily conserved, and one of the most complicated eukaryotic proteases (Bochtler et al., 1999). It is composed of two subassemblies, the 19S regulatory particle (RP) and the 20S core particle (CP) (Fig. 5) (Hershko and Ciechanover, 1998; Tanaka, 2009). The RP comprises the lid and base subcomplexes. The lid contains 13 non-ATPase subunits (Rpn1-13) (Regulatory Particle Non-ATPase) and the base contains 6 different AAA+ (ATPases associated) ATPase subunits (Rpt1-6) (Regulatory Particle Triple A) (Lander et al., 2012; Lasker et al., 2012). The RP recognizes the ubiquitylated substrates, removes the ubiquitin moieties, and translocates these substrates towards the CP for degradation (Smith et al., 2007; Tomko et al., 2010). The ability of the RP to bind ubiquitylated substrates comes from the subunits Rpn1, Rpn2, Rpn10, and Rpn13 (Elsasser et al., 2002; Rosenzweig et al., 2012; Deveraux et al., 1994; Husnjak et al., 2008). Importantly, Rpn11 in the lid subcomplex

acts as a DUB, removing ubiquitin moieties prior to targeting the substrates to the CP for degradation (Fig. 5) (Verma et al., 2002; Yao and Cohen, 2002).

The cylindrical CP is a stack of four heteroheptameric rings α7β7β'7α'7, and houses active proteolytic sites within the interior space, minimizing nonspecific proteolysis (Groll et al., 1997). The two outer rings contain seven α subunits (α1-α7), while the two inner rings contain seven β subunits (β1-β7). The β1, β2 and β5 subunits present in the CP harbor the catalytic sites of the proteasome, and are responsible for the proteolysis of substrates (Groll et al., 2000; Groll and Huber, 2003).

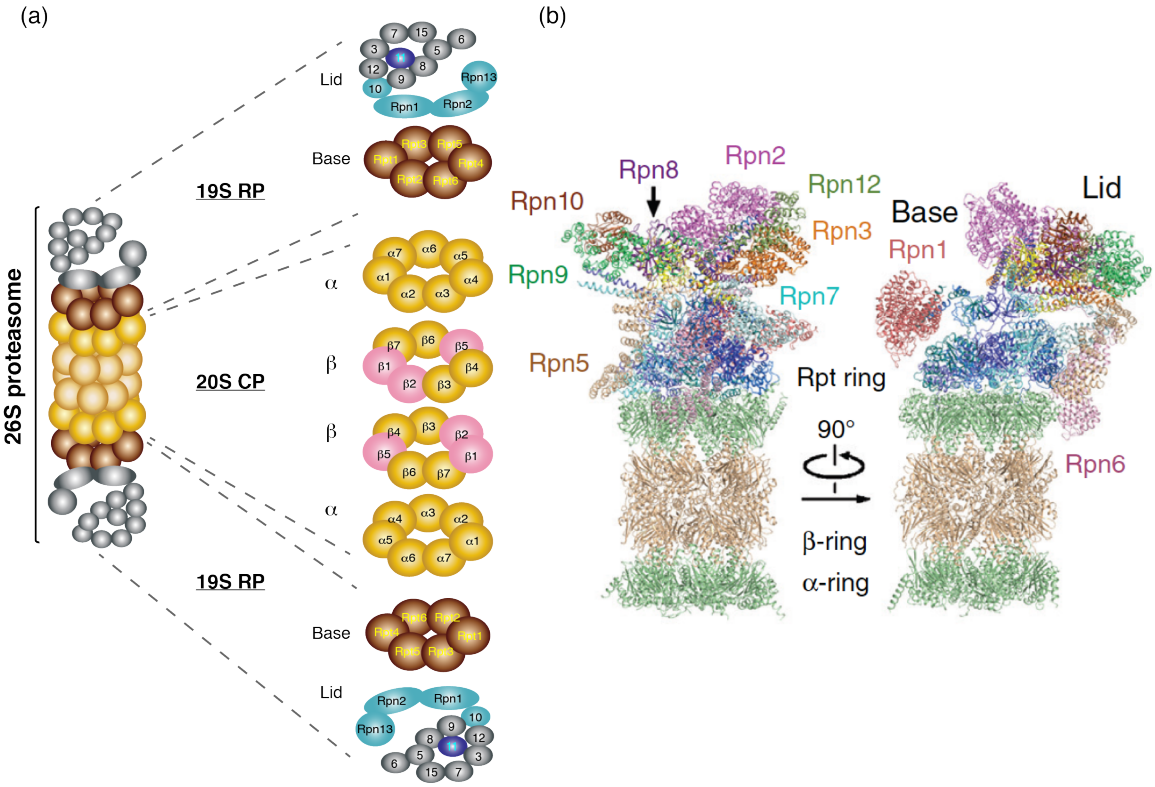


**Figure 5. The 26S proteasome complex.** (a) Schematic diagram depicting the two subassemblies of the 26S proteasome: the 19S regulatory particle (RP) and the 20S core particle (CP). The RP consists of Rpn and Rpt subunits, which forms cap on both ends of the CP. The CP consists of two outer α rings and two inner β rings. (b) Cartoon representation of the human proteasome in two perpendicular views. All RP subunits are color-coded (From Huang et al., 2016).

Proteasome activity can be perturbed upon acute oxidative stress, amino acid deprivation, or heavy metal toxicity (e.g., arsenic) (Livnat-Levanon et al., 2014; Suraweera et al., 2012; Yun et al., 2008). A defect in proteasome activity leads to an accumulation of ubiquitylated substrate proteins and aggregated proteins (Kitajima et al., 2014). Several reports have shown that a defect in proteasome activity is linked to aging and neurodegenerative disorders such as Alzheimer's (AD), Huntington's (HD), Parkinson's diseases (PD) and Amyotrophic lateral sclerosis (ALS) (Balchin et al., 2016; Labbadia

and Morimoto, 2015). Studies indicate that the other protein quality control system, autophagy, shows increased activity under conditions of impaired proteasomal activity (Nedelsky et al., 2008).

## 2.3 Macroautophagy

Autophagy is an evolutionarily conserved intracellular degradation process in eukaryotes. Three different types of autophagy have been reported till date: chaperone-mediated autophagy, microautophagy, and macroautophagy (Fig. 6). The central mechanism in all three different types of autophagy involves the proteolytic degradation of cellular components by the lysosome. Macroautophagy eliminates long-lived and aggregated proteins, macromolecular assemblies as well as damaged organelles and intracellular pathogens (Galluzzi et al., 2017).

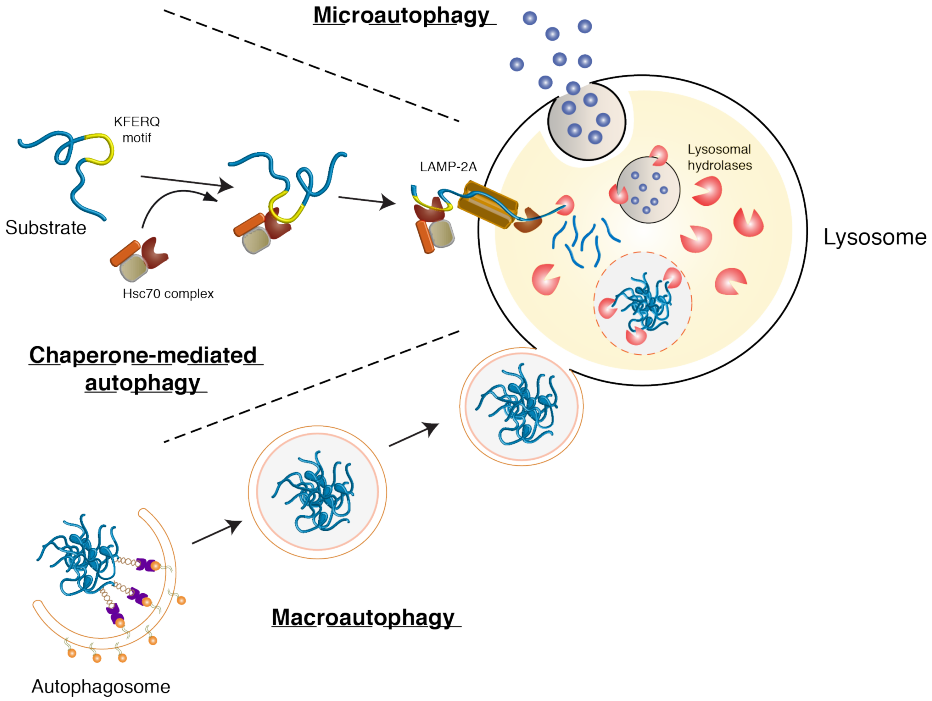


**Figure 6. Types of autophagy.** Schematic diagram representing three different types of autophagy – microautophagy, chaperone-mediated autophagy, and macroautophagy.

In mammals, macro-autophagy (referred to as autophagy hereafter) is initiated primarily at the lipid bilayer of the endoplasmic reticulum (ER), where the formation of an isolation membrane (known as phagophore) starts. The phagophore expands and forms the double-membrane bounded autophagosome, which engulfs cargo such as protein aggregates, damaged organelles, and bacterial pathogens (Fig. 6). The cargo-loaded autophagosome matures through fusion with the lysosome into an autolysosome, forming

an acidic inner compartment containing lysosomal hydrolases (Fig. 6) (Noda and Inagaki, 2015; Antonioli et al, 2016).

During autophagy, the cytosolic form of a protein called microtubule-associated protein 1A/1B-light chain 3 (LC3-I) (a mammalian homolog of yeast Atg8) is first gets covalently conjugated to phosphatidylethanolamine. This enzymatic process is facilitated by various autophagy-related genes to form lipidated LC3 (LC3-II) (Kabeya et al, 2000), resulting in its recruitment to the phagophore. The incorporated LC3-II then extends the phagophore, eventually forming the autophagosome. The LC3 family of proteins also acts as a receptor, which recruits adaptor proteins like p62, NBR1, and Nix/BNIP3L (Stolz et al, 2014; Wild et al, 2014). p62 binds to the ubiquitylated cargo proteins through its UBA domain, and incorporates it into the autophagosome *via* LIR-motif mediated binding to LC3-II (Lamark et al., 2009). p62 *via* its C-terminal UBA domain interacts preferentially with long K63-linked chains (with more than 7 ubiquitins), but it can also bind short chains linked through both K48 and K63 (Long et al., 2008; Tan et al., 2007; Wooten et al., 2008).

Autophagy plays a significant role in the clearance of intracellular aggregates and is essential for cellular survival and development. It has been suggested that its adaptive role protects organisms against a variety of diseases including cancer (Amaravadi et al, 2016), neurodegeneration (Menzies et al, 2015), cardiomyopathy (Shirakabe et al, 2016), diabetes, liver disease, autoimmune diseases (Deretic et al, 2013; Zhong et al, 2016) and infections (Deretic et al, 2013).

## 2.4 Stress granules

### 2.4.1 Formation of stress granules

In the physiological milieu, cells face a constant threat of environmental stress, and to cope with these stress conditions cells have evolved mechanisms to protect macromolecules vital for cellular viability and to conserve energy. Cells prioritize synthesis of chaperones and enzymes required for stress adaptation over the synthesis of house-keeping genes (Alberti et al., 2017).

Under normal physiological conditions, protein translation is initiated when nuclear mRNPs (messenger ribonucleoprotein) are exported to the cytosol. These cytosolic mRNPs are then bound by translation initiation factors and ribosomal subunits, and enter into the translation initiation process (Kedersha et al., 1999). Under stress conditions,

translation is halted and the polysome disassembles. As a result, mRNAs, ribosomal subunits, translation initiation factors, and several RNA binding proteins (RBPs) assemble into membrane-less compartments called stress granules (SGs) (Fig. 7) (Panas et al., 2016; Protter and Parker, 2016). Phosphorylation of translational initiation factor eIF2α on Ser51 is a pre-requisite for the assembly of almost all types of SGs in cells exposed to environmental stresses (Wek et al., 2006). Stalled mRNAs along with RBPs are kept silent and protected from the degradation inside SGs, and can re-enter translation when stress subsides (Alberti et al., 2017).

SGs are evolutionarily highly conserved membrane-less and highly dynamic cytoplasmic structures formed *via* liquid liquid phase separation (LLPS). Super-resolution microscopy studies revealed that SGs are composed of two compartments, a stable core and a phase-separated shell (Wheeler et al., 2016).

It has been shown that different stress conditions can affect specific stages of SG assembly, resulting in SGs of varying composition (Panas et al., 2016; Protter and Parker, 2016). SG assembly starts with mRNP aggregation mediated by protein(s) like TIA-1 (T-cell intracellular antigen 1), G3BP1 (Ras-GTPase-activating protein SH3-domain binding protein 1), FMRP (fragile X mental retardation protein), among others (Fig. 7) (Kedersha et al., 2000; Mazroui et al., 2002; Tourriere et al., 2003). SG assembly then continues with the help of several protein-protein interactions. For example, the G3BP protein has a dimerization domain that contributes to SG formation during arsenite stress (Tourriere et al., 2003). Moreover, several RBPs (eg. TIA-1 and TIA-R) containing Q/N-rich (glutamine/asparagine) prion-like domains are able to self-aggregate and play a major role in SG assembly (Gilks et al., 2004; Cushman et al., 2010). The stable core of a SG, surrounded by a shell assembly, forms microscopically visible SGs (Jain et al., 2016). A dynamic exchange of proteins between the core and the shell is important and is speculated to be regulated by chaperones. A defect in this dynamic exchange affects the kinetics of SGs, and leads to the formation of aberrant SGs (Jain et al., 2016).

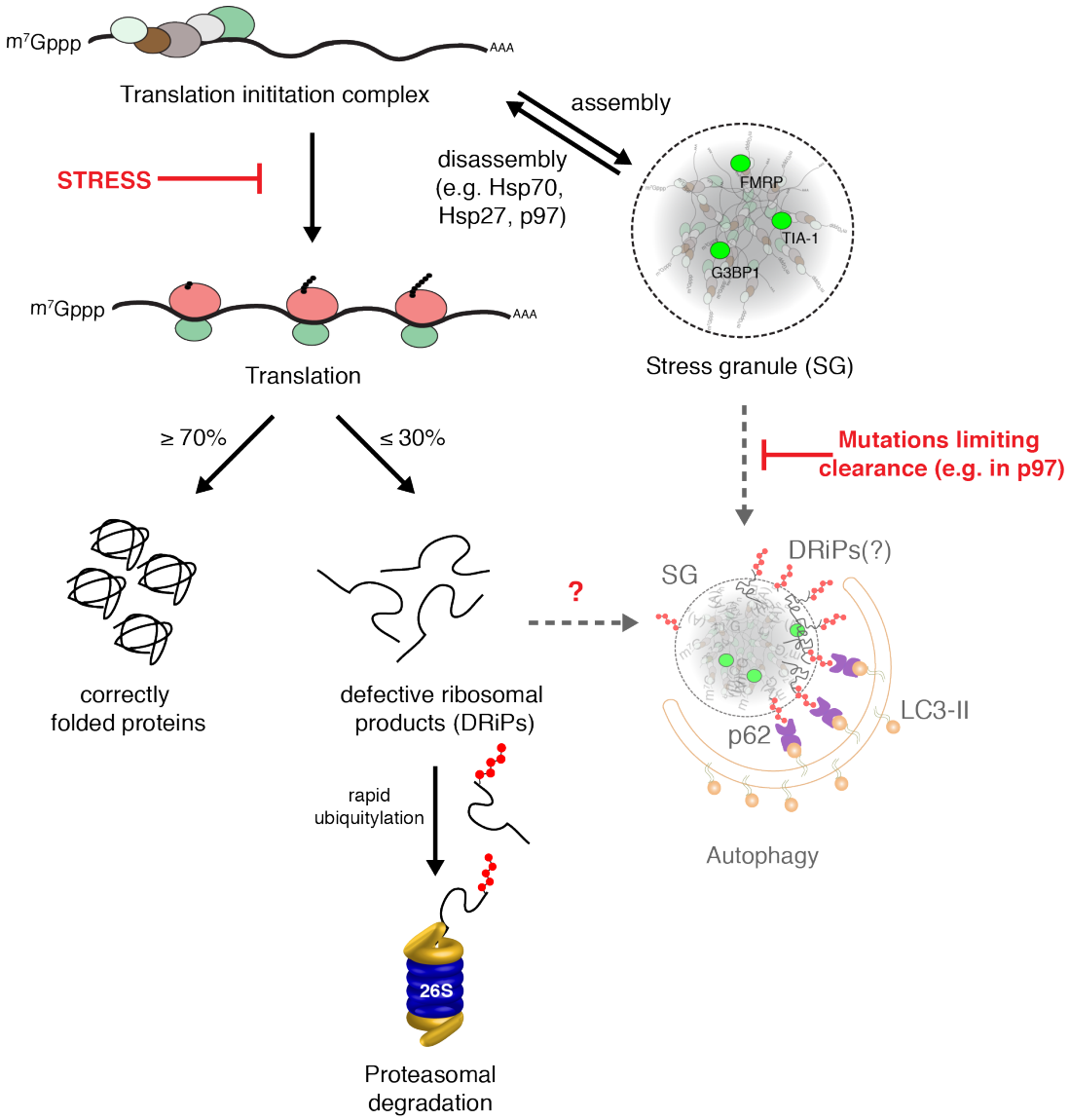


**Figure 7. Stress granule dynamics.** Schematic representation of SG formation and clearance. During translation, approximately 30% of newly synthesized proteins end up as DRiPs, which are rapidly ubiquitylated and degraded by the 26S proteasome. During stress condition, mRNPs along with vaious translation initiation factors accumulate as SGs in a reversible manner. Prolonged stress leads to accumulation of SGs, which is targeted for autophagy in a process involving p97.

### 2.4.2 Disassembly or clearance of stress granules

Typically, within a few minutes after stress conditions subside, SGs undergo disassembly, which is required for the recovery of translation. The mechanism underlying SG disassembly is poorly understood. Due to the presence of various aggregation-prone RBPs within SGs, a role for chaperones (eg. heat shock proteins) has been speculated and several chaperones including Hsp70 and Hsp27 (a.k.a. HSPB8) have also been found to localize to SGs (Fig. 7) (Kedersha et al., 1999; Gilks et al., 2004).

SGs can be cleared *via* a process involving the HSPB8-BAG3-HSP70 chaperone complex (Ganassi et al., 2016), and also with the help of p97 (Rodriguez-Ortiz et al., 2016). Interestingly, the *VCP* gene has been shown to play an important role in autophagy-mediated SG clearance. Disease-causing mutant of *VCP* causes perturbed granulostasis possibly contributing to the pathogenesis of IBMPFD/ALS (Buchan et al., 2013; Rodriguez-Ortiz et al., 2016). Importantly, a defect in SG clearance, resulting in altered SG composition and dynamics, is linked with the pathogenesis of several neurodegenerative diseases, including amyotrophic lateral sclerosis (ALS), frontotemporal lobar degeneration (FTLD), among others (Alberti et al., 2017; Ramaswami et al., 2013; Taylor et al., 2016).

## 2.5 p97/Cdc48

### 2.5.1 p97 structure

p97 (also known as VCP, Cdc48 and Ter94) is a ubiquitin-selective AAA ATPase. p97 is highly conserved among all eukaryotes and is a central regulator of the eukaryotic protein quality control system. It contains an amino-terminal N domain, two Walker-type ATPase domains, D1 and D2, and a carboxy-terminal, unstructured tail (Fig. 8a) (Meyer et al., 2012; Stolz et al., 2011). Energy derived from ATP hydrolysis is used for segregation of ubiquitylated proteins from their cellular environment (Braun et al., 2002; Jentsch and Rumpf, 2007; Buchberger, 2010). The N domain and the C-terminus of p97 can bind to various regulatory cofactors (see below).

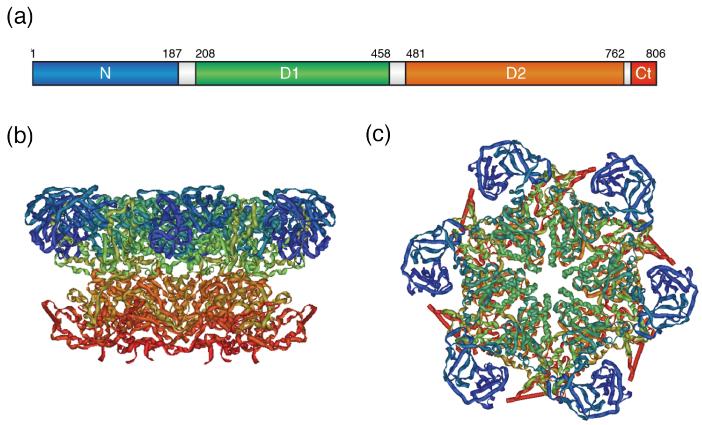


**Figure 8. Structure of AAA ATPase p97.** a) Schematic overview of the domain architecture of p97; the N-domain (blue) is followed by the two ATPase domains D1 (green), and D2 (orange). b) Sideward view of a p97 hexamer (colors as in a) c) View along the central axis (colors as in a) (From Buchberger, 2006).

p97 forms homohexameric, ring-shaped complexes (Fig. 8b,c) and is involved in a vast range of ubiquitin-related cellular processes. It binds to ubiquitylated proteins in the

cellular environment, or extracts ubiquitylated proteins from larger complexes, membranes, or chromatin, *via* its segregase activity (Buchberger, 2013; Meyer et al., 2012). The majority of these ubiquitylated proteins is then targeted to the 26S proteasome for degradation. In the past two decades, p97, apart from its role in PQC pathways like ERAD (endoplasmic reticulum associated degradation), OMMAD (outer mitochondrial membrane associated degradation), CAD (chromatin associated degradation), and RQC (ribosomal quality control), has also been found to play a major role in several other degradation pathways like cell cycle regulation, DNA damage repair, endolysosomal trafficking, and autophagy (Meusser et al., 2005; Ramadan et al., 2007; Ju et al., 2009; Tresse et al., 2010; Stolz et al., 2011; Verma et al., 2011; Xu et al., 2011; Verma et al., 2013).

### 2.5.2 p97 cofactors

The role of p97 in distinct cellular processes is tightly regulated by cofactors. p97 cofactors can be subdivided into two main categories: substrate-recruiting and substrate-processing cofactors (Fig. 9) (Jentsch and Rumpf, 2007). Substrate-recruiting cofactors typically possess a ubiquitin-binding domain and mediate the interaction between p97 and ubiquitylated substrate proteins. They can also recruit p97 to different cellular compartments (Schuberth and Buchberger, 2008). The majority of cofactors interact with p97 either by binding to the N domain or to the C-terminal tail. Most of the substrate recruiting cofactors bind to the N domain of p97 *via* their ubiquitin regulatory X (UBX), and UBX-like domains, or *via* linear sequence motifs including binding-site 1 (BS1), VCP-interacting motif (VIM), and VCP-binding motif (VBM) (Fig. 10) (Schuberth and Buchberger, 2008; Buchberger, 2010; Buchberger et al., 2015). The two most prominent and mutually exclusive substrate-recruiting cofactors are the heterodimeric Ufd1-Npl4 complex and the Shp1/p47 (Schuberth and Buchberger, 2008; Buchberger et al., 2015). On the other hand, substrate-processing cofactors possess E3-ligase or DUB activity, and can change the fate of substrate proteins by manipulating their ubiquitylation state (Rumpf and Jentsch, 2006). Some of these cofactors bind to the C-terminal tail of p97 *via* peptide N-glycosidase/ubiquitin-associated (PUB) or PLAA, Ufd3 and Lub1 (PUL) domains (Fig. 9) (Buchberger et al., 2015).

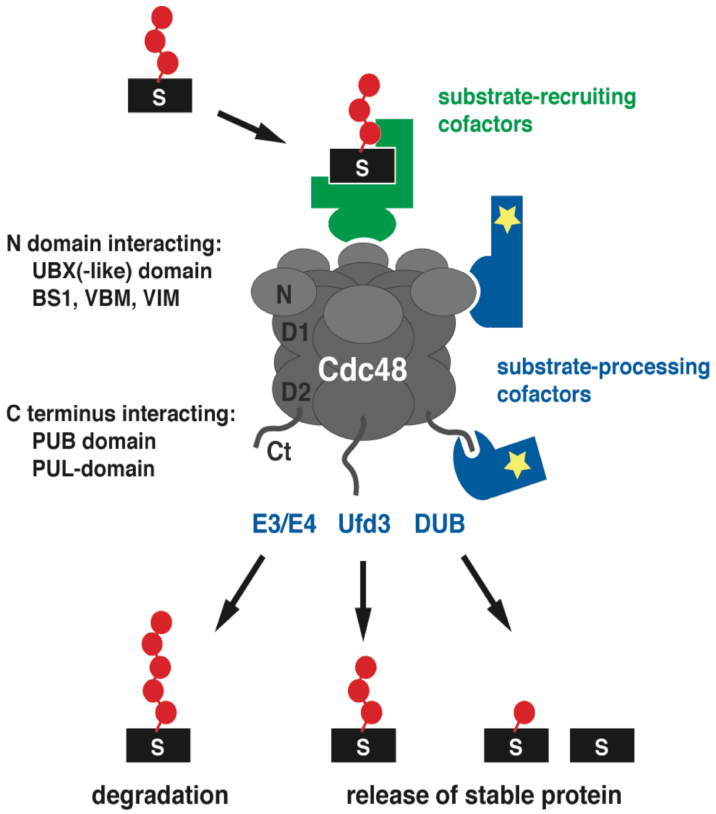


**Figure 9. Cdc48/p97 cofactors.** Ubiquitylated substrate proteins (S) are recognized by substrate-recruiting cofactors (green), and targeted towards the p97/Cdc48. On the other hand, substrate-processing cofactors (blue) can manipulate the fate of the substrate proteins by modifying ubiquitylation state (From Buchberger, 2006).

Importantly, *VCP* is an essential gene, and mutations in the human *VCP* gene cause the multisystem degenerative disorder IBMPFD/ALS (Nalbandian et al., 2011). Interestingly, this age related disease could also be caused by pathogenic mutations in the *SQSTM1* gene encoding the autophagy cargo adaptor p62, and in several genes encoding SG components. This suggests a strong interplay between protein quality control, SG homeostasis and disease (Alberti et al., 2017; Taylor et al., 2016).

## 2.6 Cellular responses to arsenite stress

### 2.6.1 Arsenic

Arsenic is a ubiquitous environmental toxin and carcinogen. However, arsenic has been used medicinally for over 2,400 years. Arsenic has been shown to induce apoptosis and inhibit proliferation, and used as a therapeutic agent for the treatment for acute promyelocytic leukemia (APL) (Waxman and Anderson, 2001). Its use has declined since the mid-1990s, due to concerns regarding its toxicity and carcinogenicity upon chronic administration.

In its trivalent oxidation state As(III), arsenic has been shown to damage cells *via* several different mechanisms including DNA damage, ROS production, and dysregulated transcription (Hughes, 2002; Khairul et al., 2017). However, the most dangerous and immediate effect of arsenic is its proteotoxicity. Arsenic can directly perturb the 26S proteasome and p97 functions (Stanhill et al., 2006; Tillotson et al., 2017). In order to adapt to arsenite toxicity, cells strongly enhance the heat shock response, the unfolded protein response, and also upregulate the amount of 26S proteasome (Guerra-Moreno et al., 2015; Hanna and Finley, 2007; Stanhill et al., 2006). However, the molecular mechanisms behind the proteasomal adaptation to arsenite stress are not well understood.

### 2.6.2 The ZFAND family

Proteins containing zinc finger domains of the AN1 type were found to play a role in arsenite proteotoxicity (Isakov and Stanhill, 2011; Stanhill et al., 2006; Yun et al., 2008). Bioinformatic analyses revealed that ZFAND1 and Cuz1, together with ZFAND2A and ZFAND2B, form a small family of proteins containing zinc fingers of the AN1 type (Kay Hofmann, University of Cologne, personal communication). Members of this family are found to contain either one or two N-terminal Zf_AN1 finger domains. Interestingly, the ZFAND1/2A/2B family of proteins contains a distinct consensus sequence (LDFLP motif) in the first AN1 finger (Sun et al., 2016), which is not present in other AN1-type domain containing proteins (Fig. 10) (Kay Hofmann, University of Cologne, personal communication). This subfamily also possesses a specific domain organization where human ZFAND2A and ZFAND2B contain an archetypical triad of two AN1 fingers separated by a UBZ-like zinc finger (Hofmann, 2009). By contrast, human ZFAND1 and most of its homologs lack the central UBZ-like finger, and Cuz1 and several fungal homologs possess just the N-terminal AN1 finger. It has been shown that the AN1 type zinc finger domain is required for binding to the 26S proteasome in case of Cuz1, ZFAND2A and ZFAND2B (Sa-Moura et al., 2013; Stanhill et al., 2006; Yun et al., 2008), suggesting that this is an evolutionarily conserved function. Interestingly, all three members of ZFAND1/2A/2B subfamily contain a distinct C-terminal domain, which might contribute specific functions (Fig. 10). Cuz1 and its human homolog ZFAND1 contain a ubiquitin-like domain (UBL) at the C-terminal region (Fig. 10), and in case of Cuz1, this UBL domain has been shown to be required for Cdc48 binding (Hanna et al., 2014; Sa-Moura et al., 2013).

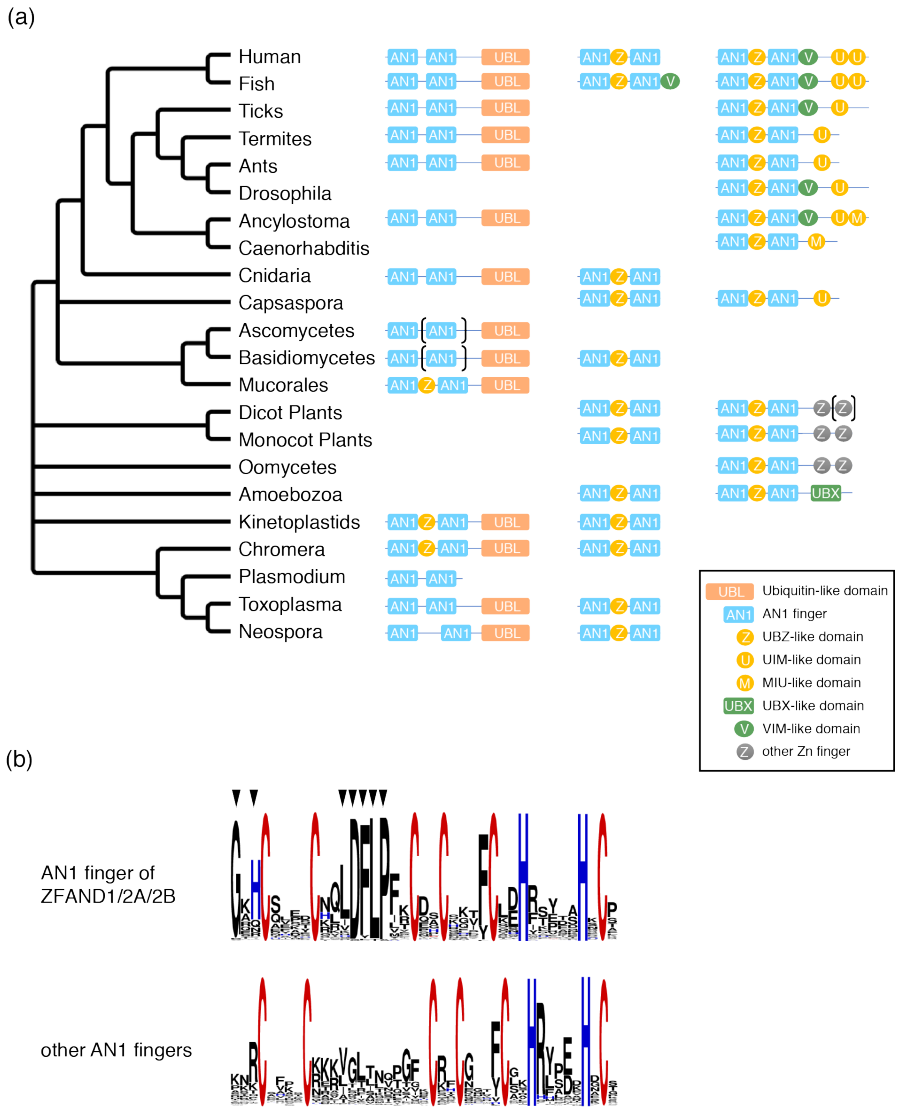


**Figure 10. Evolutionary conservation of the ZFAND1/2A/2B family.** (A) Domain organization of the ZFAND1/2A/2B family members were retrieved from the Uniprot database. Blue: AN1 fingers; orange: ubiquitin-like (UBL) domain; yellow: known or presumed ubiquitin binding domains (Z: UBZ type, M: MIU type, U: UIM type); green: known or presumed p97 binding domains (V: VIM, UBX: UBX domain); grey: other domains. (B) Consensus sequence of the family defining AN1 finger. The conserved sequence motifs defining the N-terminal AN1 finger of the ZFAND1/2A/2B family are indicated by black arrowheads (Kay Hofmann, University of Cologne, personal communication).

## 2.7 Aims

AN1-type zinc finger containing proteins including ZFAND2A and ZFAND2B are found to interact with the 26S proteasome (Isakov and Stanhill, 2011; Stanhill et al., 2006; Yun et al., 2008). However, specific cellular functions of Cuz1 and ZFAND1 have remained elusive, with ZFAND1 being completely uncharacterized till date. The major aim of this thesis is therefore to characterize the role of the UBL domain found in Cuz1 and ZFAND1, and to elucidate their cellular functions.

# 3 Results

## 3.1 Cuz1

### 3.1.1 Cuz1 interacts *via* its UBL domain with the N domain of Cdc48

Cuz1 was first identified as a novel binding partner of budding yeast Cdc48 in a yeast two-hybrid screen (Böhm, 2011). To validate this finding, interaction studies between Cuz1 and Cdc48 were performed using a variety of experiments including *in vitro* pulldown, yeast two-hybrid (Y2H), and immunoprecipitation (IP) experiments.

In order to characterize the interaction between Cuz1 and Cdc48 and to identify the region of Cuz1 involved in Cdc48 binding, different Cuz1 variants (Fig. 11a) were cloned into pGAD and pGEX4T3 vectors for yeast two-hybrid (Y2H) assays (Fig. 11b) and GST-pulldown experiments (Fig. 11c), respectively. A Y2H experiment was performed using full length Cdc48 as bait and the various Cuz1 variants as prey. Strong interactions between Cdc48 and full length Cuz1 as well as constructs lacking the AN1_ZF domain were observed, whereas a Cuz1 deletion variant lacking the UBL domain showed no interaction with Cdc48 (Fig. 11b).

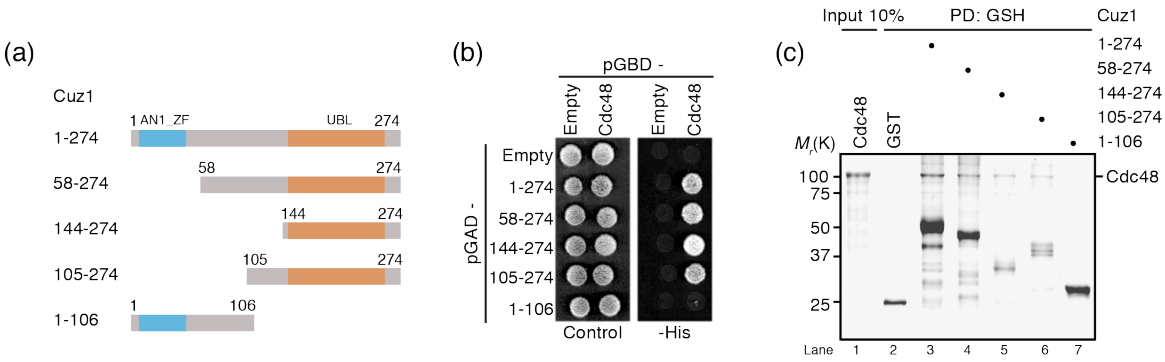


**Figure 11. Cuz1 interacts *via* its UBL domain with Cdc48.** (a) Schematic showing different variants of Cuz1 generated for Y2H experiments and *in vitro* pulldown. (b) Yeast two-hybrid assay. Yeast cells of the reporter strain PJ69-4a expressing the indicated Gal4-AD and Gal4-BD fusion proteins were spotted on SC plates lacking tryptophan and leucin (control) or additionally lacking histidine (-His). (c) GST pulldown assay. GST fusions of the Cuz1 variants shown in (a) were analyzed for their interaction with Cdc48.

*In vitro* binding assays were carried out using GST-Cuz1 constructs or GST alone, as a negative control. The proteins were immobilized on glutathione beads and then incubated with recombinant Cdc48. Full-length Cuz1, but not GST alone, was able to bind to Cdc48, indicating a direct interaction between Cuz1 and Cdc48 (Fig. 11c, lane 2,3). Consistent with the Y2H assays, deletion of the UBL domain, but not the AN1_ZF domain completely abolished Cdc48 binding (Fig. 11c, lane 7 and 4-6 respectively). This indicates that the UBL domain of Cuz1 is required for direct binding to Cdc48.

Cdc48 interacts with its cofactors through either the N-terminal domain or the C-terminal tail. In order to identify the Cuz1 binding site of Cdc48, variants of Cdc48 lacking the N domain (Cdc48ΔN) or comprising just the N domain (Cdc48-Nd) were recombinantly expressed (Fig. 12a). Two different GST-Cuz1 variants, full length and the UBL domain, were tested for binding to the Cdc48 variants. As expected, both variants of Cuz1 were able to bind to the wild-type Cdc48 (Fig. 12b, lane 4 and 7). Cdc48ΔN showed no binding to either construct of Cuz1 (Fig. 12b, lane 6 and 9). On the other hand, Cdc48-Nd was sufficient to bind Cuz1 (Fig. 12b, lane 5 and 8). This indicates that the N domain of Cdc48 is necessary and sufficient for binding to the UBL domain of Cuz1, in agreement with a recent report (Sa-Moura et al., 2013) (Fig. 12b).

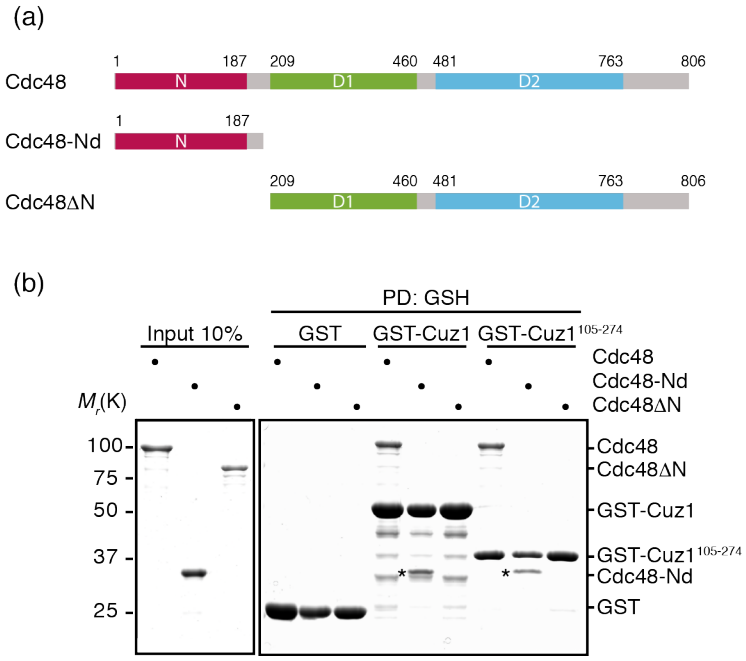


**Figure 12. Cuz1 interacts with the N domain of Cdc48.** (a) Schematic showing different variants of Cdc48 generated for *in vitro* pulldown experiments. (b) GST pulldown assay. Different Cdc48 variants shown in (a) were used to analyze the interaction with either full length ($Cuz1^{1-274}$) or the UBL domain of Cuz1 ($Cuz1^{105-274}$). * indicates Cdc48-Nd.

### 3.1.2 Arsenite strengthens the interaction between Cuz1 and Cdc48

In order to verify the interaction between Cuz1 and Cdc48 in cells, co-immunoprecipitation experiments were performed. A yeast strain expressing N-terminally HA-epitope tagged Cuz1 (3HA-Cuz1) under the control of the ADH1 promoter was used. Indeed, a clear co-immunoprecitation of Cdc48 with 3HA-Cuz1 was observed (Fig. 13). In line with a previous report (Sa-Moura et al., 2013), the interaction between Cuz1 and Cdc48 was strongly increased in a time-dependent manner upon prior addition of arsenite to the yeast culture (Fig. 13). These results, together with the

previously published finding showing a strengthened interaction of Cuz1 with the 26S proteasome upon arsenite stress (Sa-Moura et al., 2013; Hanna et al., 2014), clearly implicate Cuz1 in the arsenite stress response of yeast cells.

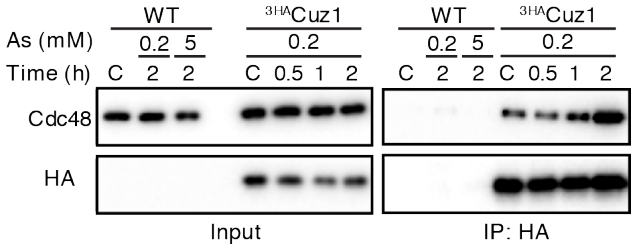


**Figure 13. The interaction between Cuz1 and Cdc48 is strengthened upon arsenite addition.** Immunoprecipitation (IP) of N-terminally 3HA epitope-tagged Cuz1 was performed either in the absence or presence of the indicated concentration of arsenite for different time intervals. WT strain was used as a negative control. Western blot against Cdc48 and HA.

### 3.1.3 Phenotypic characterization of a *Δcuz1* null mutant

In order to determine a potential role of Cuz1 in the cellular stress response, the growth of Δ*cuz1* cells under various stress conditions was analyzed on plates. No temperature (Fig. 14a) or drug sensitivity (MMS, HU or cycloheximide) of Δ*cuz1* in comparison to the wild type was observed (Fig. 14b). As a positive control, the sensitivity of the deletion strains Δ*rad18* to MMS and HU, Δ*vms1* to cycloheximide, and Δ*rpn4* to arsenite was used. These results showed no hypersensitivity of the Δ*cuz1* null mutant at all tested stress conditions.

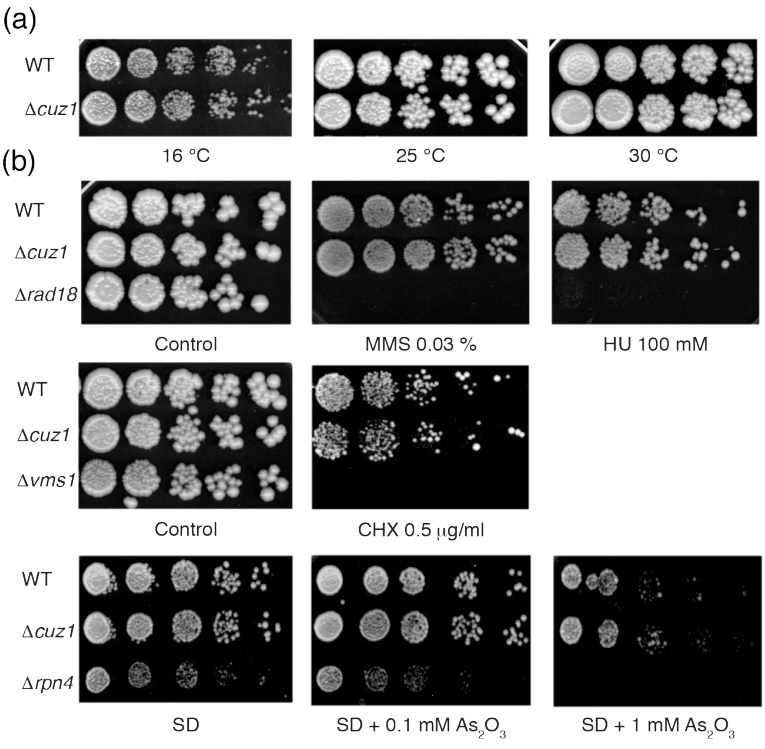


**Figure 14. The Δ*cuz1* null mutant exhibits no temperature sensitivity or hypersensitivity against various drugs.** (a) Five-fold serial dilutions of cultures of wild-type (WT) and Δ*cuz1* null mutant strains were spotted onto YPD plates and incubated at the indicated temperatures. (b) Five-fold serial dilutions of cultures of the indicated strains were spotted on YPD as control (SD plates in case of arsenite), and plates containing either 0.03% MMS, 100 mM hydroxyurea (HU) or 0.5 µg/ml cycloheximide (CHX). Sensitivity against arsenite was checked using SD plates containing 0.1 or 1 mM arsenite.

### 3.1.4 Role of Cuz1 in the clearance of arsenite-induced stress granules

A specific cellular function of Cuz1 during arsenite stress is still unknown. However, one hallmark of arsenite stress is the rapid formation of stress granules (SGs) (Kedersha et al., 1999). The strong interaction between Cuz1 and Cdc48 in the presence of arsenite (Fig. 13) and the published role of Cdc48/p97 in SG clearance (Buchan et al., 2013) hinted towards a potential involvement of Cuz1 in SG metabolism. In order to test this possibility, wild type, *cdc48-6*, and Δ*cuz1* cells were subjected to either heat shock or arsenite stress. Pbp1, a yeast homolog of Ataxin-2, is mainly nuclear under normal conditions, but localizes to SGs under several stress conditions. To study SG dynamics, Pbp1-GFP was used as SG marker protein in yeast live cell fluorescence microscopy. Wild type cells exhibited a robust formation of SGs under both stress conditions, which were cleared upon stress removal (Fig. 15). While SG formation in *cdc48-6* cells appeared normal, the SGs persisted after stress removal, particularly after heat shock, indicating an impaired SG clearance (Fig. 15, yellow arrows), as expected (Buchan et al., 2013). Δ*cuz1* cells also exhibited normal SG formation. Intriguingly, however, these cells retained a large number of arsenite-induced SGs, but not heat-induced SGs, during recovery (Fig. 15, yellow arrows). This result indicates an involvement of Cuz1 in the clearance of arsenite-induced SGs.

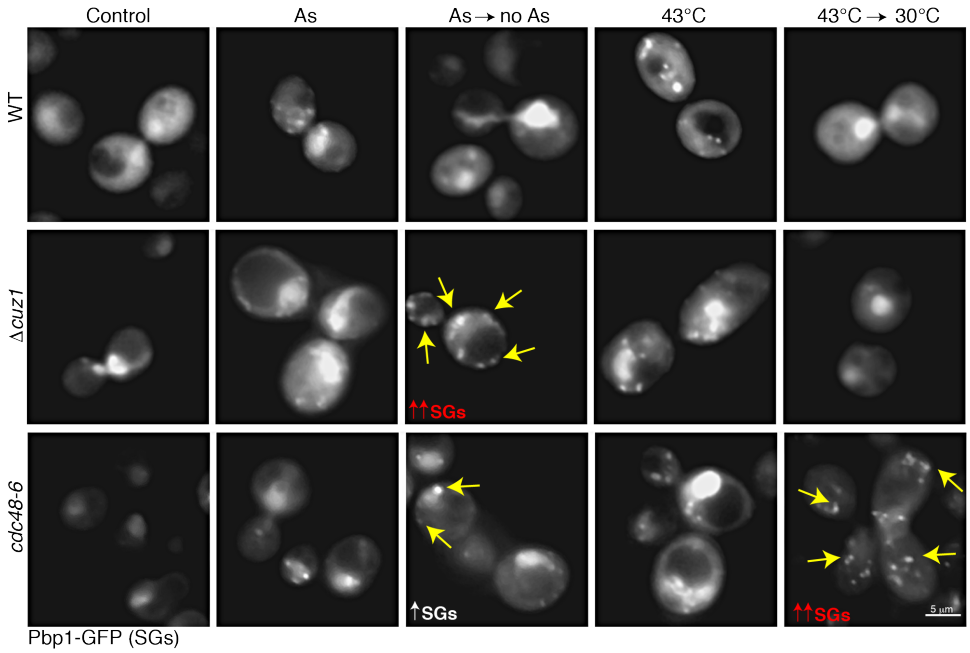


**Figure 15. The Δ*cuz1* null mutant is defective in clearance of arsenite-induced SGs.** Live cell fluorescence microscopy of exponentially growing wild type (WT), Δ*cuz1*, and *cdc48-6* cells expressing the SG marker Pbp1-GFP. Cells were treated with either 43 °C or 5 mM arsenite for 30 min. SGs were analyzed directly after stress treatment and 30 min after shifting the cells back to normal growth conditions.

Next, a complementation experiment was performed to rescue the impaired SG clearance observed in the Δ*cuz1* null mutant. A centromeric plasmid harboring the wild-type *CUZ1* gene was transformed into the Δ*cuz1* strain, whereas an empty vector was transformed as a negative control. Directly after arsenite stress, no significant increase in SG positive cells was observed in the Δ*cuz1* strain in comparison to wild type strain. On the other hand, during recovery, almost 35% of the Δ*cuz1* cells were found to contain SGs, in comparison to 12% of the wild-type cells, indicating a statistically significant defect in the clearance of the SGs. This impaired clearance of arsenite-induced SGs in Δ*cuz1* was rescued by the expression of wild-type *CUZ1* from a plasmid (Fig. 16a,b, middle and bottom row). Quantitation of the microscopy data showed that the expression of *CUZ1* in Δ*cuz1* cells reduced the number of cells exhibiting residual SGs after arsenite removal to the level of the wild type strain (~15% vs. 12% in wild-type) (Fig. 16b, top and bottom row). These results confirm that the observed phenotype of *Δcuz1* is specific to the lack of *CUZ1*, and provide formal proof for a role of Cuz1 in the clearance of arsenite-induced SGs. Importantly, this is the first description of a specific cellular function of Cuz1.

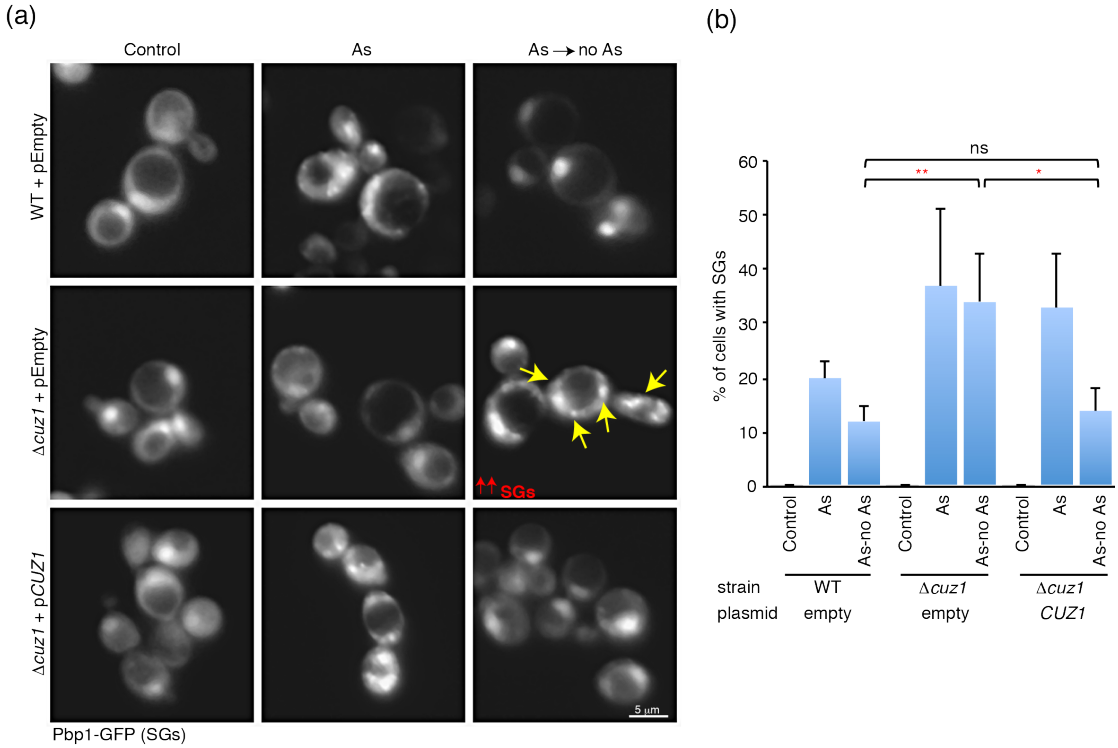


**Figure 16. Cuz1 is required for the efficient clearance of arsenite-induced SGs.** (a) Suppression of impaired SG recovery by *CUZ1*. *Δcuz1* cells were transformed with an either empty plasmid or with a centromeric plasmid encoding full-length *CUZ1*. Exponentially growing cells were treated with 5 mM arsenite, recovered for 30 min and analyzed as in Fig. 6. (b) Quantitation of the data from (a) showing the fraction of cells containing SGs. At least 100 cells per condition were analyzed. Mean values ± SEM are based on three replicate experiments *, $p<0.05$; **, $p<0.01$.

### 3.1.5 Partial co-localization of Cuz1 to SGs

In order to further investigate the role of Cuz1 in arsenite-induced SG clearance, the co-localization of Cuz1 with SGs was studied. A yeast strain expressing C-terminally GFP-tagged Cuz1 (Cuz1-GFP) was transformed with a plasmid encoding Pbp1-mCherry. In untreated control cells, Cuz1-GFP showed a diffuse cytoplasmic localization, whereas Pbp1-mCherry was mainly nuclear. By contrast, upon arsenite treatment, Cuz1-GFP formed distinct cytoplasmic foci. Importantly, many of these foci were either co-localizing with or in close proximity to the SG marker protein Pbp1-mCherry (Fig. 17). The observed partial localization of Cuz1 to SGs further confirms its involvement in SG dynamics.

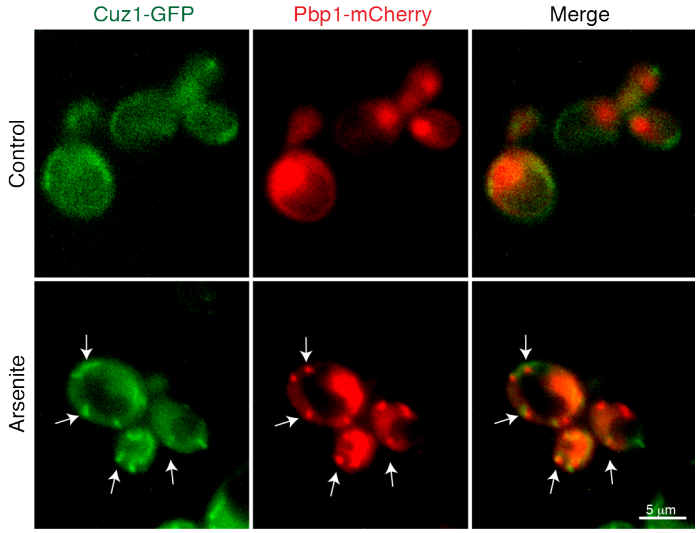


**Figure 17. Partial localization of Cuz1 to arsenite-induced SGs.** Live cell fluorescence microscopy of exponentially growing cells expressing C-terminal GFP-tagged Cuz1 (Cuz1-GFP) and Pbp1-mCherry. Cells were treated with 5 mM arsenite for 30 min.

## 3.2 ZFAND1

ZFAND1 is the hitherto uncharacterized human homolog of Cuz1 (Sa-Moura et al., 2013). Bioinformatic analyses (Kay Hofmann, University of Cologne, personal communication), identified ZFAND1 and Cuz1 as members of family of proteins characterized by the presence of an N-terminal domain containing AN1-type zinc fingers (AN1_ZF; Fig. 18), which also includes ZFAND2A/AIRAP and ZFAND2B/AIRAPL. It has been shown that ZFAND2A, ZFAND2B, and Cuz1 can interact with the 26S proteasome *via* their N-terminal AN1_ZF domain (Stanhill et al., 2006; Yun et al., 2008; Hanna et al., 2014; Sa-Moura et al., 2013). Interestingly, all of them possess a distinct C-terminal domain, possibly with distinct and specific functions.

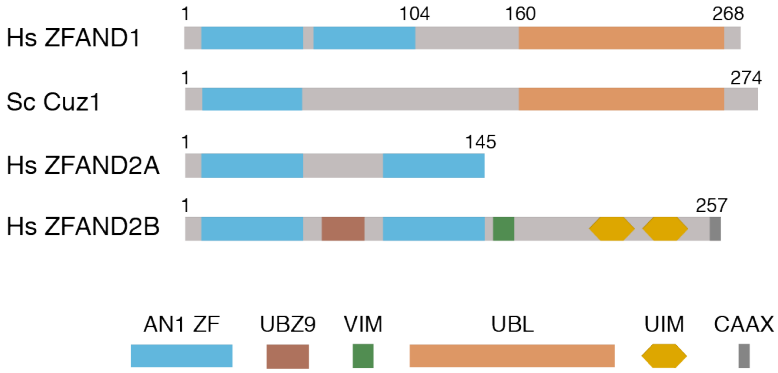


**Figure 18. The ZFAND protein family.** Schematic depicting the domain organization of human ZFAND1, its yeast homolog Cuz1, and the human relatives ZFAND2A and ZFAND2B. The key to the color-coded domains and sequence motifs is shown at the bottom: AN1_ZF, zinc finger of the AN1-type; VIM, VCP interacting motif; UIM, ubiquitin interacting motif; UBL, ubiquitin-like domain; UBZ9, UBZ9-like zinc finger; CAAX, prenylation motif.

### 3.2.1 Induction of ZFAND1 expression upon arsenite stress

Cuz1 expression was reported to be induced by arsenic treatment (Sa-Moura et al., 2013). In order to determine the effect of arsenite stress on the expression of ZFAND1, HeLa cells were treated with arsenite for up to 3 h. Interestingly, in the presence of arsenite, the level of ZFAND1 was found to increase by two-fold. In contrast, the expression of ZFAND2B remained constant or even slightly decreased upon arsenite treatment (Fig. 19), in agreement with a previous report (Yun et al., 2008). This result suggests the involvement of ZFAND1 in arsenite stress response.

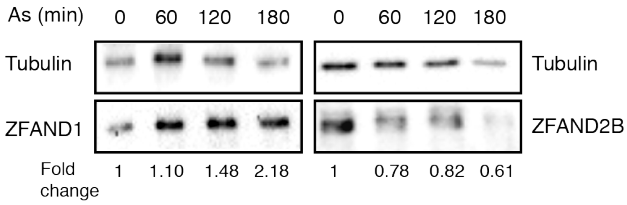


**Figure 19. ZFAND1 expression is induced upon arsenite treatment.** HeLa cells were treated with arsenite (0.5 mM) for the indicated time. Expression levels of ZFAND1 and ZFAND2B were analyzed using immunoblot analysis.

### 3.2.2 ZFAND1 interacts *via* its UBL domain with p97

ZFAND1, like its yeast homolog Cuz1, has a predicted C-terminal UBL domain (Fig. 18). For Cuz1, the UBL domain is required for Cdc48 binding both *in vitro* (Fig. 11c, Fig. 12) and *in vivo* (Sa-Moura et al., 2013). Surprisingly, in a GST-pulldown experiment, human ZFAND1, in contrast to its yeast homolog Cuz1, did not bind to p97 (Fig. 20).

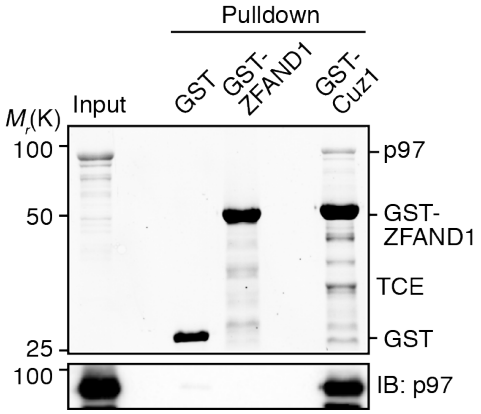


**Figure 20. Interaction between ZFAND1 and p97 *in vitro*.** Glutathione sepharose pulldown was performed using purified recombinant p97, GST, GST-ZFAND1, and GST-Cuz1. p97 binding to GST-ZFAND1 and GST-Cuz1 was analyzed by 2,2,2-trichloroethanol staining (TCE) and immunoblot (IB).

Moreover, immunoprecipitation experiments using HEK293T cells transfected with a plasmid encoding FLAG-ZFAND1 showed a very weak binding of ZFAND1 to p97 (data not shown), indicating a transient interaction. In order to obtain more robust evidence for an interaction between ZFAND1 and p97, immunoprecipitation experiments were performed with HEK293T cells co-transfected with either an empty plasmid (control) or a plasmid encoding FLAG-ZFAND1, and an ATPase-deficient trapping mutant of p97 (p97-E578Q), in order to stabilize cofactor-binding. Using this approach, an interaction of ZFAND1 with p97 was detected specifically in arsenite-treated cells, but not in untreated cells (Fig. 21a). In order to further confirm this interaction, in-cell crosslinking was performed using dithiobis[succinimidyl propionate] to stabilize p97-cofactor interactions (Xue et al., 2016). This crosslinking approach showed a binding of endogenous ZFAND1 to p97, which was also resistant to RNase treatment, indicating that the interaction resulted from protein-protein contacts (Fig. 21b).

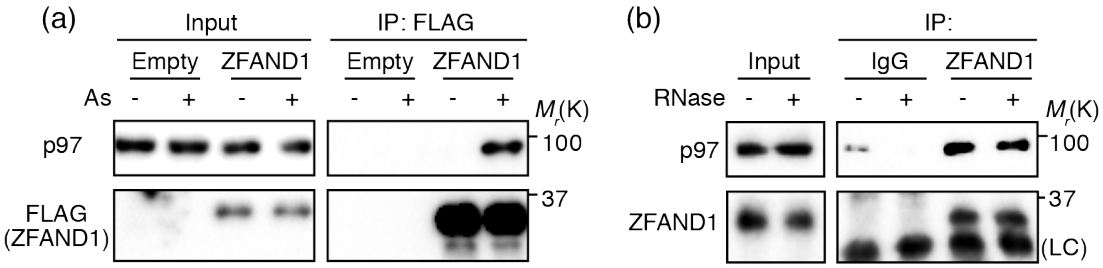


**Figure 21. ZFAND1 interacts with p97 in an arsenite dependent manner.** (a) Arsenite-dependent binding to p97. HEK293T cells were co-transfected with plasmids encoding p97-E578Q and either FLAG-ZFAND1 or empty plasmid. Cells were then treated with arsenite (0.5 mM) for 1 h, where indicated. Lysates were subjected to anti-FLAG immunoprecipitation (IP). Input and IP samples were immunoblotted for p97 and FLAG. (b) HEK293T cells were treated with arsenite (0.5 mM) for 1 h, and then subjected to crosslinking using 0.8 mM DSP (30 min, RT). Lysates were incubated with 100 µg/ml RNase A (30 min, RT) as indicated and then subjected to IP using a ZFAND1-specific antibody or unspecific IgGs.. Input and IP samples were analyzed for p97 and ZFAND1 using immunoblot. LC, antibody light chain (Experiment was performed by Susanne Meyer).

In order to determine the domain of ZFAND1 that binds to p97, a co-immunoprecipitation experiment was performed using two ZFAND1 variants, one lacking the C-terminal UBL domain, and the other lacking functional zinc fingers. The ZFAND1 variant lacking functional zinc fingers was generated by mutating zinc coordinating cysteine residues by site-directed mutagenesis. In the co-immunoprecipitation experiment, the variant lacking the functional zinc finger was able to bind p97, while the UBL deletion variant was not (Fig. 22).

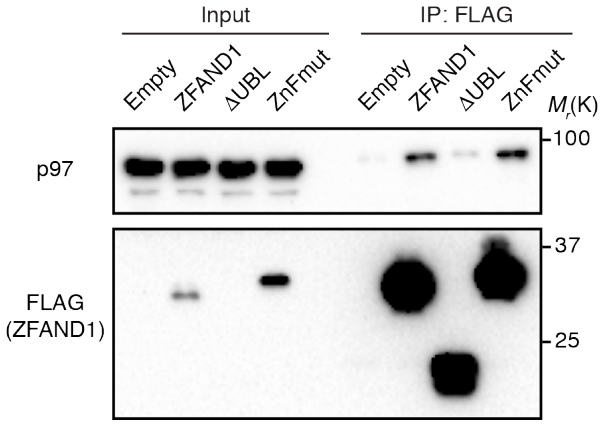


**Figure 22. ZFAND1 interacts *via* its UBL domain with p97.** UBL-dependent binding to p97. HEK293T cells were co-transfected with plasmids encoding p97-E578Q and the indicated FLAG-ZFAND1 variants or empty plasmid. Cells were then treated with arsenite (0.5 mM) for 1 h. Lysates were subjected to anti-FLAG immunoprecipitation (IP). Input and IP samples were immunoblotted for p97 and FLAG. Note: the expression of the ΔUBL variant was too low to be detected in the input (Experiment was performed by Susanne Meyer).

Collectively, these co-immunoprecipitation experiments revealed an arsenite-dependent binding of ZFAND1 to p97 that is mediated by the UBL domain of ZFAND1, like its yeast homolog Cuz1.

### 3.2.3 ZFAND1 binds to the 26S proteasome

A previous study reported that Cuz1 interacts with the proteasome (Sa-Moura et al., 2013). Apart from that, both ZFAND2A and ZFAND2B also have been shown to bind to the proteasome *via* its AN1-type zinc finger domain, where it overcomes arsenite-induced impairment effect on the 26S proteasome (Stanhill et al., 2006).

In order to analyze proteasome binding of ZFAND1, an *in vitro* pulldown experiment was performed using human 26S proteasome and purified recombinant GST-ZFAND1. In line with the previously characterized interaction of Cuz1 with the yeast 26S proteasome (Sa-Moura et al., 2013; Hanna et al., 2014), the interaction of ZFAND1 to both 19S and 20S subunit of the 26S proteasome was detected (Fig. 23). This experiment clearly indicates a direct interaction between ZFAND1 and the 26S proteasome. Importantly, these results for the first time revealed an ATP-depletion dependent binding of ZFAND1 to proteasome.

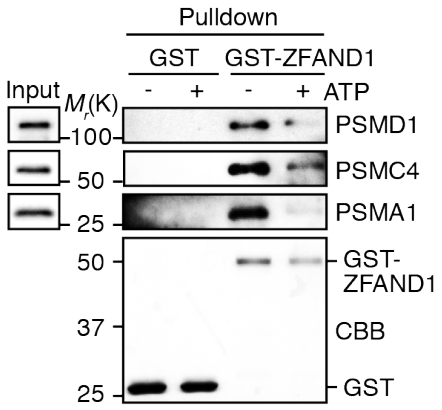


**Figure 23. Interaction between ZFAND1 and the 26S proteasome *in vitro*.** Glutathione sepharose pulldown was performed by incubating the recombinantly purified GST-ZFAND1 with the human 26S proteasome in the absence and presence of 5 mM ATP. 19S subunits PSMD1 and PSMC4, and the 20S subunit PSMA1 were analyzed by immunoblotting. Immobilized GST and GST-ZFAND1 were detected by Coomassie staining (CBB).

To investigate the binding of ZFAND1 to the 26S proteasome in cells, co-immunoprecipitation experiments were performed using a HEK293T cell line transfected with a plasmid encoding C-terminally FLAG epitope-tagged ZFAND1 (ZFAND1-FLAG). Indeed, interaction between ZFAND1 and the 19S proteasome subunit

(PSMD1) was observed. This binding was only observed when the cell lysate was ATP depleted using hexokinase and glucose, and was reduced significantly upon addition of ATP to the lysate (Fig. 24a), consistent with the result *in vitro* (Fig. 23).

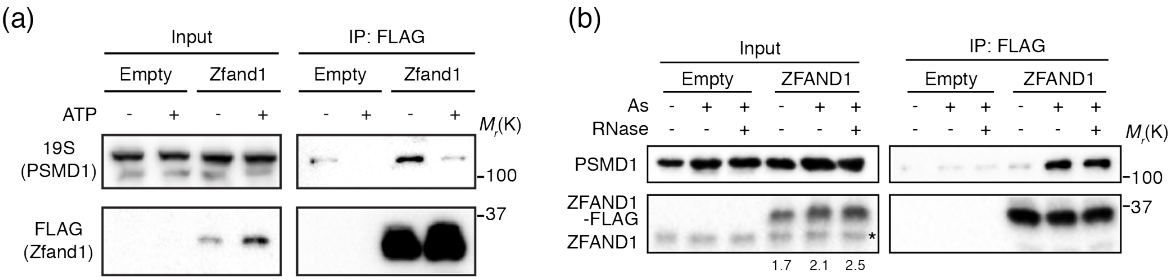


**Figure 24. Interaction between ZFAND1 and the proteasome *in vivo*.** Binding to the 19S proteasome. (a) HEK293T cells transfected with either plasmid encoding ZFAND1-FLAG or empty plasmid. Lysates were depleted of ATP by addition of hexokinase and glucose for 15 min and subjected to FLAG-IP. Input and IP samples were immunoblotted for the 19S subunit PSMD1 and FLAG. (b) HEK293 Flp-In T-REx cells stably expressing ZFAND1-FLAG were induced using tetracycline (10 ng/ml) for 24 h. Cells were then treated with arsenite (0.5 mM) for 1 h, where indicated. Lysates were subjected to FLAG-IP after ATP depletion as in (a). Input and IP samples were immunoblotted for the 19S subunit PSMD1 and ZFAND1.

To confirm this interaction at more physiological expression levels, co-immunoprecipitation was performed using a stable HEK293 cell line expressing C-terminally FLAG epitope-tagged ZFAND1. Low concentration of tetracycline was used to express ZFAND1-FLAG at close to endogenous level, and lysates were depleted for ATP. Using this approach, binding of ZFAND1 to the 19S proteasome subunit PSMD1 was detected (Fig. 24b). Similar to p97 binding, this interaction was significantly strengthened upon arsenite treatment and resistant to RNase treatment.

In order to identify the domain of ZFAND1 responsible for proteasome binding, a co-immunoprecipitation was performed using arsenite-treated HEK293T cells transfected with a plasmid encoding either C-terminally FLAG epitope-tagged wild-type or AN1_ZF mutant variant of ZFAND1 (ZFAND1 ZnFmut-FLAG), or empty vector. The ZFAND1 construct lacking the functional AN1_ZF domain showed strongly reduced proteasome binding (Fig. 25).

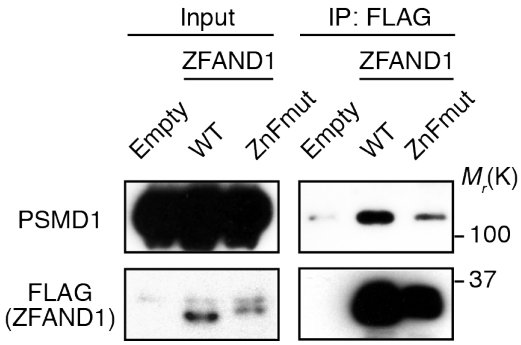


**Figure 25. ZFAND1 interacts *via* its AN1_ZF domain to the proteasome.** Lysates of HEK293T cells transfected with plasmids encoding the indicated ZFAND1-FLAG variants were arsenite-treated, ATP depleted and subjected to FLAG-IP as in (Fig. 25a). Inputs and IP samples were immunoblotted for the 19S subunit PSMD1 and FLAG.

### 3.2.4 Proteomic study of ZFAND1 binding proteins

In order to identify the ZFAND1 interactome and to obtain a more complete picture of the interaction between ZFAND1 and the 26S proteasome, affinity purification and mass spectrometry analysis was performed. For this, a stable HEK293 cell line expressing C-terminally FLAG epitope-tagged ZFAND1 (ZFAND1-FLAG) was used. Intriguingly, the mass spectrometry analysis revealed a strong enrichment of all subunits of the 19S proteasome (Fig. 26; https://chorusproject.org/; project ID 1382).

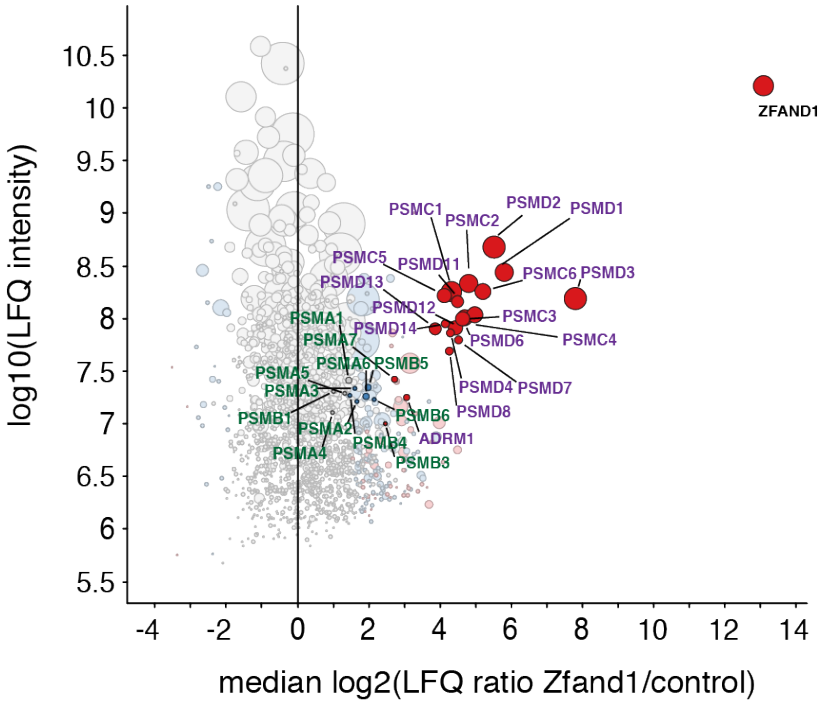


**Figure 26. Mass spectrometric analysis for ZFAND1 binding proteins.** Identification of proteins interacting specifically with ZFAND1 by Co-IP and quantitative mass spectrometry. Median values calculated from triplicate experiments were plotted. The 19S and 20S proteasomal subunits are labeled in magenta and green, respectively.

Again, these interactions were ATP depletion-dependent (data not shown). In addition, many 20S proteasome subunits were detected, but not as strongly enriched as 19S subunits. Together, these data strongly indicate that ZFAND1 is an interactor of the intact 26S proteasome.

### 3.2.5 Function of ZFAND1 in SG clearance

#### 3.2.5.1 ZFAND1 associates with SGs upon arsenite stress

The cellular function of ZFAND1 is uncharacterized till date. The yeast homolog of ZFAND1, Cuz1, is required for efficient clearance of SG clearance (Fig. 16). To test a potential SG localization of ZFAND1, immunofluorescence (IF) experiments were performed using HeLa cells. TIA-1, which is known to accumulate in SGs upon various stress conditions (Kedersha et al., 1999), was used as a SG marker protein. Under control conditions, a diffuse signal of ZFAND1 was found in the cytoplasm (Fig. 27, top row). Interestingly, an accumulation of ZFAND1 at TIA-1 positive speckles was observed upon arsenite stress (Fig. 27, middle row). By contrast, no co-localization of ZFAND1 was observed with heat-induced SGs, indicating an arsenite-specific role of ZFAND1 (Fig. 27, bottom row).

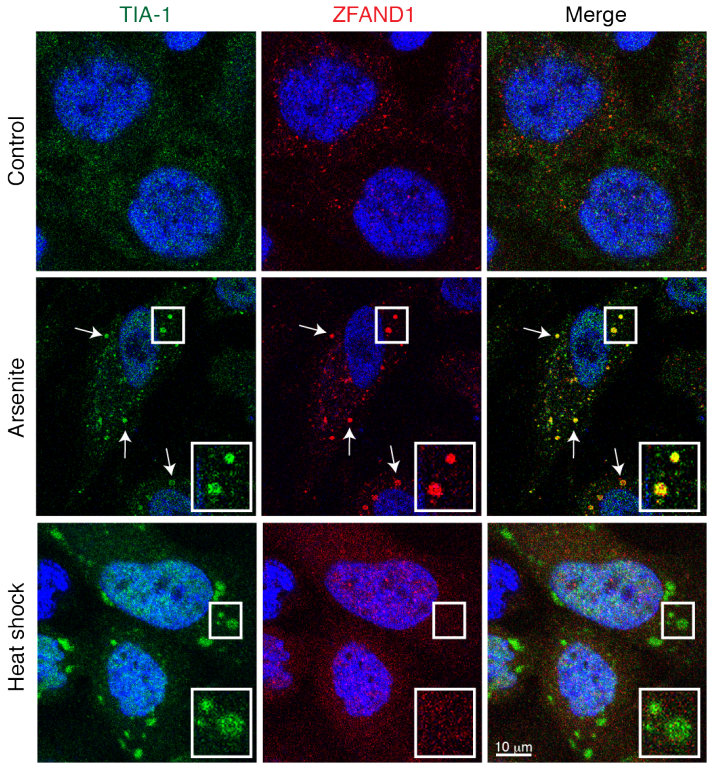


**Figure 27. ZFAND1 associates with arsenite-induced SGs.** HeLa cells were subjected to either arsenite treatment (0.5 mM) for 1 h or heat shock (43 °C) for 2 h. Confocal microscopy was performed to visualize the localization of endogenous TIA-1 and ZFAND1. Representative co-localized foci are marked by arrows or magnified in the inset (2x zoom).

In order to exclude the possibility of non-specific staining by the ZFAND1 antibody, a HeLa Flp-In T-Rex cell line stably expressing FLAG-ZFAND1 was used. Expression of ZFAND1 was induced using tetracycline, and an IF was performed using an anti-FLAG antibody. A strong co-localization of ZFAND1 with TIA-1 was observed under arsenite stress, which was also confirmed in IFs of G3BP1, a cytoplasmic protein that is known to accumulate in SGs upon various stress conditions (Fig. 28a,b, bottom rows). This result shows an association of ZFAND1 with SGs that is specific to arsenite stress.

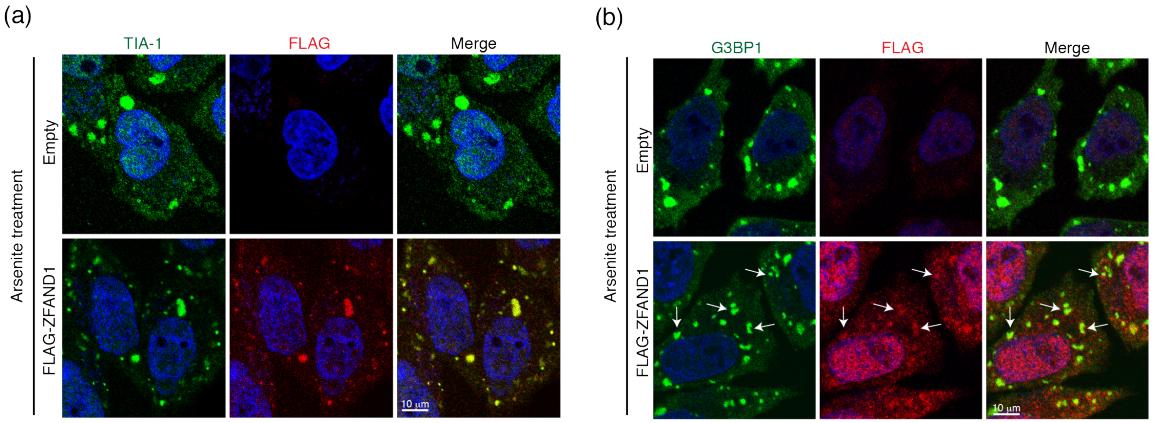


**Figure 28. Co-localization of ZFAND1 to arsenite-induced SGs.** (a) HeLa Flp-In T-REx cells were induced to express FLAG-ZFAND1 using tetracycline (1 µg/ml, 24 h) and subjected to arsenite treatment (0.5 mM) for 1 h. Confocal microscopy was performed to visualize the localization of FLAG-ZFAND1 and endogenous TIA-1. (b) Same as in (a) except localization of G3BP1 was analyzed instead of TIA-1.

In order to determine which domain of ZFAND1 mediates the assocation with SGs, HeLa ZFAND1 knockout cells (Source: Dr. Gabriella Marincola, Buchberger lab) generated by CRISPR/Cas9-mediated genome editing were used. We ectopically expressed wild-type and mutant ZFAND1 variants in ZFAND1 knockout HeLa cells (Fig. 29a,b). Whereas ZFAND1-ZnFmut exhibited the same strong association with arsenite-induced SGs as wild-type ZFAND1, the p97 binding deficient ZFAND1-ΔUBL variant did not localize to SGs (Fig. 29), suggesting that the UBL domain mediates association of ZFAND1 to SGs.

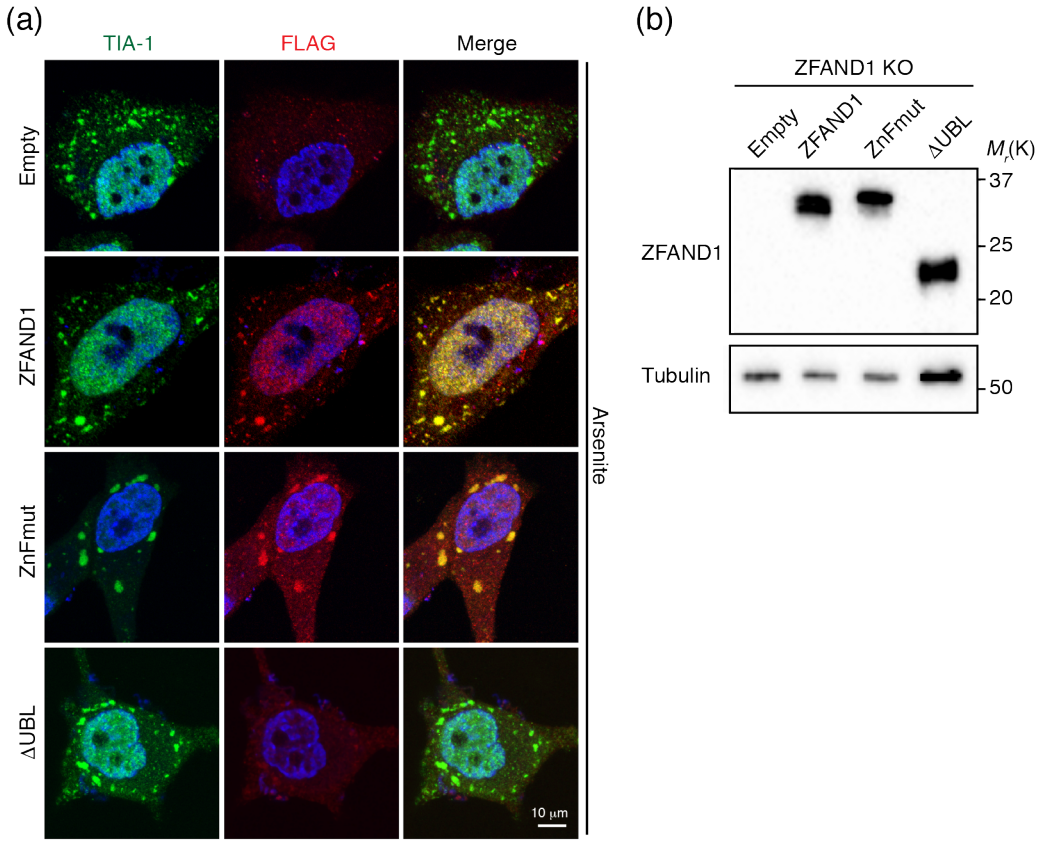


**Figure 29. The UBL domain-dependent association of ZFAND1 to SGs.** (a) ZFAND1 KO HeLa cells ectopically expressing the indicated FLAG-ZFAND1 variants were analyzed as in (Fig. 28). (b) Immunoblot showing FLAG-ZFAND1 protein levels in cells from (a).

### 3.2.5.2 ZFAND1 is required for the clearance of arsenite-induced SGs

The association of ZFAND1 with SGs and a role of its yeast homolog Cuz1 in the clearance of arsenite-induced SG suggested a possibility of an evolutionarily conserved function in SG clearance.

In order to get insight into the role of ZFAND1 in SG dynamics, HeLa cells were treated with siRNA against ZFAND1 or luciferase (used as a control) and subjected to arsenite stress. SG formation was observed using FMRP as an SG marker protein (Fig. 30a). FMRP has been shown to translocate to SGs upon several stress conditions. A robust formation of FMRP-positive SGs was observed in both control- and ZFAND1-depleted HeLa cells upon arsenite stress (Fig. 30a, middle column). Importantly, when shifted back to the normal growth condition for recovery after arsenite removal, ZFAND1-depleted cells, unlike control-depleted cells, were unable to efficiently clear arsenite-induced SGs (Fig. 30a). Quantitation of the microscopy data showed a statistically significant effect, with ZFAND1-depleted cells possessing much more SGs than control-depleted cells (50% compared to 14%) (Fig. 30b). This observed defect in the clearance of arsenite-induced

SGs in ZFAND1-depleted HeLa cells, along with the function of its yeast homolog Cuz1 (Fig. 15,16), demonstrates an evolutionarily conserved function of ZFAND1.

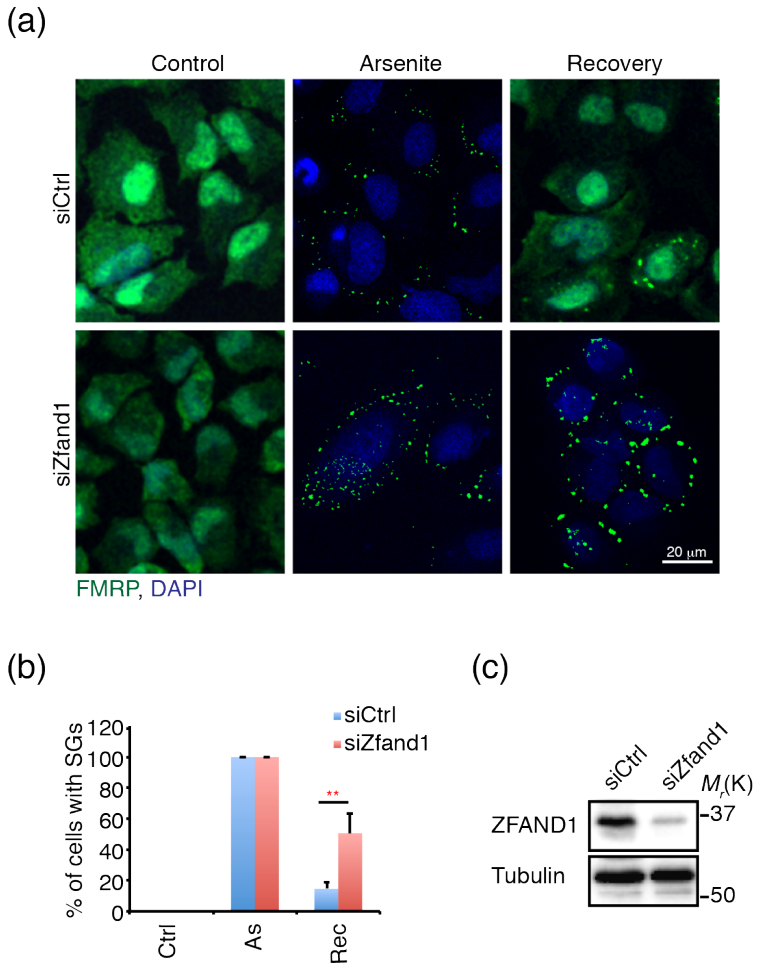


**Figure 30. ZFAND1 is required for the clearance of arsenite-induced SGs**. (a) HeLa cells were transfected with the indicated siRNAs for 48 h. Cells were then subjected to arsenite treatment (0.5 mM) for 1 h, and allowed to recover for 2 h. Confocal microscopy was performed to visualize FMRP. (b) Quantitation of cells with SGs in (a); mean ± SD; n = 3 with ≥ 100 cells per condition; **p < 0.01. (c) Depletion of ZFAND1 in cells from (a) was confirmed using immunoblot analysis.

ZFAND1 knockout cells were used in order to further confirm the observed results (Fig 31a). All three ZFAND1 KO clones exhibited a highly significant SG clearance defect, which was even stronger than that of siRNA-depleted cells for two of the three clones (Fig 31b,c). This confirms a specific role of ZFAND1 in SG clearance.

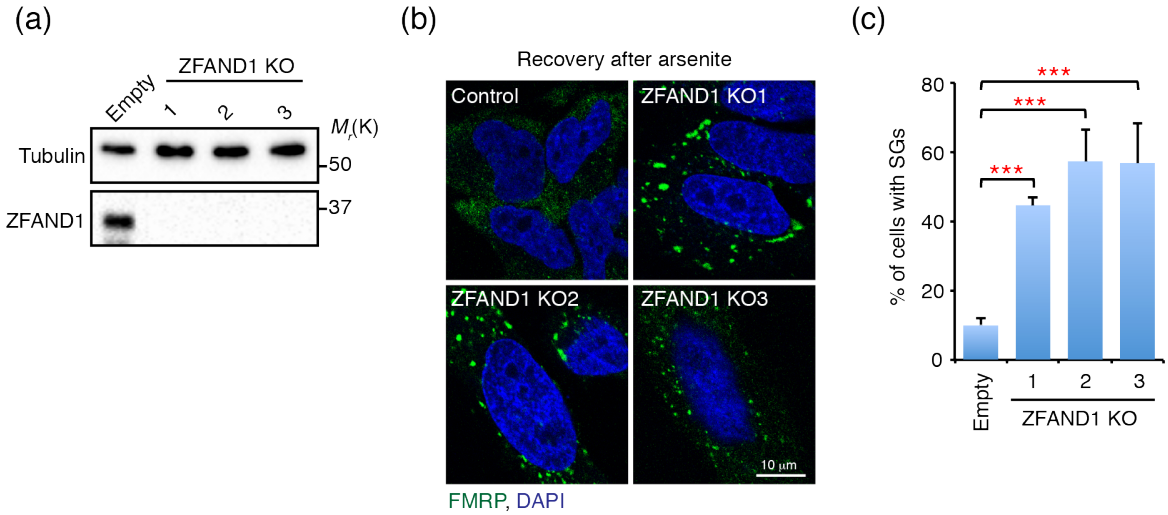


**Figure 31. Validation of SG clearance defect using *ZFAND1* knockout clones.** (a) Lack of ZFAND1 in the KO HeLa clones was confirmed using immunoblot analysis. (b) Three Zfand1 knockout (KO) and one control HeLa clones were subjected to arsenite treatment (0.5 mM) for 1 h, and recovered for 2 h. Confocal microscopy was performed to visualize FMRP. (c) Quantitation of cells with SGs in (b).

### 3.2.5.3 ZFAND1 has a conserved and specific function in SG clearance

In order to rescue the impairment in SG clearance observed upon ZFAND1 depletion, a complementation experiment was performed. ZFAND1-depleted HeLa cells co-transfected with a plasmid encoding the wild-type *ZFAND1* gene reduced the number of SG-positive cells to the level of the control-depleted cells (~20% vs. 22% SG-positive cells) (Fig. 32a,b).

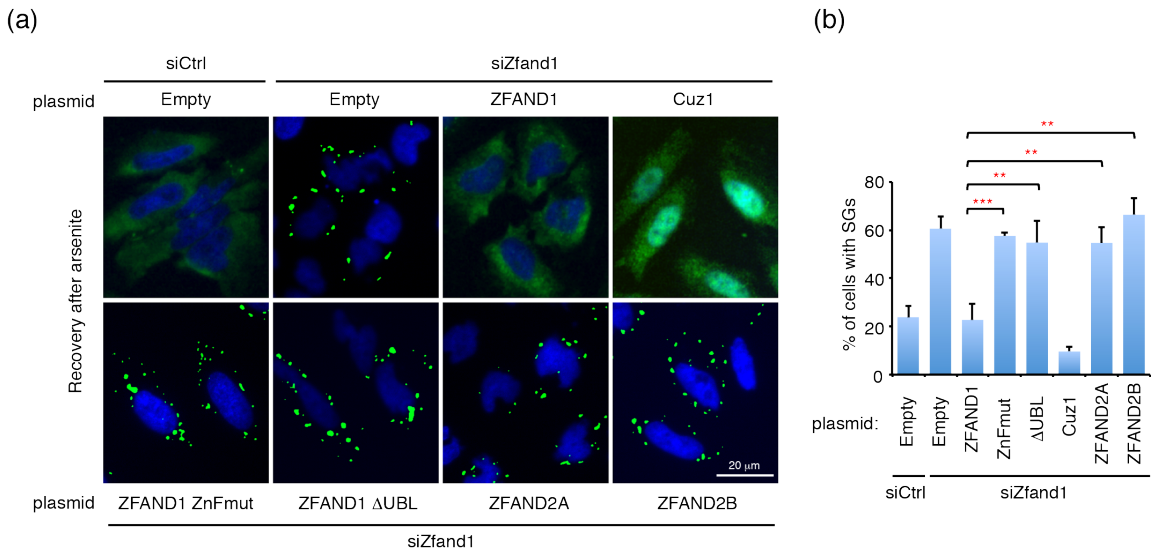


**Figure 32. Specific and conserved function of ZFAND1 in arsenite-induced SG clearance.** (a) HeLa cells were co-transfected for 48 h with the indicated siRNAs and plasmids encoding ZFAND1, FLAG-Cuz1, ZFAND1 ZnFmut, FLAG-ZFAND1ΔUBL, ZFAND2A or FLAG-ZFAND2B. Cells were then subjected to arsenite treatment (0.5 mM) for 1 h, and recovered for 2 h. Confocal microscopy was performed to visualize FMRP. (b) Quantitation showing cells with SGs in (a).

More importantly, a similar suppression was observed when ZFAND1-depleted cells were complemented with a plasmid encoding the wild-type yeast *CUZ1* gene (Fig. 32a,b). In contrast, no rescue was observed using a plasmid encoding wild-type *ZFAND2A* or *ZFAND2B*, which suggests that *ZFAND1* has a function distinct from other AN1_ZF family members (Fig. 32a,b).

In order to investigate the domain of ZFAND1 responsible for its role in SG clearance, a complementation experiment was performed, where ZFAND1-depleted cells were transfected with variants of ZFAND1, either lacking functional zinc fingers or lacking the C-terminal UBL domain. Neither of these constructs was able to rescue the impaired SG clearance (Fig. 32a,b).

Together, these complementation experiments reveal an evolutionarily conserved and specific function of ZFAND1 in SG clearance, which is mediated *via* both domains of ZFAND1, the zinc fingers and the UBL domain.

To investigate if the function of ZFAND1 in SG clearance is specific to arsenite stress, various other stress conditions were tested, including heat shock (43 °C, 2 h) (Fig. 33a,b), treatment with 0.6 M sorbitol or with 2 mM hydrogen peroxide (Fig. 33c,d). Intriguingly, however, no defect in SG clearance was observed under any of these conditions. This result indicates that a function of ZFAND1 in SG clearance is specific to arsenite stress, and not required under other stress conditions.

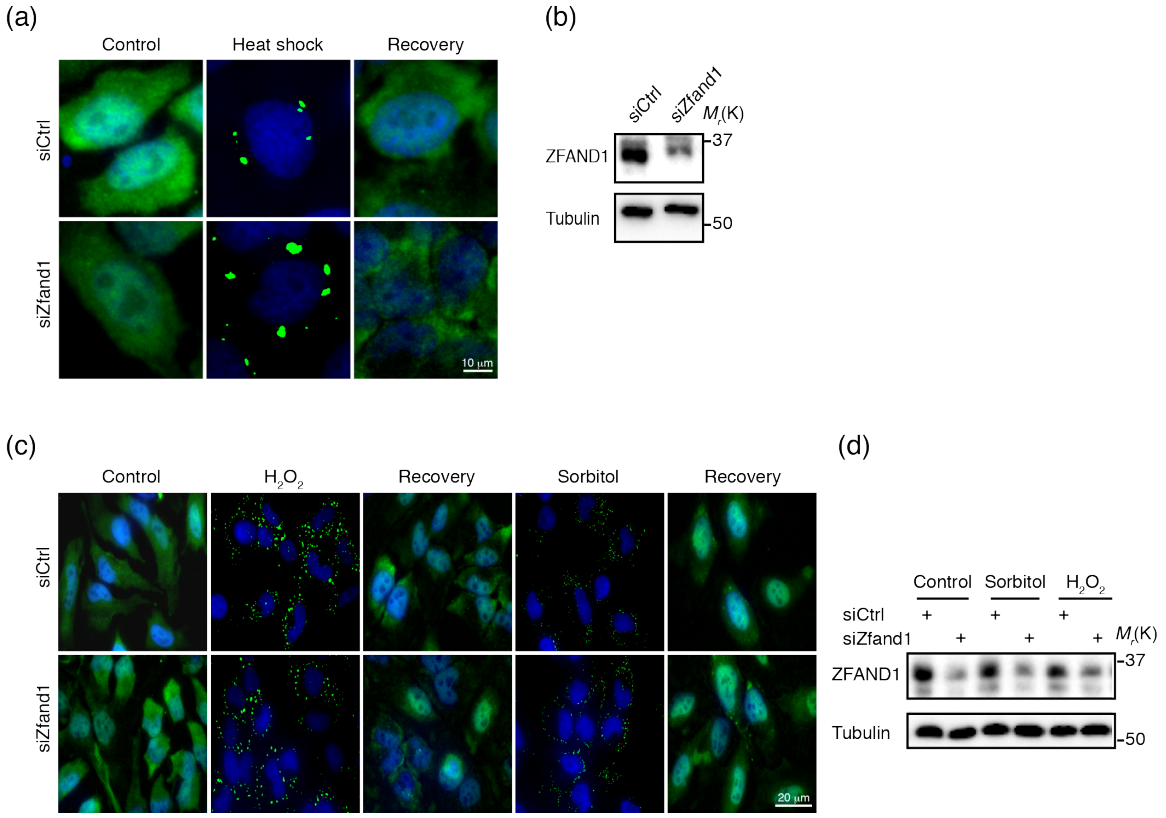


**Figure 33. No role of ZFAND1 in heat-, sorbitol-, and $H_2O_2$-induced SG clearance.** (a) HeLa cells were transfected with the indicated siRNAs targeting either ZFAND1 (siZFAND1) or control (siCtrl) for 48 h. Cells were then subjected to heat shock (43 °C) for 2 h, and allowed to recover for 2 h. Confocal microscopy was performed to visualize FMRP. (b) Depletion of ZFAND1 in cells from (a) was confirmed using immunoblot analysis. (c) Same as in (a) except cells were treated with either $H_2O_2$ (2 mM, 1 h) or sorbitol (0.6 M, 1 h), and allowed to recover for 2 h. (d) Depletion of ZFAND1 in cells from (c) was confirmed using immunoblot analysis.

The AN1_ZF family member ZFAND2B has been shown to interact with both, the 26S proteasome *via* its AN1_ZF domain, and p97 *via* its VIM motif (Yun et al., 2008; Glinka et al., 2013) (Fig. 18). This binding pattern of ZFAND2B prompted us to test if ZFAND2B has a similar function in SG clearance as ZFAND1. HeLa cells were depleted for ZFAND2B using a specific siRNA, and an IF experiment was performed to study the formation and clearance of SG. Interestingly, no defect either in the formation or in the clearance of SGs was observed upon ZFAND2B depletion (Fig. 34a), which is in line with the observed rescue defect in Fig. 32. This result implies that ZFAND1, among other AN1_ZF family members, has a specific role in the clearance of arsenite-induced SGs.

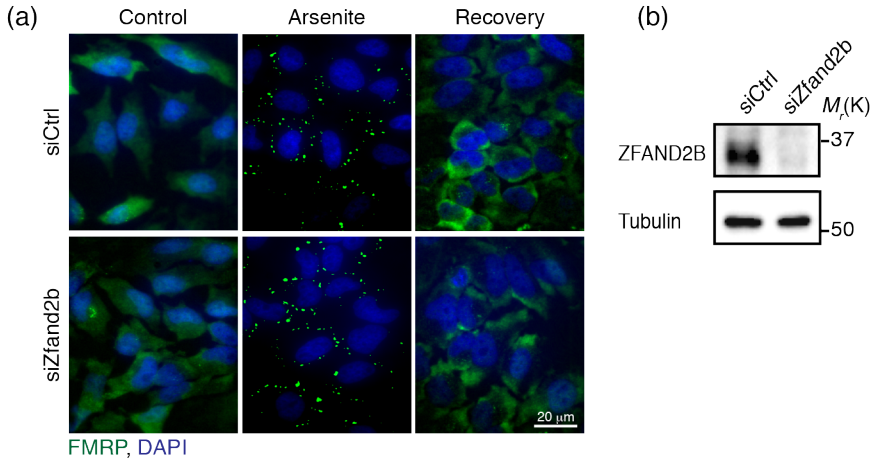


**Figure 34. ZFAND2B is not required for arsenite-induced SG clearance.** (a) HeLa cells were treated with either control siRNA or ZFAND2B siRNA for 48 h. Cells were then subjected to arsenite treatment (0.5 mM) for 1 h, and allowed to recover for 2 h. Confocal microscopy was performed to visualize FMRP. (b) Depletion of ZFAND2B in cells from (a) was confirmed using immunoblot analysis.

#### 3.2.5.4 ZFAND1 mediates the recruitment of p97 and the 26S proteasome

ZFAND1 interacts with p97 (Fig. 22) and with the proteasome in a UBL- and AN1_ZF domain-dependent manner, respectively (Fig. 25). In order to get detailed insight into the molecular mechanism behind the cellular function of ZFAND1 in SG clearance, an IF was performed to analyze if ZFAND1-positive SGs also contain p97 and/or the 26S proteasome.

HeLa cells were treated with either siZFAND1 or siCtrl. After arsenite treatment, an IF was performed in order to analyze the localization of ZFAND1, p97, and the 26S proteasome. Co-localization of ZFAND1 with p97 at SGs in siCtrl treated HeLa cells was observed (Fig. 35a, top row). Interestingly, in ZFAND1-depleted HeLa cells, a diffuse signal of p97 was observed. No co-localization of p97 to SGs was observed under this condition (Fig. 35a, bottom row).

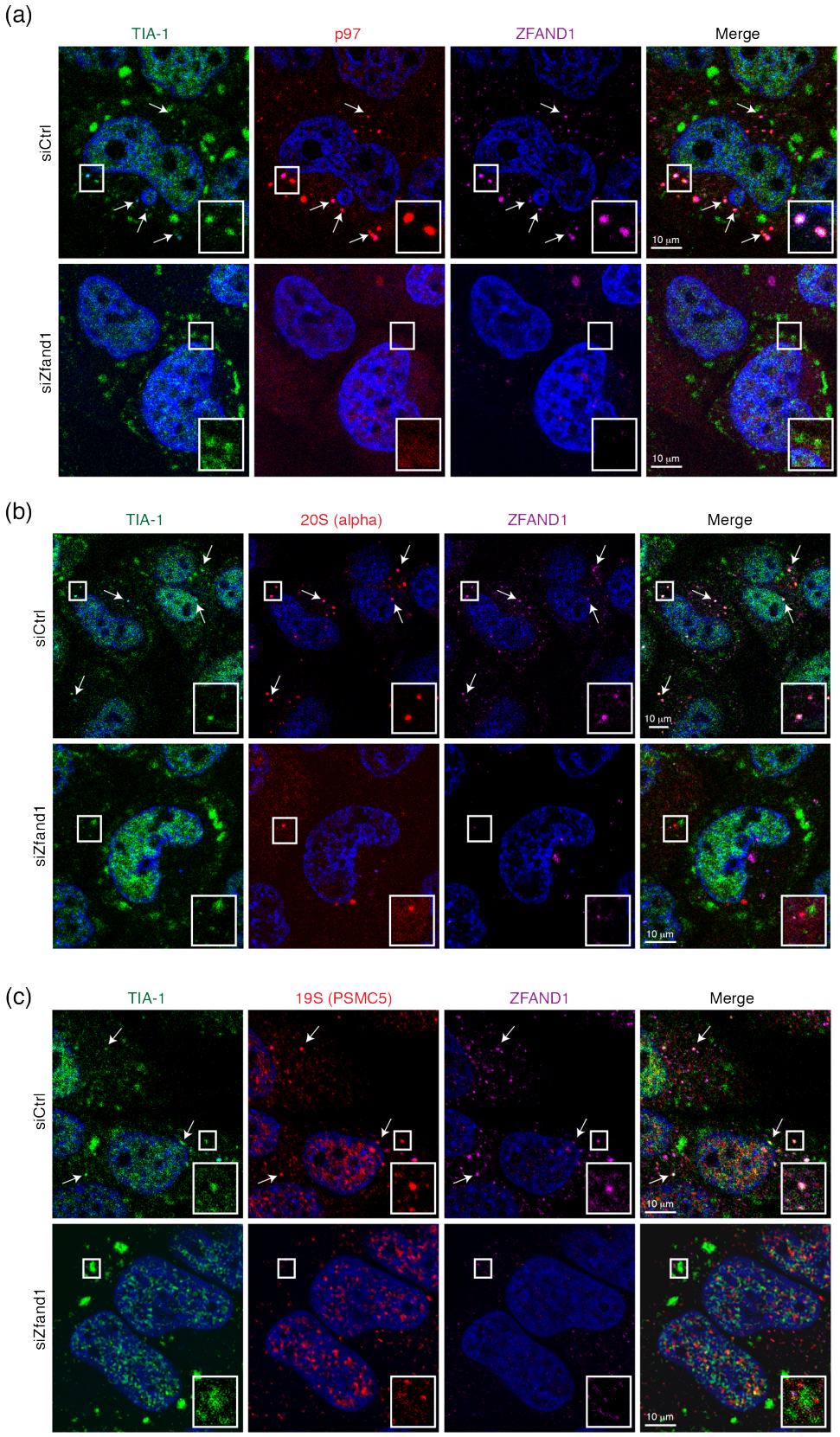


**Figure 35. ZFAND1 mediates the recruitment of p97 to arsenite-induced SGs.** HeLa cells transfected with the indicated siRNA for 48 h were subjected to arsenite treatment (0.5 mM) for 1 h. Confocal microscopy was performed to visualize the localization of endogenous TIA-1, ZFAND1 and either (a) p97, (b) 20S alpha subunits or (c) PSMC5. Representative co-localized foci are marked by arrows or magnified in the inset (2x zoom).

A similar result was observed in IFs performed with either anti-19S proteasome (PSMC5 subunit) or with anti-20S proteasome (alpha subunits) antibodies (Fig. 35b,c). The localization of p97 and the 26S proteasome to SGs in a ZFAND1-dependent manner strongly indicates a role of ZFAND1 as an adaptor or a recruitment factor for targeting both, p97 and the 26S proteasome to SGs.

It has been shown previously that p97 co-localizes with SGs generated during various different stress conditions including heat shock, arsenite, sorbitol and clotrimazole stress (Buchan et al., 2013). In order to understand if the role of ZFAND1 in p97 recruitment is specific to arsenite, the localization of p97 to heat-induced SGs in ZFAND1-depleted cells was analyzed. Localization of p97 to heat-induced SGs was observed (Fig. 36a, top row), in line with a previous report (Buchan et al., 2013). Interestingly, no difference in the localization of p97 to heat-induced SGs, in contrast to arsenite-treated cells, was observed in ZFAND1-depleted cells (Fig. 36a, bottom row). Importantly, this observation implies that ZFAND1 acts as a recruitment factor for p97 in an arsenite-dependent manner.

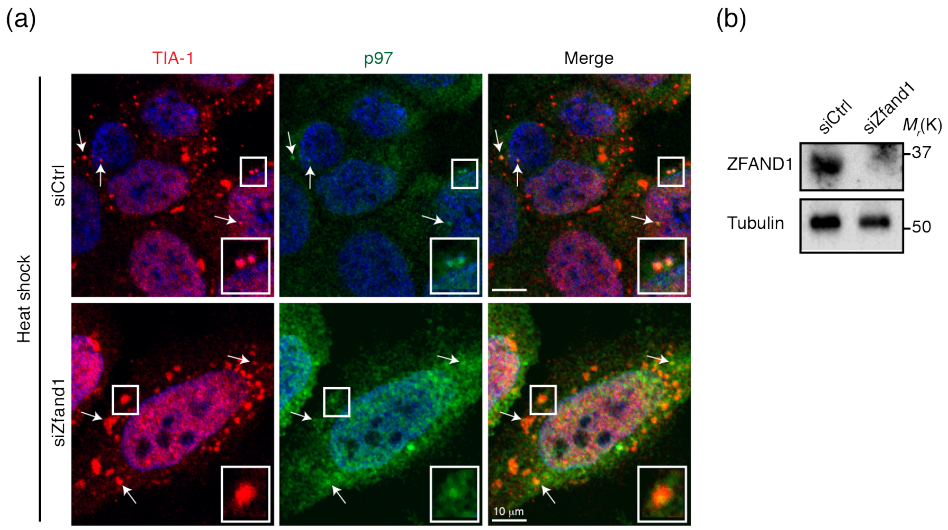


**Figure 36. ZFAND1 independent recruitment of p97 to heat-induced SGs.** (a) HeLa cells treated with indicated siRNA targeting either ZFAND1 (siZFAND1) or control (siCtrl) for 48 h, were subjected to heat shock (43 °C) for 2 h. Confocal microscopy was performed to visualize endogenous TIA-1 and p97. (b) Depletion of ZFAND1 in cells from (a) was confirmed using immunoblot analysis.

To map the domains of ZFAND1 that mediate the SG recruitment of p97 and the 26S proteasome, respectively, we analyzed their localization in ZFAND1 knockout HeLa cells ectopically expressing wild-type and mutant ZFAND1 (Fig. 37). Whereas wild-type ZFAND1 was proficient in the recruitment of both p97 and the proteasome to SGs,

ZFAND1-ZnFmut mediated the recruitment of p97, but not the proteasome, consistent with the immunoprecipitation data (Fig. 25). Importantly, the ZFAND1-ΔUBL variant unable to associate with SGs (Fig. 29) was unable to recruit either p97 or the 26S proteasome, as expected (Fig. 37). These data confirm that the ZFAND1-mediated recruitment of the 26S proteasome to arsenite-induced SGs is required for their efficient clearance. They also show that p97 recruitment to SGs is necessary, but not sufficient for normal clearance.

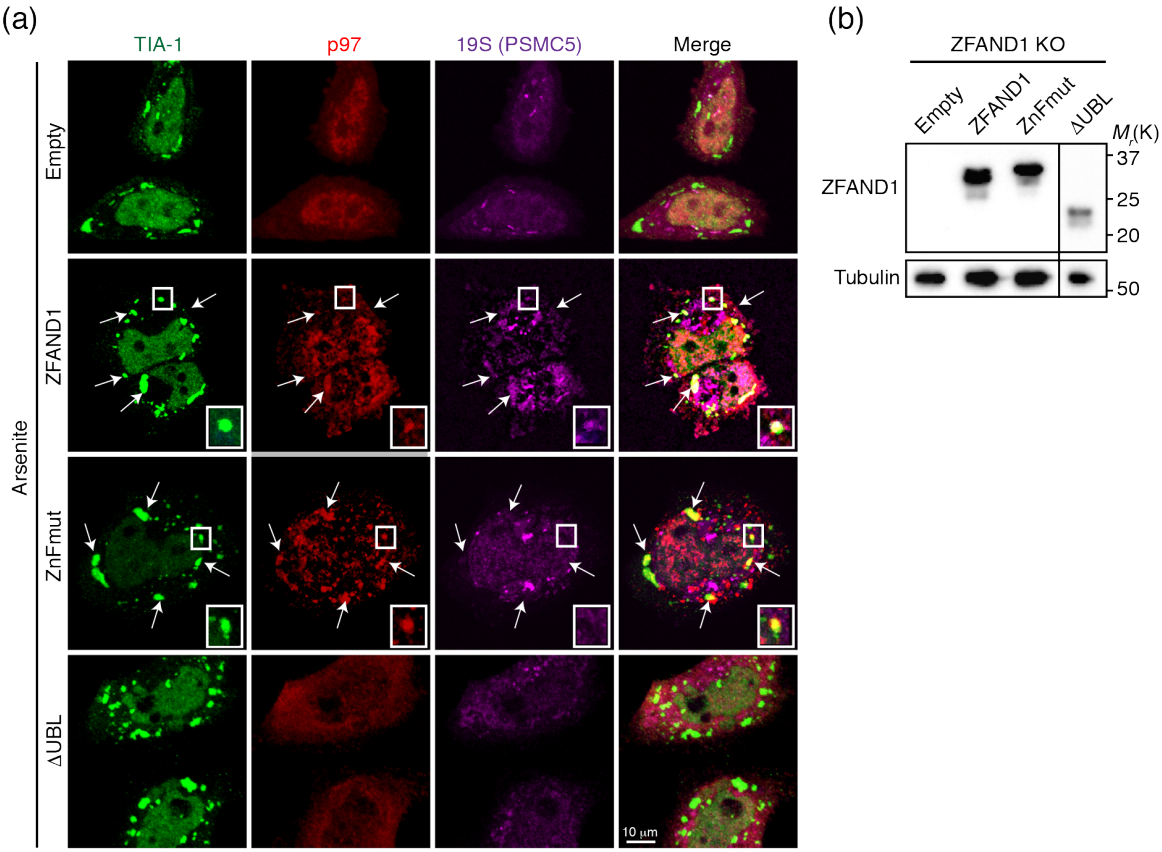


**Figure 37. ZFAND1-mediated recruitment of p97 and the 26S proteasome to SGs.** (a) ZFAND1 KO HeLa cells ectopically expressing the indicated FLAG-ZFAND1 variants were subjected to arsenite treatment (0.5 mM, 1 h). Endogenous TIA-1, p97 and the 19S subunit PSMC5 were visualized by confocal microscopy. Representative p97- and 19S-positive SGs are marked by arrows or magnified in the inset (2x zoom). (b) Immunoblot showing FLAG-ZFAND1 protein levels in cells from (a). The vertical line indicates that an irrelevant lane of the original blot was removed. All lanes of a given panel are from the same blot and were processed identically.

### 3.2.6 Potential relevance of ZFAND1 in human diseases

#### 3.2.6.1 Link between ZFAND1 function and neurodegenerative diseases

Mutations in the p97/valosin-containing protein (VCP) gene cause the multisystem degenerative disorder IBMPFD/ALS (inclusion body myopathy, Paget´s disease of bone, frontotemporal dementia, and amyotrophic lateral sclerosis). However, the mechanism by

which p97 mutant proteins contribute to the pathogenesis of this disease remains unknown. A recent study showed that disease-causing p97 variants carrying the missense mutations R155H or A232E are impaired in the clearance of arsenite-induced SG clearance, which may then lead to skeletal muscle degeneration (Rodriguez-Ortiz et al., 2016).

In order to test if ZFAND1 and p97 function in the same pathway for arsenite-induced SG clearance, control- or ZFAND1-depleted HeLa cells were co-transfected with either p97 WT, p97-R155H or with empty vector, and arsenite-induced SG formation and clearance was studied using IF (Fig. 38).

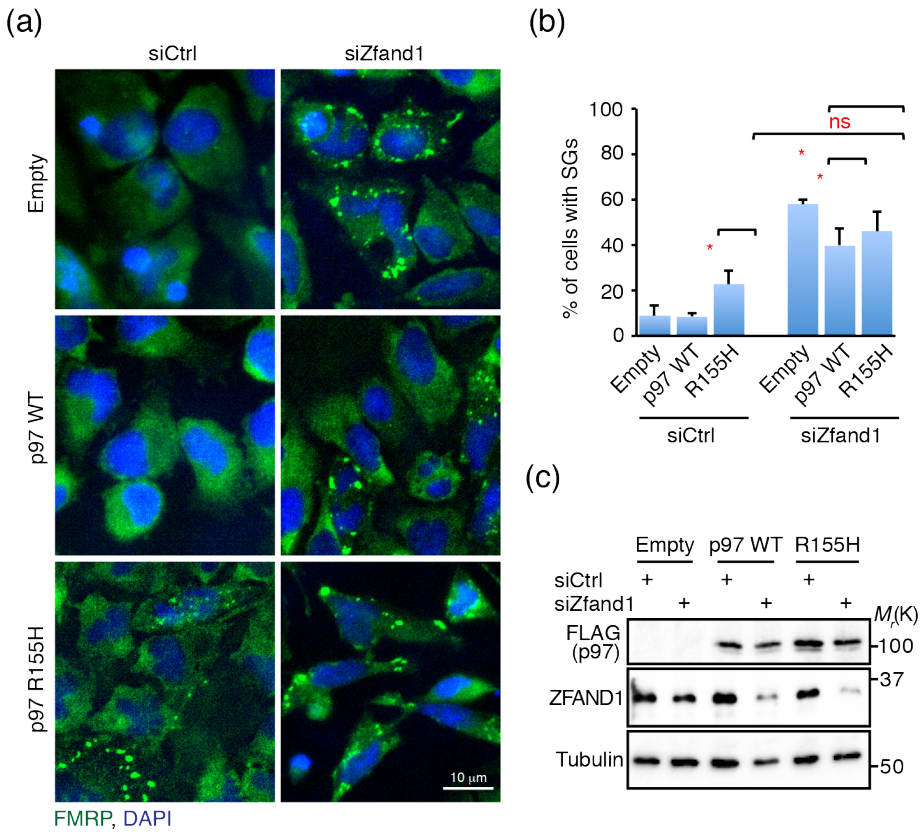


**Figure 38. Impaired ZFAND1 function is linked to neurodegenerative disease.** (a) HeLa cells were co-transfected with either an empty plasmid or a plasmid encoding wild-type p97 or the p97-R155H mutant, along with the indicated siRNAs for 48 h. Cells were then subjected to arsenite treatment (0.5 mM) for 1 h, and allowed to recover for 2 h. Fluorescence microscopy was performed to visualize FMRP. (b) Quantitation of cells with SGs in (a). (c) Expression of p97 and ZFAND1 in cells from (a) was confirmed using immunoblot analysis.

A defect in SG clearance was observed in control-depleted cells expressing p97-R155H, compared to control-depleted cells expressing p97 WT (Fig. 38a, left column), in line with a previous report (Rodriguez-Ortiz et al., 2016). In ZFAND1-depleted cells, the defect in SG clearance (in the presence of an empty plasmid) was much stronger as

compared to that in the control-depleted cells (Fig. 38a, top row). However, no additive defect in SG clearance was observed in ZFAND1-depleted cells in the presence of p97-R155H (Fig. 38a,b). This lack of additive defects points towards an epistatic relationship between ZFAND1 depletion and expression of disease-causing mutant of p97. It implies that ZFAND1 and p97 function in one pathway required for efficient SG clearance.

### 3.2.6.2 Link between ZFAND1 function and cancer

Interestingly, *ZFAND1* was found to be amplified in several cancer types (www.cbioportal.org). Morever, several mutations in *ZFAND1* have been found in different cancer types. Among these mutations, a nonsense mutation at amino acid residue 130 (R130*) is seen to occur most frequently, and mainly in colorectal and prostate adenocarcinoma (www.cbioportal.org). Importantly, this nonsense mutation (R130*) is located C-terminal of the AN1_ZF domains (which ranges from amino acid residues 1-104) and generates a variant lacking the UBL domain. The ZFAND1-R130* variant was tested for a potential SG clearance defect in a complementation experiment as described above. Indeed, ZFAND1-R130* was found to be impaired in the clearance of arsenite-induced SGs in a similar manner as the ZFAND1ΔUBL variant (Fig. 39). This result may suggest a link between perturbed SG clearance and tumorigenesis.

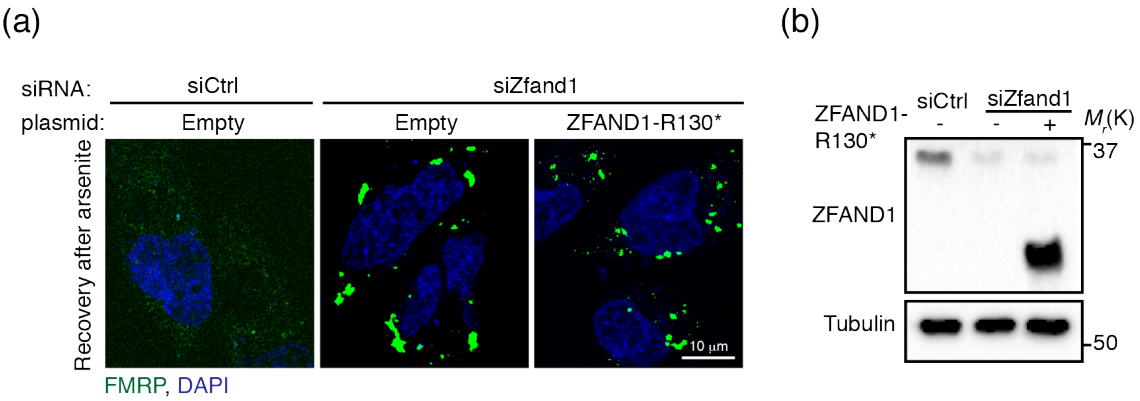


**Figure 39. Impaired ZFAND1 function is linked to cancer.** (a) HeLa cells were co-transfected for 48 h with the indicated siRNAs and either with an empty plasmid or a plasmid encoding the cancer-derived ZFAND1-R130* mutant. Cells were then subjected to arsenite treatment (0.5 mM) for 1 h, and allowed to recover for 2 h. Confocal microscopy was performed to visualize FMRP. (b) ZFAND1 protein levels in cells from (a) were detected using immunoblot analysis.

### 3.2.7 ZFAND1 depletion causes the formation of aberrant SGs

Recent reports suggest that SGs positive misfolded proteins also contain chaperones like p97, Hsp70, and Hsp27 (Mateju et al., 2017). A defect in the removal of misfolded

proteins from SGs can lead to the transformation of normal SGs into aberrant SGs. These aberrant SGs persist and have to be cleared *via* autophagy (Buchan et al., 2013).

In order to analyze if the persistent SGs in ZFAND1-depleted cells are aberrant, DRiPs (Defective Ribosomal Products) localization was analyzed. DRiPs are prematurely terminated and/or misfolded polypeptides that are released from ribosomes. It has been shown that DRiPs get ubiquitylated and rapidly degraded by the 26S proteasome (Yewdell et al., 2011). If not degraded by the 26S proteasome, DRiPs can accumulate in proximity to or at SGs, which likely leads to the transformation of normal into aberrant SGs (Ganassi et al., 2016). The persistent SGs in ZFAND1-depleted cells were tested for a possible co-localization with DRiPs, which could explain the mechanism underlying the SG clearance defect.

In order to analyze the formation and clearance of DRiPs, O-Propargyl-puromycin (OP-puro) was used. OP-puro is an alkyne analog of puromycin, which is incorporated into nascent polypeptide chains in order to generate DRiPs in cellulo. The cells are then fixed and permeabilized, and DRiPs can be coupled to azide-fluorophores by a CuAAC (Copper-catalyzed Azide-Alkyne Cycloaddition) reaction, and further analyzed using fluorescence microscopy (Liu et al., 2012).

Interestingly, upon OP-puro treatment for 45 min, ZFAND1-depleted HeLa cells showed a significant increase in the number of DRiPs compared to control-depleted cells (Fig. 40a,b). This result indicates that ZFAND1 might play a role in the degradation of DRiPs.

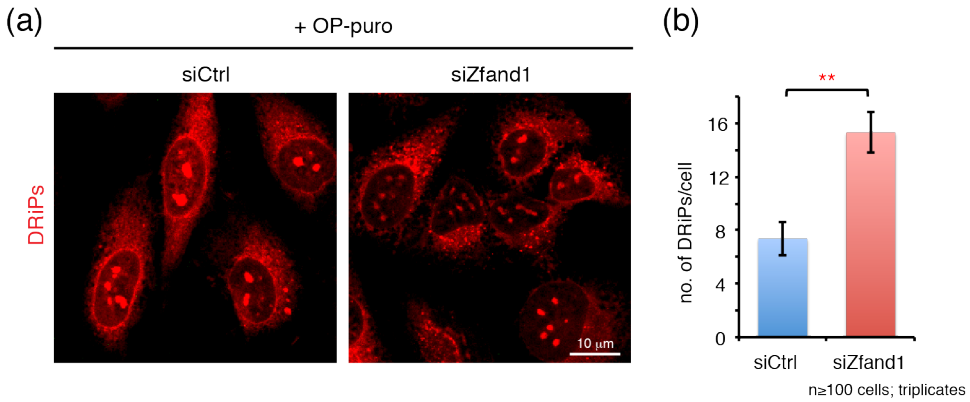


**Figure 40. DRiP accumulation upon ZFAND1 depletion** (a) HeLa cells were transfected with the indicated siRNA for 48 h, subjected to OP-puro (40 µM) treatment. OP-puro-labeled DRiPs were detected using Alexa594-azide and visualized by confocal microscopy. (b) Quantitation showing number of DRiPs/cell in (a).

A possible involvement of DRiPs in the SG clearance defect observed in ZFAND1-depleted cells was analyzed. ZFAND1- and control-depleted cells were treated simultaneously with arsenite and OP-puro for 45 min and recovered for 1 h. Treated cells were then analyzed for SG and DRiP formation using an IF.

ZFAND1- and control-depleted HeLa cells treated with Op-puro in the absence of arsenite stress showed formation of OP-puro-labeled DRiPs, but not SGs (data not shown). This control shows that treatment with Op-puro does not lead to formation of SGs. In the presence of ZFAND1, SGs produced under arsenite stress did not co-localize with DRiPs, and both DRiPs and SGs were efficiently cleared during recovery (Fig. 41, 1st and 2nd column). Interestingly, in cells depleted for ZFAND1, significant co-localization of SGs and DRiPs was observed immediately after arsenite treatment (Fig. 41, 3rd and 4th column). This observation suggests that SGs produced in the absence of ZFAND1 accumulate DRiPs and transform into *bona fide* aberrant SGs, which is a rarely observed phenotype.

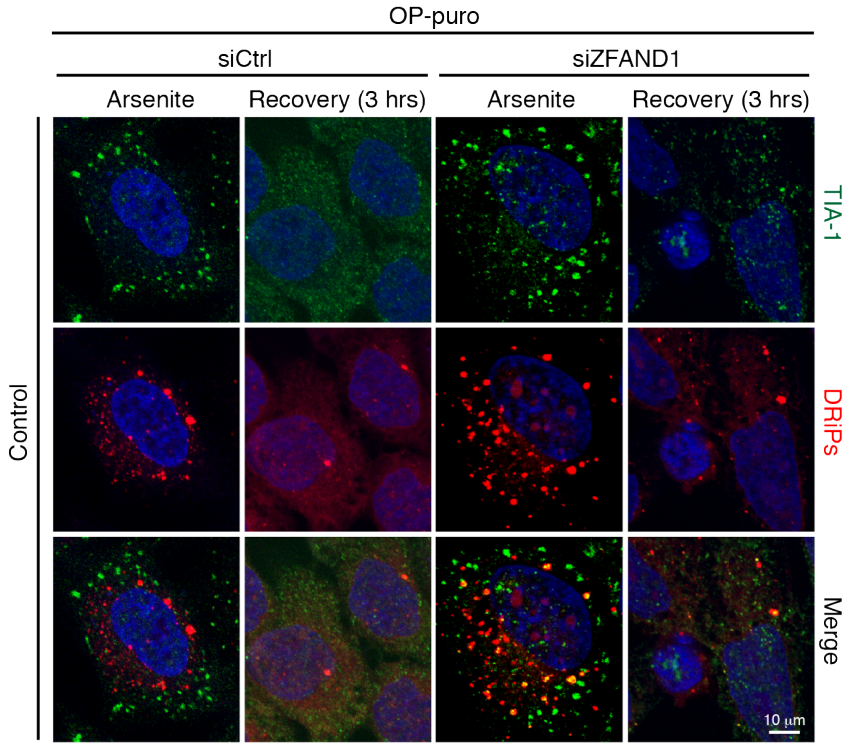


**Figure 41. Lack of ZFAND1 causes the formation of aberrant SGs.** HeLa cells were transfected with the indicated siRNA for 48 h. Cells were then subjected to simultaneous treatment with OP-puro (40 µM) and arsenite (0.5 mM) for 45 min, and allowed to recover for 3 h. OP-puro-labeled DRiPs were detected using Alexa594-azide. Confocal microscopy was performed to visualize TIA-1 and DRiPs.

### 3.2.7.1 Involvement of proteasome in SG clearance

In order to get an insight into the involvement of the 26S proteasome in formation or clearance of aberrant SGs, cells were treated with proteasome inhibitor and arsenite. Proteasome inhibitor MG132 itself has been shown to induce the formation of SGs (Mazroui et al., 2007), making the analysis of SG clearance difficult. To avoid this complication, we used the proteasome inhibitor bortezomib instead at concentrations and incubation times that did not result in SG formation *per se* (Fig. 42a).

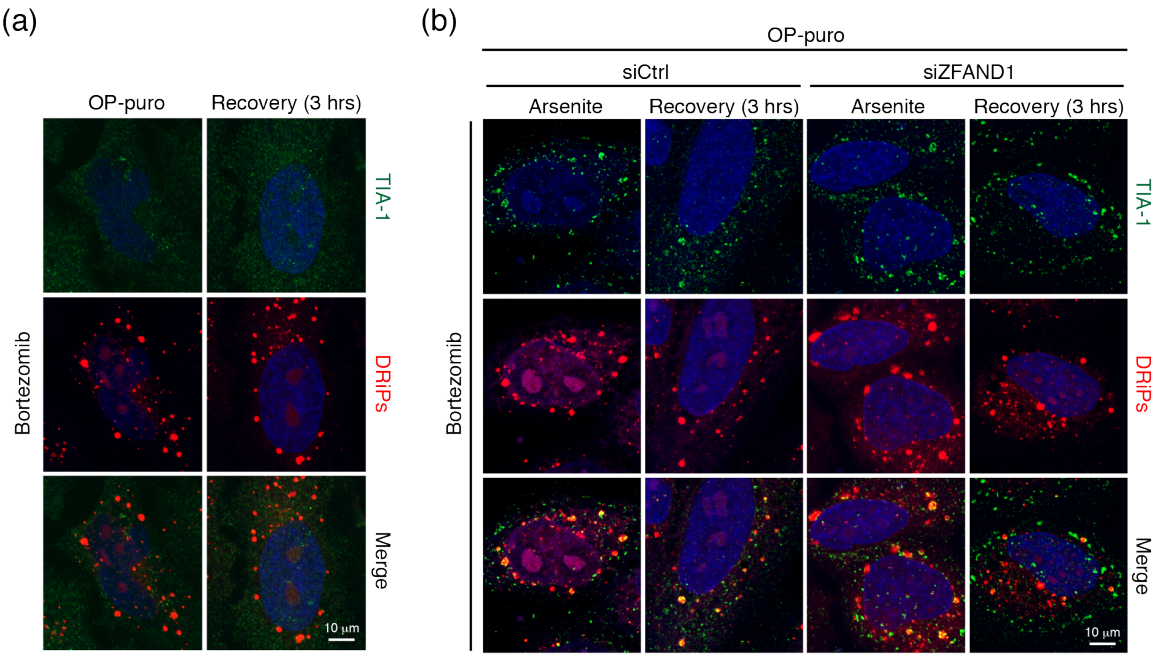


**Figure 42. Effect of proteasome inhibition on the aberrant SGs dynamics.** (a) HeLa cells were subjected to simultaneous treatment with bortezomib (5 µM) and OP-puro (40 µM), and were recovered for 3 h in the presence of bortezomib. OP-puro-labeled DRiPs were detected using Alexa594-azide. Confocal microscopy was performed to visualize TIA-1 and DRiPs. (b) Same as (Fig. 41), but bortezomib (5 µM) was added 15 min prior to the simultaneous treatment with OP-puro (40 µM) and arsenite (0.5 mM). Cells were then allowed to recover for 3 h in the presence of bortezomib. OP-puro-labeled DRiPs and TIA-1 was visualized as in (a).

Bortezomib was added 15 min prior to arsenite treatment and was maintained during recovery. Intriguingly, aberrant SGs were observed directly after arsenite stress under these conditions, and were not efficiently cleared after 3 hours of recovery, even in the presence of ZFAND1 (Fig. 42b, 1$^{st}$ and 2$^{nd}$ column). This suggests that proteasome activity is required for the efficient clearance of arsenite-induced SGs. Importantly, the effect of bortezomib was very similar to that of ZFAND1 depletion, and combining both did not significantly increase the number of aberrant SGs after arsenite stress or recovery (compare Fig. 42b 3$^{rd}$ and 4$^{th}$ column to Fig. 41 3$^{rd}$ and 4$^{th}$ column). Together, these

results points towards the importance of proteasome activity at SGs for the efficient clearance of SGs.

### 3.2.7.2 Involvement of autophagy in the clearance of aberrant SGs

To study the effect of autophagy on SG clearance, cells were treated with the autophagy inhibitor bafilomycin as explained above for bortezomib (Fig. 43).

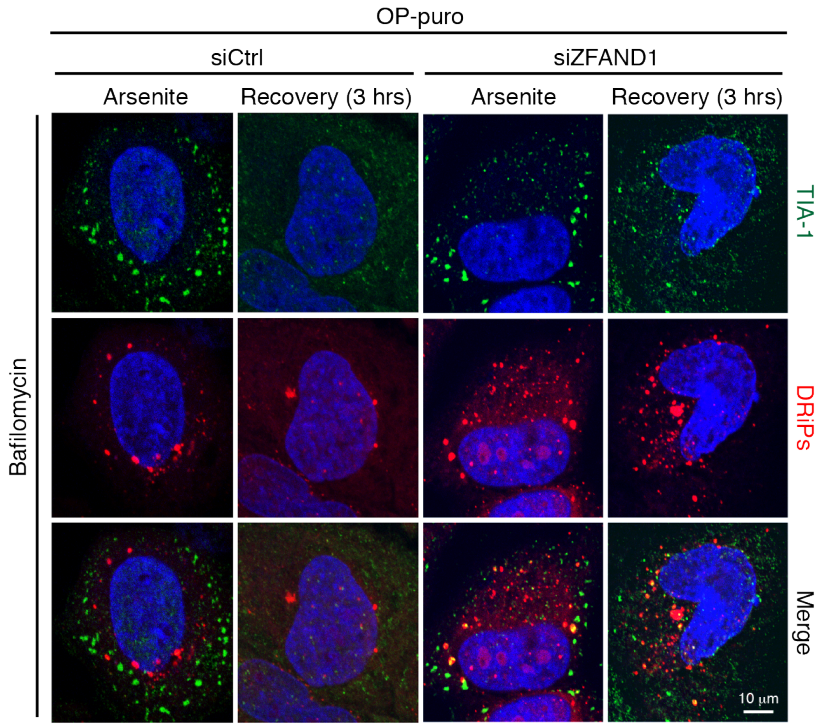


**Figure 43. Effect of autophagy inhibition on the aberrant SGs dynamics.** HeLa cells were transfected with the indicated siRNA for 48 h. Cells were then treated same as (Fig. 41), but bafilomycin (200 nM) was added 15 min prior to the simultaneous treatment with OP-puro (40 µM) and arsenite (0.5 mM). Cells were then allowed to recover for 3 h in the presence of bafilomycin. OP-puro-labeled DRiPs and TIA-1 was visualized as in (a).

In contrast to proteasome inhibition, autophagy inhibition did not lead to induction of aberrant SGs directly after arsenite treatment (compare Fig. 43 1$^{st}$ column to Fig. 42b 1$^{st}$ column). However, after 3 h recovery from arsenite stress, ZFAND1-depleted cells showed a significant increase in the number of aberrant SGs, when treated with bafilomycin (5.57±0.32 *versus* 1.09±0.06 DRiP-positive SGs in the presence and absence of bafilomycin, respectively; 50 cells quantified, n=2) (compare Fig. 43 4$^{th}$ column to Fig. 41 4$^{th}$ column). This accumulation of aberrant SGs upon bafilomycin treatment confirms the involvement of autophagy in the clearance of aberrant SGs.

In order to further analyze the property of remaining SGs, the possible co-localization of the accumulated SGs with autophagy marker proteins, including the cargo adaptor p62, LC3B and ubiquitin was investigated (Fig. 44).

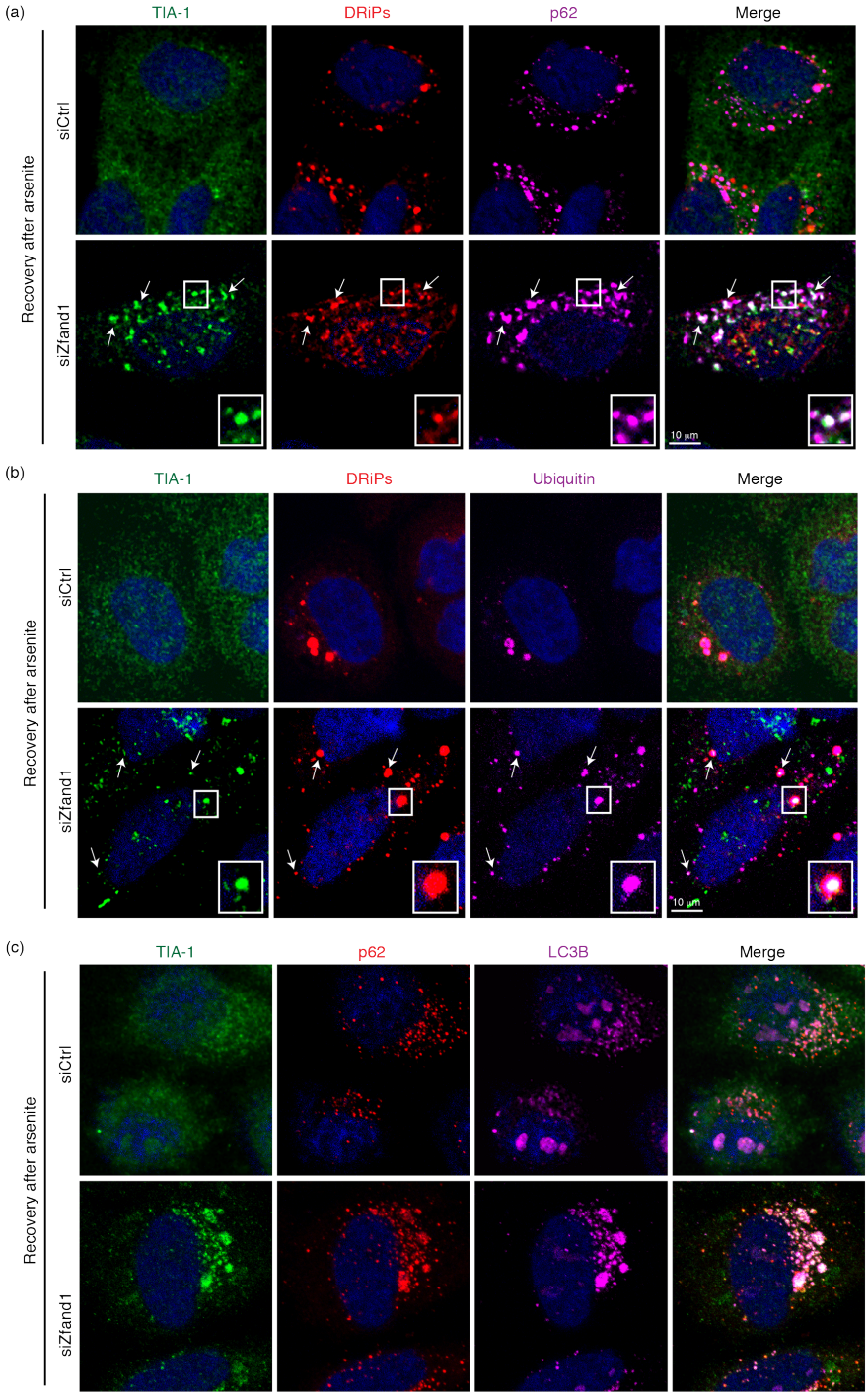


**Figure 44. Aberrant SGs formed in the absence of ZFAND1 are targeted by autophagy** (a) HeLa cells were transfected with the indicated siRNA for 48 h. Cells were then subjected to simultaneous treatment with OP-puro (40 µM) and arsenite (0.5 mM) for 45 min, and allowed to recover for 1 h. OP-puro-labeled DRiPs were detected using Alexa594-azide. Confocal microscopy was performed to visualize the co-localization of TIA-1 and DRiPs with p62 (a) and ubiquitin (b) or co-localization of TIA-1, p62 and LC3B (c). Representative co-localized foci are marked by arrows or magnified in the inset (2x zoom).

Importantly, in ZFAND1-depleted cells, the DRiP-positive SGs were observed to be positive for p62 (Fig. 44a, bottom row), ubiquitin (Fig. 44b, bottom row), and LC3B (Fig. 44c, bottom row), which was not the case in control-depleted cells. Taken together, these results clearly demonstrate that the lack of ZFAND1 causes the transformation of normal SGs into aberrant SGs upon arsenite stress.

# 4 Discussion

In this work, ZFAND1 was identified as a novel and critical regulator of arsenite-induced SG turnover. ZFAND1 recruits p97 and the 26S proteasome to arsenite-induced SGs, and prevents the transformation of normal SGs into aberrant SGs.

## 4.1 Model of ZFAND1 function in SG clearance

This study demonstrates the requirement of ZFAND1 for efficient clearance of arsenite-induced SGs (Fig. 45). Similar to other stress conditions, such as heat shock, oxidative stress and osmotic stress, arsenite causes translational stalling and thus induces SG formation. SGs can have a varied composition depending on the stress condition (Panas et al., 2016; Protter and Parker, 2016), but mainly consist of stalled translation initiation complexes, untranslated mRNAs, RNA binding proteins with low-complexity regions such as TIA-1, G3BP1 and FMRP, and many of additional proteins contributing to SG structure and dynamics (Jain et al., 2016; Panas et al., 2016; Protter and Parker, 2016). ZFAND1 *via* its UBL domain associates with arsenite-induced SGs. ZFAND1 also interacts with both, p97 and the 26S proteasome, and recruits them specifically to arsenite-induced SGs for their normal clearance (Fig. 45, left half). During recovery from arsenite stress, SGs have been shown to dissociate in a chaperone-dependent manner (Ganassi et al., 2016), by which stalled mRNPs can reenter translation. During this work, the involvement of p97 and the 26S proteasome in the disassembly of SGs, allowing translation to recommence was found. In addition to SGs, arsenite stress also induces the accumulation of ubiquitylated DRiPs. In the presence of ZFAND1, normal clearance of arsenite-induced SGs occurs, and DRiPs get degraded rapidly *via* the 26S proteasome.

On the other hand, in the absence of ZFAND1 (Fig. 45, right half), arsenite-induced SGs lack p97 and the 26S proteasome, and DRiPs co-localize to SGs. Importantly, a significant fraction of SGs cannot be cleared under these conditions. During recovery, SGs co-localize with DRiPs, and become aberrant. It has been shown that presence of other misfolded, prion domain-containing or ubiquitylated proteins at SGs make them aberrant. These transformed aberrant SGs, which are positive for DRiPs, are then recruited into LC3-positive autophagosomes by p62, and degraded *via* autophagy.

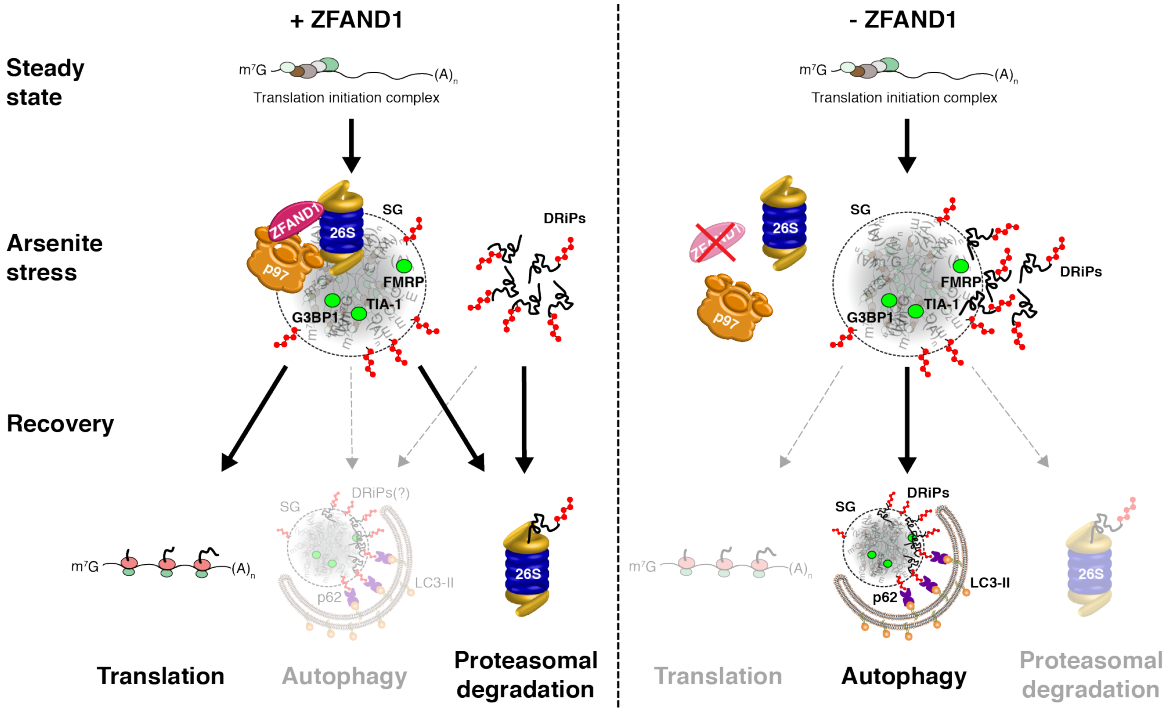


**Figure 45. Model for the role of ZFAND1 in the turnover of arsenite-induced SGs.** SG, stress granule; DRiPs, defective ribosomal products. Ubiquitylation of DRiPs and (unknown) SG proteins is indicated by red lollipop structures. See text for details.

## 4.2 Function of p97 in SG turnover

Intriguingly, p97, apart from its central role in many of the proteasomal degradation pathways, was also found to be involved in SG dynamics. There are different hypotheses regarding the role of p97 in SG dynamics, and roles of p97 in both formation and clearance of SG has been reported.

A recent study showed that impairment of either p97 function or autophagy could affect SG assembly (Seguin et al., 2014), suggesting their involvement in SG formation. SGs in cells treated with p97 siRNA or autophagy inhibitor were found to be smaller in size as compared to SGs formed in control cells. By contrast, in our study, apparently normal formation of SGs was observed upon p97 knockdown (data not shown) or autophagy inhibition (Fig. 43), excluding the possible involvement of p97 and autophagy in SG formation. In order to further investigate this, careful analysis of number and size of SGs formed during different conditions needs to be done. Data from this study points towards the possibility that the function of p97 and the 26S proteasome at SGs is rather to remove misfolded or ubiquitylated proteins from SGs as a prerequisite for its normal clearance, but not in the formation of SGs.

A study by Buchan et al. showed an involvement of p97 in SG clearance *via* autophagy (Buchan et al., 2013). They could show that p97 knockdown leads to a defect in SG clearance. Interestingly, in this study, the p97-binding deficient construct of ZFAND1 (lacking the UBL domain) was found defective in SG clearance, demonstrating a direct role of p97 in normal clearance of SGs. Intriguingly, the UBL domain alone of ZFAND1 was unable to rescue the SG clearance defect (Fig. 32). This important observation shows the requirement of both p97 and the 26S proteasome in normal clearance of SG. In addition, disease-causing mutant of p97 was found to be defective in SG clearance (Fig. 38) that could possibly contribute to the pathogenesis of IBMPFD/ALS, in line with a recent report (Rodriguez-Ortiz et al., 2016). p97 is also known to be involved in the fusion of autophagosomes to lysosomes, which might could explain an observed SG clearance defect in the presence of disease-causing mutant of p97. These findings together suggest an additional role of p97, which is in the normal clearance of SGs, but the exact mechanism by which p97 plays a role SG turnover remains to be analyzed.

In this study, the recruitment of p97 to SGs was observed that is in line with previous reports (Fig. 35, 36). However, recruitment of p97 to arsenite-induced SGs was found to be ZFAND1-dependent (Fig. 35). Interestingly, under stress conditions other than arsenite, p97 was found to be recruited to SGs in a ZFAND1-independent manner (Fig. 36). This finding indicates the possibility that there might be specific cofactors of p97 that are required for its recruitment to SGs induced by different stress conditions.

### 4.3 Function of the 26S proteasome in SG turnover

This study, for the first time, shows a direct role of the 26S proteasome in SG turnover. Previously, proteasome function was assumed to be required for SG formation *via* an unknown mechanism. In this study, both 19S and 20S subunits were found to localize to arsenite-induced SGs in a ZFAND1-dependent manner (Fig. 35). Immediate localization of the proteasome to SGs following arsenite treatment suggests a direct role of the 26S proteasome in SG dynamics. This study mainly focuses on arsenite stress, but the co-localization of the 26S proteasome and its requirement in SG turnover should be analyzed in other stress conditions as well.

A careful analysis was performed in order to understand the function of the 26S proteasome in SG turnover, using different proteasome inhibitors. MG132, when used for 3-4 h, itself is known to induce formation of SGs, which are eventually cleared in a HSP70-dependent manner following prolonged treatment (> 6 h) (Mazroui et al., 2007).

This effect of MG132 in SG metabolism makes it complicated to carefully study the role of the proteasome in SG turnover. In order to avoid this complication, we used bortezomib (a selective 20S proteasome inhibitor) in our study at a concentration that inhibits the proteasome but cannot induce SG formation itself (Fig. 42a). Seguin et al. showed that a short treatment with bortezomib induces DRiP accumulation in close proximity to SGs after arsenite treatment (Seguin et al., 2014). Interestingly, overnight treatment with bortezomib was found to inhibit the formation of SGs, and thus likely to interfere with SG assembly (Seguin et al., 2014). In order to confirm this, careful analysis of dose- and time-dependent effects of bortezomib needs to be done. In line with this report, bortezomib treatment was found to induce the formation of aberrant SGs (co-localization of DRiPs to SGs) immediately after arsenite stress even in the presence of ZFAND1 (Fig. 42b). This interesting finding not only confirms the role of the 26S proteasome in the clearance of DRiPs, but also suggests its involvement in preventing aberrant SG formation.

Interestingly, localization of the proteasome to SGs was detected in the presence of ZFAND1 (Fig. 35), a condition where DRiPs did not co-localize with SGs (Fig. 41). This indicates that apart from DRiPs, there might be other ubiquitylated substrates present at SGs. In line with previous studies, arsenite-induced SGs were found to be ubiquitin positive (data not shown), thus indicating a requirement for the 26S proteasome at these SGs (Kwon et al., 2007; Seguin et al., 2014). It would be interesting to identify the specific ubiquitylated substrates for the proteasome present inside these SGs.

The proteasome-binding deficient construct of ZFAND1 (mutated in the AN1_ZF domain) was found to be defective in SG clearance. However, it is important to note that ZFAND1 lacking the UBL domain (but containing an intact AN1_ZF domain) was not able to rescue the defect in SG clearance (Fig. 32a), suggesting that the AN1_ZF domain of ZFAND1 alone is unable to function in SG clearance. This was further confirmed by analyzing the SG clearance defect in a rescue experiment using ZFAND2A and ZFAND2B, which contain a similar AN1_ZF domain but not the UBL domain. These observations together suggest that the 26S proteasome alone is not sufficient to mediate SG clearance.

### 4.4 ZFAND1, SG metabolism, and its relevance to diseases

Defects in either the formation or clearance of SGs leads to a perturbed SG homeostasis (granulostasis). It can occur either because of mutations in important SG components

leading to increased SG formation (e.g. TIA-1, HNRNPA1, FUS, TARDBP), or mutational impairment in proteostasis factors responsible for SG clearance (e.g. VCP, SQSTM1, BAG3, HSPB8). Perturbed granulostasis has been linked to the pathogenesis of a majority of neuro- and muscular degenerative disorders including ALS, IBMPFD, and some others (Alberti et al., 2017; Ramaswami et al., 2013; Taylor et al., 2016). SGs accumulating under these conditions might act as a seed for fibrillary aggregates that possibly contributes to the pathogenesis of these diseases.

Importantly, p97 seems to play a central role in maintaining granulostasis as it has been found to play a role of in autophagy-mediated clearance of aberrant SGs, and our work suggests an additional function of p97 together with the 26S proteasome in the normal clearance of SGs. It is important to note that both functions of p97 are affected by disease-mutants of p97 strongly suggesting a relationship between perturbed granulostasis and neurodegenerative diseases. Findings from this research work suggesting the role of ZFAND1 as a recruitment factor for both p97 and the proteasome could play an important role in analyzing the function of both the proteasome and p97 in SG dynamics in future studies. Furthermore, given the close functional relationship between ZFAND1 and p97 in SG clearance, it will be interesting to systematically check for ZFAND1 mutations in proteinopathy patients lacking mutations in any of the known SG-related candidate genes.

Perturbed granulostasis is not only involved in the pathogenesis of multiple neurodegenerative, immunological, and infectious diseases (Alberti et al., 2017; Ramaswami et al., 2013; Taylor et al., 2016), but also thought to be involved in the initiation and progression of cancer (Anderson et al., 2015). Cancer cells have been shown to utilize post-transcriptional control mechanisms to re-program gene expression in order to enhance cell survival, and SGs are thought to contribute to this process by modulating cellular signaling pathways. SGs have been found to contain several signaling molecules and may thus act as signaling hubs. SG can alter multiple signaling pathways such as the JNK, Wnt and mTOR pathways (Kedersha et al., 2013) to ensure cell adaptation to stress. Importantly, the *ZFAND1-R130** loss-of-function mutation, which is also found to be defective in SG clearance (Fig. 39), has been identified in tumors from ovarian, prostate, lung, colorectal and some other cancers, and is the most frequent somatic *ZFAND1* mutation in human cancers (Cerami et al., 2012). This finding suggests a link between perturbed SG clearance and tumorigenesis, perhaps *via* alterations in signaling pathways.

## 4.5 Outlook

This research work focusing on ZFAND1 raises various interesting questions, and answers to these could provide a deeper insight into the functional relevance of Cuz1/ZFAND1 for proteostasis.

Firstly, binding interactions studies performed during this work between Cuz1/ZFAND1 and Cdc48/p97 revealed an interesting difference between Cuz1 and its human homolog ZFAND1. Both Cuz1 and its human homolog ZFAND1 contain an UBL domain near the C-terminus that readily fits to the structure of ubiquitin (90% confidence score over 79 residues; Phyre2 structural modeling program). The second AN1 finger is not conserved in Cuz1. Cuz1 has been shown to interact with Cdc48 *via* its UBL domain (Sa-Moura et al., 2013). In line with this report, we could also confirm the UBL domain-dependent binding of Cuz1 to Cdc48 *in vivo* and *in vitro* (Fig. 11-13). Cuz1 could also bind to the human homolog of Cdc48, p97, *in vitro* (data not shown). Surprisingly, this was not the case for its human homolog, ZFAND1. Although there is a clear homology between the UBL domains of Cuz1 and ZFAND1, binding of ZFAND1 to p97 was not detected *in vitro* and *in vivo* experiments (Fig. 20, 21). Understanding the differences between the two UBL domains by analyzing a potential involvement of a posttranslational modification or a difference in the structural conformation might be the key to the elucidation of the reason for this different binding pattern.

In contrast to Cuz1, the binding of ZFAND1 to p97 was found to be either very weak or highly dynamic, as it was detected only during arsenite stress, and in the presence of a p97-trapping mutant (p97-E578Q) or using cross-linking (Fig. 21). One possibility behind this binding pattern could be the involvement of a posttranslational modification on ZFAND1 that might be responsible for arsenite-dependent binding to p97. Since the direct intereaction between ZFAND1 and p97 was not observed during this study, another possibility points towards an indirect binding between ZFAND1 and p97 that could be mediated *via* other p97 cofactors. These interesting aspects need to be elucidated in future studies in order to understand the mechanism behind arsenite-dependent binding of ZFAND1 to p97.

Secondly, As SGs are known to be of varied composition under different stress conditions (Panas et al., 2016; Protter and Parker, 2016), the arsenite specific localization and function of ZFAND1 (Fig. 29, 30, 33) identified in this study raises a question – why the recruitment of ZFAND1 to SGs is specific to arsenite stress? One possibility could be that

ZFAND1 binds to RNA upon arsenite stress and is thus recruited to SGs, which needs to be carefully studied. Since the recruitment of ZFAND1 to SGs seems to occur upstream of p97 and the 26S proteasome (Fig. 35), one interesting aspect that needs to be addressed is, is there any specific binding partner or substrate of ZFAND1 present inside arsenite-induced SGs? Although the recruitment of ZFAND1 to SG was found to be mediated *via* its UBL domain (Fig. 29), there might be a possible involvement of an unstructured region present between AN1_ZF domain and the UBL domain in this recruitment that needs to be analyzed.

Thirdly, the binding of ZFAND1 *via* its AN1_ZF domain to the 26S proteasome was found *in vivo* (Fig. 24-26), which was also found to be strengthened upon arsenite stress similar to p97 binding (Fig. 24). Intriguingly, mass spectrometry experiments using lysates from ZFAND1 immunoprecipitations revealed the presence of almost all 19S and 20S subunits (Fig. 26), suggesting that ZFAND1 is an interaction partner of the 26S proteasome. Interestingly, in a previously reported study by Stanhill et al., ZFAND2A was also found to interact with and increase the activity of the 26S proteasome upon arsenite stress (Stanhill et al., 2006); however, the mechanism behind this is not understood. As our work shows the binding of ZFAND1 to the 26S proteasome, it would be interesting to study the influence of ZFAND1 on the 26S proteasome activity.

Fourthly, a recent study showed the presence of a conserved LDFLP motif in the first AN1 zinc finger in ZFAND1/2A/2B that appears to be a distinct feature of this subfamily (Sun et al., 2016). This conserved motif was found to be dispensable for binding to either the proteasome or p97. This study suggests that the function of ZFAND1 in the SG clearance pathway is independent of the LDFLP motif, because the zinc finger mutant of ZFAND1 possessing the LDFLP motif was unable to rescue the SG clearance defect. However, there might be a possibility that the zinc finger mutant ZFAND1 has altered 3D structure or orientation of the LDFLP motif that is unable to bind to the 26S proteasome. It would be interesting to carefully analyze the role of this motif in proteasome binding and to identify its functional relevance in future studies.

Lastly, SGs have been shown to disassemble in a chaperone dependent manner. A recent study showed the importance of the HSPB8-BAG3-HSP70 chaperone complex in preventing the transition from normal to aberrant SGs (Ganassi et al., 2016). In a similar line, another study also showed the involvement of the HSP70 chaperone in SG turnover (Mateju et al., 2017). Mateju et al showed the presence of misfolded proteins such as

ALS-associated variants of SOD1 and FUS in SGs. FUS is a RNA binding protein and thus recruited to SGs. On the other hand, SOD1 has no RNA binding motif, but its ALS-variant that behaves as a misfolded protein is also found to be recruited to SGs. This finding suggests the involvement of two distinct protein clearance machineries at SGs, chaperone-mediated normal clearance of SGs and the proteasome-mediated degradation of misfolded proteins from SGs. This finding together with our study showing accumulation of misfolded protein like DRiPs at SGs might explain the requirement of the 26S proteasome (Fig. 41). A possible involvement of the 26S proteasome was further supported by the presence of ubiquitylated proteins in SGs. Interestingly, in our study, apart from the effect of arsenite, an increased number of DRiPs was also observed during knockdown of ZFAND1 alone (Fig. 40). Together these findings point towards a direct relationship between ZFAND1 and proteasomal activity that is independent of arsenite and SGs, which needs to be investigated further.

# 5 Materials and Methods

## 5.1 Materials

### 5.1.1 Chemicals and reagents

Commonly used chemicals were obtained from Roth, Sigma Aldrich, Merck, and Serva unless otherwise indicated.

### 5.1.2 *S. cerevisiae* media and plates

Yeast rich (YPD) and minimal (SC) media were prepared according to the following mentioned protocols:

YPD (Yeast Peptone Dextrose)

2% (w/v) glucose

1% (w/v) bacto yeast extract (Difco, BD)

2% (w/v) bacto peptone (Difco, BD)

SC (Synthetic Complete)

2% (w/v) glucose added after autoclaving

0.67% (w/v) yeast Nitrogen Base (Difco, BD)

0.2% (w/v) drop-out mixture

Drop-out mixtures for SC-media and plates

36.7 g master-mix

addition of the following supplements with the exception of the drop-out(s) of interest

2 g histidine, 4 g leucine, 2 g uracil, 2 g tryptophan, 2 g methionine, 0.5 g adenine

Master-mix for drop-out mixtures

20 g of each alanine, arginine, asparagine, aspartic acid, cysteine, glutamine, glutamic acid, glycine, inositol, isoleucine, lysine, phenylalanine, proline, serine, threonine, tyrosine, valine, and 2 g of para-aminobenzoic acid

YPD and SC- plates

2% (w/v) agar (Difco, BD) was added to YPD medium directly and to 2x medium after autoclaving

Plates for phenotypic analysis

The indicated drugs and compounds were added to YPD/ 2 % (w/v) agar after autoclaving at approximately 55 °C.

### 5.1.3 Strains and cell lines

#### 5.1.3.1 *E. coli* strains

XL1 Blue: *supE44, hsd R17, rec A1, gyr A46, thi, rel A1, lac-, F' [proAB +, lac lq, lacZ M15, Tn10(tet r)]*

XL10 Gold: *Tetr Δ(mcrA)183 Δ(mcrCB-hsdSMR-mrr)173 endA1 supE44 thi-1 recA1 gyrA96 relA1 lac I [F' proAB lacIqZΔM15 Tn10 (Tetr) Amy Camr]*

#### 5.1.3.2 *S. cerevisiae* strains

**Table 1** - List of yeast strains used in this study.

| Strain/Reference number | Genotype | Source |
|---|---|---|
| PJ69-4a (YAB697) | MATa *ura3-52, trp1-901, his3Δ200, leu2-3,112, gal4Δ, gal80Δ, GAL2-ADE2, LYS2::GAL1-HIS3, met2::GAL7-lacZ* | James et al., 1996 |
| DF5 (YAB698) | MATa *ura3-52, lys2-801, trp1-1, his3Δ200, leu2-3,112* | Finley et al., 1987 |
| DF5 *Δcuz1* (YAB1243) | MATa *his3-Δ200, leu2-3,2-112, lys2-801, trp1-1, ura3-52 Δcuz1::HIS3MX6* | This study |
| DF5 *cdc48-6* (YAB694) | MATa *ura3-52, lys2-801, trp1-1, his3Δ200, leu2-3,112, cdc48-6* | Buchberger lab collection |
| MHY500 FLAG-*CUZ1* (YAB 1920) | MATa *his3-Δ200 leu2-3,112 ura3-52 lys2-801 trp1-1* FLAG-*CUZ1* | Hochstrasser lab |
| DF5 *Δrpn4* (YAB787) | MATa *ura3-52, lys2-801, trp1-1, his3Δ200, leu2-3,112 Δrpn4::natNT2* | Buchberger lab collection |
| DF5 *Δrad18* (YAB1152) | MATa *his3-Δ200, leu2-3,2-112, lys2-801, trp1-1, ura3-52, rad18::LEU2* | Buchberger lab collection |

#### 5.1.3.3 Cell lines

**Table 2** - List of mammalian cell lines used in this study.

| Cell line | Source |
|---|---|
| HeLa | ATCC #CCL-2 |
| HEK293T | ATCC # CRL-3216 |
| HeLa Flp-In T-Rex | Prof. Thomas Mayer, University of Konstanz |
| HEK 293 Flp-In T-Rex | Invitrogen (R780-07) |
| HeLa Flp-In T-Rex *ZFAND1-FLAG* | This work |

| Cell line | Source |
|---|---|
| HeLa Flp-In T-Rex *FLAG-ZFAND1* | This work |
| HEK 293 Flp-In T-Rex *ZFAND1-FLAG* | This work |
| HEK 293 Flp-In T-Rex *FLAG-ZFAND1* | This work |
| HeLa *ZFAND1* -/- knockout | Dr. Gabriella Marincola, Buchberger lab |

### 5.1.4 Plasmids

**Table 3** - List of plasmids used in this study.

| Reference number | Plasmid | Source |
|---|---|---|
| pAB413 | pCMV-Tag 2B | Stratagene |
| pAB597 | pCMV-Tag 4A | Stratagene |
| pAB595 | pCMV-Tag 3B | Stratagene |
| pAB2305 | FLAG-ZFAND1 (pCMV2B) | This study |
| pAB2394 | ZFAND1-FLAG (pCMV4A) | This study |
| pAB2306 | FLAG-ZFAND1ΔUBL (pCMV2B) | This study |
| pAB2487 | ZFAND1ΔUBL-FLAG (pCMV4A) | This study |
| pAB2375 | FLAG-ZFAND1 ZnFmut (pCMV2B) | This study |
| pAB2392 | ZFAND1 ZnFmut-FLAG (pCMV4A) | This study |
| pAB2473 | FLAG tagged ZFAND1 R130* (pCMV4A) | This study |
| pAB2381 | ZFAND1 untagged (pCMV4A) | This study |
| pAB2387 | ZFAND1 ZnFmut untagged (pCMV4A) | This study |
| pAB2309 | FLAG-ZFAND2B (pCMV2B) | This study |
| pAB2308 | FLAG-Cuz1 (pCMV2B) | This study |
| pAB2384 | ZFAND2A untagged (pCMV4A) | This study |
| pAB2174 | p97-E578Q (pCMV3B) | Buchberger lab collection |
| pAB1953 | pOG44 | Life technologies |
| pAB1952 | pcDNA5-FRT/TO | Life technologies |
| pAB2342 | FLAG-ZFAND1 (pcDNA5-FRT/TO) | This study |
| pAB2344 | ZFAND1-FLAG (pcDNA5-FRT/TO) | This study |
| pAB1331 | FLAG-p97 (pCMV2B) | Buchberger lab collection |
| pAB1333 | FLAG-p97 R155H (pCMV2B) | Buchberger lab collection |
| pAB2106 | Pbp1-GFP Edc3-mcherry | Swisher & Parker, 2010 |
| pAB1029 | Cuz1 (YCplac33) | This study |

| Reference number | Plasmid | Source |
|---|---|---|
| pAB826 | YCplac33 | Gietz & Sugino, 1988 |
| pAB2203 | GST-Cuz1 (pGEX4T3) | This study |
| pAB2204 | GST-Cuz1$^{144-274}$ (pGEX4T3) | This study |
| pAB2197 | GST-Cuz1$^{105-274}$ (pGEX4T3) | This study |
| pAB2508 | GST-Cuz1$^{1-106}$ (pGEX4T3) | This study |
| pAB2509 | GST-Cuz1$^{58-274}$ (pGEX4T3) | This study |
| pAB1046 | Cuz1 (pGAD) | This study |
| pAB2513 | Cuz1$^{144-274}$ (pGAD) | This study |
| pAB2512 | Cuz1$^{105-274}$ (pGAD) | This study |
| pAB2510 | Cuz1$^{1-106}$ (pGAD) | This study |
| pAB2511 | Cuz1$^{58-274}$ (pGAD) | This study |
| pAB2067 | GST-ZFAND1 (pGEX4T1) | This study |

### 5.1.5 Antibodies

#### 5.1.5.1 Primary antibodies

**Table 4** - List of primary antibodies used in this study.

| Antigen | Manufacturer | Dilution | | Lab collection number |
|---|---|---|---|---|
| | | WB | IF | |
| Rabbit polyclonal anti-ZFAND1 | Sigma-Aldrich | 1:250 | 1:50 | 180 |
| Rabbit polyclonal anti-ZFAND2B | Ron lab | 1:3000 | | 203 |
| Mouse monoclonal anti-VCP | Abcam | 1:2000 | 1:50 | 36 |
| Mouse monoclonal anti-FMRP | Fischer lab | | 1:200 | N/A |
| Rabbit polyclonal anti-TIA1 | Abcam | | 1:100 | 198 |
| Goat polyclonal anti-TIA1 | Santa Cruz | | 1:100 | N/A |
| Mouse monoclonal anti-G3BP1 | Abcam | | 1:100 | 261 |
| Rabbit polyclonal anti-FLAG | Sigma-Aldrich | 1:1000 | | 90 |
| Rabbit polyclonal anti-19S subunit S3 | Thermo | 1:1000 | | 196 |
| Mouse monoclonal anti-20S alpha 1+2+3+5+6+7 | Abcam | 1:1000 | 1:100 | 197 |
| Rabbit polyclonal anti-PSMD1 | Abcam | 1:2000 | | 205 |
| Mouse monoclonal anti-19S Rpt6 (PSMC5) (p45-110) | Enzo | | | 206 |

| Antigen | Manufacturer | Dilution | | Lab collection number |
|---|---|---|---|---|
| | | WB | IF | |
| Rabbit polyclonal anti-Tbp7 (PSMC4) | Abcam | 1:1000 | | 248 |
| Rabbit polyclonal anti-PSMA1 | Thermo | 1:2000 | | 262 |
| Mouse monoclonal anti-SQSTM1 (D3) | Santa Cruz | 1:500 | 1:300 | 18 |
| Rabbit polyclonal anti-LC3B | Sigma-Aldrich | 1:1000 | 1:100 | 199 |
| Mouse monoclonal anti-alpha Tubulin | Sigma-Aldrich | 1:2000 | | N/A |
| Rabbit polyclonal anti-c-myc (9E10) | Santa cruz | 1:1000 | | 144 |
| Mouse monoclonal anti-HA (F7) | Santa cruz | 1:1000 | | 15 |
| Rabbit polyclonal anti-Cdc48 | Buchberger lab collection | 1:1000 | | 95 |
| Rabbit polyclonal anti-Cuz1 | Immunoglobe | 1:10000 | | 200 |

#### 5.1.5.2 Secondary antibodies

**Table 5** - List of secondary antibodies used in this study.

| Antibody | Manufacturer | Dilution | |
|---|---|---|---|
| | | WB | IF |
| Alexa Fluor 488 Goat anti-Rabbit IgG (H+L) | Thermo | | 1:500 |
| Alexa fluor 488 Goat anti-Mouse IgG (H+L) | Thermo | | 1:500 |
| Alexa fluor 594 Goat anti-Rabbit IgG (H+L) | Thermo | | 1:500 |
| Alexa Fluor 594 Goat anti-Mouse IgG (H+L) | Thermo | | 1:500 |
| Alexa fluor 647 Goat anti-Rabbit IgG (H+L) | Thermo | | 1:500 |
| Alexa fluor 488 Donkey anti-Goat IgG (H+L) | Thermo | | 1:500 |
| Peroxidase AffiniPure Goat anti-Mouse IgG (H+L) | Dianova | 1:7500 | |
| Peroxidase AffiniPure Goat anti-Rabbit IgG (H+L) | Dianova | 1:7500 | |
| Peroxidase IgG Fraction monoclonal Mouse anti-Rabbit IgG, light chain specific | Dianova | 1:7500 | |

### 5.1.6 Inhibitors

**Table 6** - List of chemical inhibitors used in this study.

| Name | Manufacturer | Stock solution |
|---|---|---|
| MG132 | Selleckchem | 25 mM in DMSO |
| Bortezomib | Selleckchem | 25 mM in DMSO |
| NMS-873 | Sigma-Aldrich | 10 mM in DMSO |
| Bafilomycin | Sigma-Aldrich | 100 µM in DMSO |
| Chloroquine | Sigma-Aldrich | 50 mM in $dH_2O$ |
| Rapamycin | Sigma-Aldrich | 2 mM in DMSO |

### 5.1.7 Reagents for OP-puro labeling

**Table 7** - List of chemical reagents for OP-puro labeling of nascent polypeptides.

| Name | Manufacturer | Stock solution |
|---|---|---|
| OP-puro | Jena Bioscience | 20 mM in DMSO |
| Alexa fluor 594 azide | Life Technologies | 2 mM in DMSO |
| $CuSO_4$ | Sigma-Aldrich | 20 mM in $dH_2O$ |
| (+) Sodium-L-ascorbate | Sigma-Aldrich | 100 mM in $dH_2O$ (fresh) |
| THPTA (Tris-Hydroxy Propyl Triazolylmethyl Amine) | Sigma-Aldrich | 10 mM in $dH_2O$ |

### 5.1.8 Small interfering RNAs (siRNAs)

Lyophilized small interfering RNAs (siRNAs) were dissolved in 1X siRNA buffer to 50 µM concentration and stored aliquoted at -80 °C.

**Table 8** - List of siRNAs used in this study.

| siRNA | Target sequence | Manufacturer |
|---|---|---|
| Luciferase | CGUACGCGGAAUACUUCGA | MWG |
| GFP | GCAAGCUGACCCUGAAGUUC | MWG |
| p97_A | CCCAAGAUGGAUGAAUUGCAGUUGU | Life Technologies |
| p97_B | CACCUUCCAAGGGAGUUCUGUUCUA | Life Technologies |
| Zfand1_20 | GAUGCAUGCUGAUGGCGAU | Dharmacon |
| Zfand2b_20 | UGUGAACGCUGUAGCCGAA | Dharmacon |

### 5.1.9 Transfection reagents

Transfection of siRNAs and DNA was performed using TransIT-X2® (Mirus) or Jet PRIME® (Polyplus Transfection) kit as per manufacturer's protocol.

## 5.2 Methods

### 5.2.1 Molecular biology methods

#### 5.2.1.1 Polymerase chain reaction (PCR)

DNA fragments from plasmids or genomic DNA amplified using Phusion DNA polymerase (NEB). Annealing temperature was calculated depending on the length and nucleotide composition of the primer using below mentioned formula. Elongation time was calculated depending on the length of the DNA fragment to be amplified (1 kb/min). By default, 25 ng of plasmid DNA was used as template.

Annealing temperature of oligonucleotides for PCR:

$T_m$ (°C) = 81.5 + 0.41(%GC) - (675/N)

%GC = the percentage of G and C nucleotides in the oligo

N = the length of the oligo given in nucleotides

Standard PCR protocol:

25 ng template DNA

10 µl 5x HF buffer

1 µl dNTPs (10 mM) (2.5 mM each)

1 µl 3' primer (10 µM)

1 µl 5' primer (10 µM)

1 µl Phusion DNA Polymerase

ad 50 µl with $ddH_2O$

Purification of the PCR product was performed using NucleoSpin Extract Kit (Macherey-Nagel) as per manufacturer's protocol.

In order to amplify the knockout and tagging cassettes for yeast strain constructions, OneTaq polymerase (mixture of Taq and Vent polymerases) (NEB) was used and PCR reactions were performed as described (Knop et al., 1999; Janke et al., 2004).

#### 5.2.1.2 Site-directed mutagenesis

Site-directed mutagenesis was carried out using the QuikChange XLII and Lightning Kits (Stratagene/Agilent) according to the manufacturer's protocol and verified by sequencing of both strands.

#### 5.2.1.3 Restriction digest

For the sequence-specific cleavage of plasmid DNA or PCR fragments, DNA was incubated with restriction enzymes (NEB or Fermentas) in the appropriate buffer

recommended by the manufacturer. Restriction digestion was performed generally for 2 h at 37 °C. For cloning usually 1-2 µg of plasmid DNA was used. Restriction analysis of mini-prep DNA was performed using 600 ng of DNA.

#### 5.2.1.4 Agarose gel electrophoresis and DNA extraction

For the separation of DNA fragments according to their size, 1-2% agarose gels in 1X TBE buffer were used. In order to visualize DNA, 0.2 µg/ml of ethidium bromide (Roth) was added to the agarose gels. DNA samples were loaded with loading buffer (0.1 M EDTA, 1% SDS, 20% glycerol, 0.2% bromophenol blue and xylencyanol). Agarose gel electrophoresis was performed at a voltage up to maximum 80-110 V. After 20- 60 min DNA was visualized using a UV-transilluminator (300 nm wavelength). In case of preparative digests for cloning, the appropriate DNA fragment was excised using a scalpel. The DNA was isolated from the agarose as described in the manufacturer's protocol using a gel extraction kits (Macherey Nagel). The DNA was then typically eluted in 30 µl of the supplied elution buffer.

#### 5.2.1.5 Vector dephosphorylation and ligation

Digested vector fragments were dephosphorylated using Antarctic Phosphatase (NEB) according to the manufacturer's protocol. Approximate amounts of dephosphorylated vector and insert were visually determined after agarose gel electrophoresis, and a ratio of about 5:1 for insert to vector was used for the ligation reaction. DNA fragments were ligated using T4 DNA ligase (NEB), and in most cases the reaction was carried out at 16 °C overnight. Desalting of the ligation product was performed by dialyzing it against dd$H_2O$ using a 0.05 µm filter membrane (Millipore). 5 ul of desalted ligation product was then used for transformation into electrocompetent *E. coli* cells.

#### 5.2.1.6 Sequencing

Sequencing reactions were performed by either GATC Biotec or Eurofins/MWG. Sequencing results were analyzed using the Lasergene software (DNASTAR, Inc.).

### 5.2.2 Protein biochemical methods

#### 5.2.2.1 SDS-PAGE and Western blotting

Denatured protein samples were seperated by SDS-PAGE (using a Hoefer mini-gel system) and transferred onto PVDF membrane (Millipore immobilion) by Western blotting. The membrane was blocked with 5% milk in Tris-buffered saline (TBS) (50 mM Tris-HCl. 150 mM NaCl, pH 7.4) with 0.2% Triton X-100 and incubated with the indicated primary antibody diluted in blocking solution overnight at 4 °C. The membrane

was then washed three times (10 min each) with TBST and stained with the appropriate HRP-conjugated secondary antibody (Dianova) diluted 1:7,500 in TBST for 1 h at RT. The membrane was washed three times (10 min each) with TBST and incubated with ECL reagent mixture (GE Healthcare). Chemiluminescence signals were detected using the Molecular Imager® Gel Doc™ XR+ System (Biorad) or high performance chemiluminescence film (GE Healthcare).

#### 5.2.2.2 Recombinant protein purification

Expression of GST-tagged or $His_6$-tagged proteins in *E. coli* BL21(DE3)/pRIL was induced by addition of 1 mM IPTG and overnight growth at 18 °C.

Purification of GST fusion Proteins

Cells were harvested by centrifugation (10 min, 5,000 g, 4 °C) and resuspended in 20-40 ml lysis buffer (50 mM Tris-HCl, 150 mM NaCl, 5 mM DTT, 1 mM PMSF, 1x Roche complete protease inhibitor, pH 7.4). Cells were lysed using an EmulsiFlex-C5 (Avestin Europe GmbH) high-pressure homogenizer, and the supernatant was collected by centrifugation (45,000 g, 4 °C, 45 min). The supernatant was then incubated with 1-6 ml of pre-washed Glutathione-Sepharose 4B bead slurry (GE Healthcare) for 1 h at 4 °C. Unbound proteins were removed by three washing steps each with low salt buffer (50 mM Tris-HCl, 150 mM NaCl, 5 mM DTT, pH 7.4) and high salt buffer (50 mM Tris-HCl, 650 mM NaCl, 5 mM DTT, pH 7.4), respectively. GST-tagged proteins were eluted using 1-4 ml of elution buffer (50 mM Tris-HCl, 150 mM NaCl, 5 mM DTT, 10 mM reduced gluthatione, pH 7.4). All recombinant proteins were dialyzed against 1x TBS containing 2 mM DTT overnight at 4 °C, aliquoted, flash frozen in liquid nitrogen and stored at -80 °C.

Purification of $His_6$-tagged Proteins

$His_6$-tagged proteins were purified using $Ni^{2+}$-Agarose bead slurry and eluted using a buffer containing 250 mM imidazole. Similar protocol was used as described above for the purification of GST-fusion proteins except the use of the following buffers.

Lysis buffer: 40 mM Tris-HCl, 500 mM NaCl, 10 mM imidazol, 10 mM β-mercaptoethanol, 1 mM PMSF, 1x Roche complete protease inhibitor, pH 7.5

Wash buffer: 40 mM Tris-HCl, 500 mM NaCl, 20 mM imidazol, 10 mM β-mercaptoethanol, pH 7.5

Elution buffer: 40 mM Tris-HCl pH 7.4, 500 mM NaCl, 250 mM imidazol, 10 mM β-mercaptoethanol, pH 7.5

#### 5.2.2.3 Glutathione-sepharose pulldown assays

To test the interaction of Cdc48 or p97 with GST-tagged Cuz1 variants or ZFAND1, *in vitro* pulldowns with recombinant proteins were performed. For each reaction, 0.76 nmol of GST-tagged proteins were incubated with 20 µl of pre-washed Glutathione Sepharose® 4B (GE Healthcare) bead slurry for 1 h at 4 °C in a total volume of 150 µl (1X TBS, 1 mM DTT, 0.1% Triton X-100). Beads were collected by centrifugation (1,020 g, 5 min, 4 °C) and washed three times with 800 µl buffer (1X TBS, 1 mM DTT, 0.1% Triton X-100) in order to remove unbound protein. Beads were then incubated with 0.1 nmol of p97 or Cdc48 variants (non GST-tagged) for 1 h at 4 °C in a total volume of 100 µl. Unbound protein was removed by washing the beads three times. The final washing step was performed using the same buffer lacking Triton X-100. Beads were then boiled in 30 µl of SDS loading buffer at 99 °C for 2 min. Following centrifugation (13,000 rpm, 2 min), 4-6 µl of each sample was loaded on SDS-PAGE and detected by coomassie staining.

To analyze the binding of the 26S proteasome, GST-tagged Cuz1 or ZFAND1 were immobilized on Glutathione Sepharose® 4B (GE Healthcare) bead slurry, and washing steps were performed as described above, except for the different buffer (50 mM Tris-HCl pH 7.5, 150 mM NaCl, 10% glycerol, 5 mM $MgCl_2$, 0.1% Triton X-100). Binding reactions were then performed using 7 µg of purified human 26S proteasome (Enzo Life Sciences) for 2 h at 4 °C in a final volume of 100 µl of pulldown buffer, supplemented with 5 mM ATP where indicated. Beads were washed three times with 1x PBS (137 mM NaCl, 2.7 mM KCl, 10 mM $Na_2HPO_4$, 2 mM $KH_2PO_4$, pH 7.4) containing 0.2% Tween20, and bound proteins were eluted by boiling the beads in 30 µl of SDS loading buffer.

### 5.2.3 *E. coli* methods

#### 5.2.3.1 Preparation of competent *E. coli* cells

Electrocompetent *E. coli*

An overnight culture of XL1 blue cells (in LB-tetracycline) was inoculated in LB medium to reach a final $OD_{600nm}$ of 0.7 at 37 °C. The culture was then incubated on ice for 30-60 min. Cells were harvested by centrifugation (10 min, 4 °C), washed quickly with 500 ml sterile ice-cold $ddH_2O$, resuspended in 250 ml sterile ice-cold 10% glycerol and then incubated on ice for 30 min. The cells were then again pelleted by centrifugation and resuspended in 10 ml ice-cold 10% glycerol and again incubated on ice for 30 min. After

pelleting the cells (6000 rpm, 10 min), the pellet was resuspended in an approximately equal volume of 10% glycerol, aliquots were flash frozen in liquid nitrogen and stored at -80 °C.

$CaCl_2$ competent *E. coli*

An overnight culture of XL1 blue cells (in LB-tetracycline) was inoculated in LB medium to reach a final $OD_{600nm}$ of 0.7 at 37 °C. Cultures were then cooled on ice and cells were harvested by centrifugation. The pellet was resuspended in 100 mM ice-cold sterile $CaCl_2$ solution and incubated on ice for 10 min. Cells were pelleted (5000 rpm, 4 °C, 10 min) and the pellet was resuspended in 1/10 volume $CaCl_2$, incubated for 10 min on ice and DMSO was then added to a final concentration of 10%. Cells were aliquoted, flash frozen in liquid nitrogen and stored at -80°C.

#### 5.2.3.2 Transformation of *E. coli* cells

Transformation of $CaCl_2$ competent *E. coli* cells was performed by incubating 50 µl of cells with approximately 300 ng of plasmid DNA on ice for 10 min. Cells were then subjected to heat-shock for 1 min at 42 °C and cooled on ice. LB medium was added, and phenotypic expression was carried out for at least 30 min at 37 °C.

Transformation into electrocompetent cells was performed by transferring the mixture of 50 µl cells and either 5 µl ligation product or plasmid DNA into a 0.1 cm electroporation cuvette (BioRad). The pre-installed settings for *E. coli* electroporation were used (1.8 kV, 1 pulse; Micropulser, BioRad). After electroporation, LB medium was added and phenotypic expression was carried out for 1 h at 37 °C.

#### 5.2.3.3 Plasmid isolation from *E. coli* cells

Overnight cultures of single colonies in 5 ml LB medium containing appropriate antibiotics was used for plasmid isolation, which was performed as per manufacturer's protocol (Machery Nagel, Zymoprep, Jena Bioscience).

### 5.2.4 *S. cerevisiae* methods

#### 5.2.4.1 Preparation of competent yeast cells

Overnight cultures of yeast strains grown in the appropriate selection medium were diluted to $OD_{600nm}$ of 0.1 and grown at 25 °C or 30 °C to reach a final $OD_{600nm}$ of 0.5-0.7. The cells were then harvested by centrifugation (1000 g, 5 min, RT) and washed once with an equal volume of sterile $ddH_2O$. The cells were pelleted again and were resuspended in 0.2 volumes of SORB buffer (100 mM LiOAc, 10 mM Tris-HCl pH 8,

1 mM EDTA/ NaOH pH 8, 1 M Sorbitol; pH 8 with acetic acid). After centrifugation excess SORB buffer was removed and the pellet was resuspended in 360 µl SORB buffer per 50 ml culture volume. 40 µl of denatured salmon sperm DNA (10 mg/ml, Invitrogen) were added and the competent cells were aliquoted and stored at -80 °C.

#### 5.2.4.2 Transformation of competent yeast cells

In order to transform the yeast competent cells either with plasmid DNA or PCR products and integrative plasmids, 10 or 50 µl competent cells were thawed, respectively. After addition of the DNA, six volumes of PEG buffer (10 mM Tris-HCl pH 8.0; 1 mM EDTA; 100 mM lithium acetate; 40% PEG3350) was added, the mixture was then vortexed and incubated for 30 min at RT. Prior to the heat shock, 1/9 volume of DMSO was added and the transformation mixture was then incubated at 42 °C for 15 min in a water bath (8-10 min for ts alleles). The mixture was then incubated on ice for 2-3 min, the cells were pelleted (500 g, 2 min, 24°C) and resuspended in $ddH_2O$ or SC-medium and plated on the respective selection plates. For PCR cassettes with antibiotic resistance markers, the transformed cells were incubated in 5 ml YPD for 3 h (G418) or 6 h (hph-NT1, nat-NT2) and then pelleted and plated on the antibiotic containing plates.

#### 5.2.4.3 Strain construction

Overnight cultures of yeast strains with the opposite mating types were inoculated to $OD_{600nm}$ 0.1 and incubated for approximately 3 h in order to reach the logarithmic growth phase. 10 µl of each culture, adjusted to an equal $OD_{600nm}$, was spotted on top of each other on a pre-warmed YPD plate, and incubated for 4-5 h at 30 °C. Zygotes were selected by streaking on appropriate selection plates, incubated for 1-2 days at 30 °C. The resulting diploid heterozygotes (zygotes) were sporulated and dissected to verify 2:2 marker segregation and to isolate haploid strains. Genotypes of the haploid strains were identified using marker selection, colony-PCR and Western blot. Complete lists of *Saccharomyces cerevisiae* strains used in this study can be found in 4.1.3.2.

#### 5.2.4.4 Spotting assays

Overnight cultures in YPD were diluted with sterile $ddH_2O$ to an $OD_{600nm}$ of 0.1, and further fivefold serial dilutions were made in microtiter plates. 5 µl of each dilution were transferred to agar plates using a pin stamp. The plates (containing drugs as indicated) were then incubated at the indicated temperature for 3-7 days.

#### 5.2.4.5 Yeast two-hybrid assay

Protein-protein interactions were analyzed using the yeast two-hybrid assay. Expression constructs for bait and prey fusion proteins were transformed into PJ69-4a yeast cells (James et al., 1996). After 2-3 days, an amount of cells equal to $OD_{600nm}$ 0.5 was spotted on SC-Leu-Trp (control), SC-Leu-Trp-His and SC-Leu-Trp-Ade and incubated for 3-7 days at 30 °C.

#### 5.2.4.6 Yeast whole cell lysates - TCA precipitation

The amount of cells equal to $OD_{600nm}$ 1, from plates was resuspended in 1 ml $ddH_2O$. In order to lyse the cells, 150 µl 1.85% NaOH/ 7.5% β-mercaptoethanol was added, vortexed and incubated on ice for 10 min. Then 150 µl 55% TCA was added to the samples, vortexed and again incubated on ice for 10 min. Protein precipitates were pelleted by centrifugation (20,000 g, 10 min, 4 °C) and the supernatant was aspirated. Pellets were then resuspended in 50 µl HU/DTT buffer and incubated at 65 °C for 10 min. If necessary the pH of the samples was adjusted by addition of 2-4 µl of 2 M Tris-base.

#### 5.2.4.7 Immunoprecipitation (IP) from yeast lysate

Overnight cultures of yeast strains in YPD medium were diluted to $OD_{600nm}$ 0.2 and grown at 30 °C until they reached an $OD_{600nm}$ 1. Cells were harvested (1,500 g, 4 °C, 5 min) and washed once with cold $ddH_2O$ containing 1 mM PMSF. Cells were then lysed in IP buffer (50 mM Tris-HCl pH 7.5, 150 mM NaCl, 2 mM $MgCl_2$, 0.1% nonidet P-40 substitute, 10% glycerol, 2 mM PMSF, complete protease inhibitor cocktail [Roche]) by addition of zirconia beads (Biospec) and vortexing (6x 30 sec, kept on ice for 30 sec in between). After lysis, the nonidet P-40 substitute concentration was increased to 1%, vortexed, and subjected to centrifugation at 5,500 g at 4 °C for 5 min. The supernatant was collected in a new eppendorf tube and again subjected to centrifugation at 20,000 g at 4 °C for 25 min. The supernatant was then collected into a fresh eppendorf tube, and an input sample (15 µl) was collected and denatured by adding an equal amount of HU/DTT and incubation at 65 °C for 10 min. The residual supernatants were incubated with 20 µl pre-coupled HA-beads (Santa Cruz Biotechnology Inc.) at 4 °C overnight. Beads were collected (3,000 g, 4 °C, 3 min) and washed five times with 600 µl of IP buffer (two times with 1% nonidet P-40 substitute, two times with 0.1% nonidet P-40 substitute, and one time without nonidet P-40 substitute). Protein complexes were eluted using 25 µl HU/DTT, 10 min, 65 °C. Beads were then subjected to centrifugation (14,000 g, RT,

2 min), and the supernatant was collected in a new eppendorf tube for subsequent Western blot analysis.

#### 5.2.4.8 Yeast live microscopy

Overnight cultures of yeast strains carrying the indicated plasmid in the appropriate sterile-filtered SC medium were diluted to $OD_{600nm}$ = 0.1 and grown at 30 °C until they reached an $OD_{600nm}$ of 0.4 to 0.5. Cultures were then incubated for 30 min with 5 mM arsenite at 30 °C or without arsenite at 43 °C. Subsequently, the cells were pelleted by centrifugation (1,000 g, 5 min, RT) and washed twice with SC medium. For stress recovery, the resuspended cells were grown for an additional 30 min at 30 °C. For microscopy, 2 ml culture were harvested by centrifugation (1,000 g, 5 min, RT), and cells were resuspended in 20-30 µl of sterile filtered SC medium. Cells were immobilized on coverslips using 0.1% low melting agarose prepared in SC medium.

Yeast live-cell microscopy was performed on a Zeiss Axiovert 200M microscope equipped with a Plan-Apochromat 63x/1.4 oil immersion objective (Zeiss) and filter set FITC (#10) (BP 450-490). Images were captured using an AxioCam MRm TV2/3" 0.63x camera (Zeiss) and AxioVision LE software (Zeiss). Images were processed using ImageJ (https://imagej.nih.gov/ij/), Fiji software (http://fiji.sc), and Photoshop (Adobe Photosystems). Cells containing SGs were counted manually using ImageJ.

### 5.2.5 Mammalian cell culture

#### 5.2.5.1 Cultivation of cells

All eukaryotic cells were grown and maintained in Dulbecco`s modified Eagle medium (DMEM) (GIBCO), supplemented with 10% fetal bovine serum (FBS) and 1% Penicillin/Streptomycin at 37 °C in a humidified atmosphere with 5% $CO_2$. Cells were plated at a density of 20% and split whenever they reached 90% confluence. For splitting, the medium was aspirated and the cells were washed gently with 5 ml PBS. After aspirating the PBS, the cells were detached using 2 ml trypsin-EDTA solution for 5 min at 37 °C and 5% $CO_2$. Trypsin was inhibited by the addition of fresh DMEM medium. Subsequently, cells were mixed with the fresh medium (1:7 ratio) and added into a new culture dish.

#### 5.2.5.2 Transfection of HEK293T cells

HEK293T cells were transfected by the calcium phosphate method. One day prior to transfection, cells were seeded in 10 cm dishes to achieve about 70% confluence on the next day. Immediately before transfection, 40 µM chloroquine was added to the cells. For

transfection, 12 µg plasmid DNA (total; consisting of 6-7 µg specific plasmid DNA, 1 µg pEGFP as transfection control, remainder empty vector) were diluted into 450 µl $ddH_2O$. 50 µl $CaCl_2$ solution (2.5 M) were added and vortexed immediately for 10 seconds. Then 500 µl of 2x HBS (274 mM NaCl, 10 mM KCl, 40 mM HEPES, 1.7 mM $Na_2HPO_4$; pH 7.05) were added dropwise to the mixture from the edge of the reaction tube. The reaction mixture was mixed by inverting the tube 2-3 times. After an incubation of 3-5 min at RT, the solution was added dropwise to the cells. After 4 h, the medium was changed, and the cells were incubated for further 48 h.

#### 5.2.5.3 Transfection of HeLa and MEFs cells

Cells were transfected at approximately 70% confluence with either jetPRIME® (Polyplus-transfection®) or Mirus TransIT-X2® according to the manufacturer's protocol. For 12 well plate the final concentration of siRNAs was 25-50 nM, and 0.5 µg plasmid was used.

#### 5.2.5.4 Preparation of stable HeLa and HEK 293 cell lines

To generate stable cell lines, Flp-In T-REx HeLa (Thomas Mayer, University of Konstanz) and HEK293 cells (Life Technologies) in antibiotic-free culture medium were co-transfected with the plasmids pOG44 (Life Technologies) and pcDNA5/FRT/TO (Life Technologies) constructs encoding either N- or C-terminally FLAG epitope-tagged Zfand1. Positive clones were selected using medium supplemented with 5 µg/ml puromycin and 400 µg/ml hygromycin (HeLa) or 10 µg/ml blasticidin and 100 µg/ml hygromycin (HEK293). Single clones were isolated and tested by Western blot for the expression of FLAG epitope-tagged Zfand1 after induction with 0.5 µg/ml tetracycline. Cryo cultures were prepared for positive clones and kept for storage in liquid nitrogen.

#### 5.2.5.5 Immunoprecipitation experiments

Co-immunoprecipitation of p97 with ZFAND1

HEK293T cells were seeded to 60% confluence in 10 cm dishes. Cells were then co-transfected with a pCMV-Tag 3B plasmid encoding a trapping mutant of p97 (p97-E578Q) (3 µg) and the indicated FLAG-ZFAND1 constructs or empty vector (pCMV-Tag 2B) (5 µg). 48 h after transfection, cells were treated with 0.5 mM arsenite for 1 h as indicated. After arsenite treatment, medium was aspirated carefully and cells were suspended in cold 1x PBS and collected in a 15 ml falcon tube. Cells were collected (1400 g, 5 min, RT) and washed twice using 1x PBS, and resuspended in 600 µl of lysis buffer (50 mM Tris-HCl pH 7.6, 150 mM NaCl, 2 mM $MgCl_2$, 1% NP40, 10% glycerol,

1 mM DTT) containing protease inhibitors (1 mM PMSF, 1x Roche complete protease inhibitor mix). Lysates were transferred into a 1.5 ml eppendorf tube and lysed on ice for 10 min. Cell debris was removed by centrifugation (20,000 g, 20 min, 4 °C). The supernatant was pre-cleared by incubation with protein G sepharose beads (GE Healthcare) for 1 h at 4 °C. After centrifugation (1,400 g, 4 min, 4 °C), the pre-cleared supernatant was transferred to a fresh 1.5 ml reaction tube. 50 µl were taken as input sample, mixed with 2x sample buffer and heat denatured. 500 µl of the pre-cleared supernatant were incubated overnight at 4 °C with 30 µl FLAG-M2 agarose beads (Sigma-Aldrich) on a rotating wheel. Beads were collected by centrifugation (1,400 g, 4 min, 4 °C), and the supernatant was aspirated. Beads were washed twice with lysis buffer containing inhibitors and once with lysis buffer without inhibitors (5 min each). A final washing step was performed using 1x TBS (10 min). The beads were boiled in 30 µl of 1x sample buffer at 95 °C for 10 min, and the soluble sample was collected after centrifugation (13,000 g, 2 min, RT). ZFAND1 and p97 were detected by SDS-PAGE and Western blot as described above.

For the co-immunoprecipitation of p97 with endogenous ZFAND1, HEK293T cells were seeded till 90% confluence on three 15 cm dishes, and treated with 0.5 mM for 1 h as indicated. Arsenite-treated HEK293T cells were first washed two times with cold 1x PBS and then subjected to crosslinking using 0.8 mM dithiobis[succinimidyl propionate] (DSP; 30 min, RT) before harvesting. The crosslinker was then reacted to completion with 25 mM Tris HCl pH 7.6 for (10 min, RT). Cells were lysed in 1.2 ml of lysis buffer as described above, except that the lysis buffer did not contain DTT. Where indicated, the lysate was incubated with 100 µg/ml RNase A (30 min, RT). Lysates were pre-cleared using 20 µl of protein G sepharose beads (1 h, 4 °C). Pre-cleared lysates were then incubated with either 6 µg of ZFAND1 antibody or rabbit IgG (2 h, 4 °C). Antibody complexes were captured by incubating lysates with 25 µl of protein G sepharose beads (2 h, 4 °C). Beads were washed and co-immunoprecipitation of p97 was detected as described above.

Co-immunoprecipitation of proteasomal 19S subunits with ZFAND1

Stable HEK293 Flp-In T-Rex cells expressing ZFAND1-FLAG were seeded in three 15 cm dishes. At 70% confluence, expression of ZFAND1-FLAG was induced using 10 ng/ml tetracycline for 24 h; parental HEK293 Flp-In T-Rex cells served as negative

control. Before harvesting, cells were treated with 0.5 mM arsenite for 1 h as indicated, and harvested and lysed as described above. The lysates were depleted of ATP by incubation with hexokinase (Sigma-Aldrich) (150 µg/ml lysate) and 20 mM glucose for 30 min at RT. Where indicated, 100 µg/ml RNase A were added to the lysates before ATP depletion. Subsequently, the lysates were incubated with 30 µl FLAG-M2 agarose beads for 2 h at 4 °C, followed by wash steps as described above. ZFAND1-FLAG and interacting proteins were eluted from the antibody beads using 100 µl of 1x FLAG peptide (DYKDDDDK; 200 µg/ml in 1x TBS) at RT for 20 min. Eluted proteins were TCA-precipitated and denatured in 30 µl 1x sample buffer at 95 °C for 10 min.

For the co-immunoprecipitation of PSMD1 with mutant ZFAND1 variants, HEK293T cells were seeded to 60% confluence on 10 cm dish. Cells were then transfected with the indicated ZFAND1-FLAG expression constructs or empty vector (pCMV-Tag 4A) (5 µg). 48 h after transfection, cells were treated with 0.5 mM arsenite for 1 h as indicated, and harvested and lysed as described above. Lysates were ATP depleted and subjected to immunoprecipitation using FLAG-M2 agarose beads exactly as described above. ZFAND1 and PSMD1 were detected by SDS-PAGE and Western blot as described above.

#### 5.2.5.6 Mass spectrometry analysis

For mass spectrometry analysis, stable HEK293 Flp-In T-Rex cells expressing ZFAND1-FLAG were used. Cells were seeded in three 15 cm dishes, and were grown to 70% confluence. Cells were then treated with 0.5 µg/ml tetracycline for 24 h to induce the expression of ZFAND1-FLAG. Parental HEK293 Flp-In T-Rex cells served as negative control. Before harvesting, cells were treated with 0.5 mM arsenite for 1 h where indicated. Subsequently, cells were resuspended in 1.6 ml of lysis buffer (50 mM Tris-HCl pH 7.6, 150 mM NaCl, 2 mM $MgCl_2$, 1% NP40, 10% glycerol, 1 mM DTT) containing protease inhibitors (1 mM PMSF, 1x Roche complete protease inhibitor mix). The lysates were incubated with hexokinase (150 µg/ml lysate) and 20 mM glucose for 15 min on ice for ATP depletion. Subsequently, the lysates were incubated with 75 µl FLAG-M2 agarose beads (Sigma-Aldrich) for 2 h at 4 °C. Beads were collected by centrifugation (1,400 g, 4 min, 4 °C), and the supernatant was aspirated. Beads were washed twice with lysis buffer containing inhibitors and once with lysis buffer without inhibitors (5 min each). A final washing step was performed using 1x TBS (10 min). Elution was performed using 300 µl of 1x FLAG® tag (DYKDDDDK) peptide (200 µg/ml in 1x TBS) at RT for 20 min. 3% of the eluate was used for Western blot analysis, and the

remaining eluate was analyzed on the mass spectrometry platform of the University of Würzburg (Prof. Andreas Schlosser).

#### 5.2.5.7 OP-puro labeling of cultured cells

HeLa cells were seeded to 60% confluence on coverslips 24 h prior to treatment. Cells were then subjected to transfection with siRNAs whenever required. Before harvesting, cells were treated with 40 µM O-Propargyl-puromycin (OP-puro), which was added directly into complete DMEM medium for 45 min. The OP-puro treated cells were then washed two times with cold 1x PBS. Cells were fixed with cold methanol for 2-3 min at -20 °C. The cells were washed with cold 1x TBS for 5 min, permeabilized with TBST (TBS with 0.2% Triton X-100) for 30 min at 4 °C, and washed again with cold 1x TBS for 5 min. OP-puro incorporated into nascent polypeptides was then labeled using Copper(I)-catalyzed Azide-Alkyne Cycloaddition (CuAAC) chemistry. First, 50 µM $CuSO_4$ and 250 µM THPTA (Tris-Hydroxy Propyl Triazolylmethyl Amine) were mixed together and incubated for 5 min at RT. Then, freshly prepared 2.5 mM ascorbic acid was added to the premix of $CuSO_4$ and THPTA. 1x PBS was added to this mixture, and then 20 µM Alexa594-azide was added. Coverslips were stained using this mixture (70 µl per coverslip) for 30 min at 4 °C. After staining, the coverslips were washed three times with TBST (5 min each) and mounted using mounting medium containing DAPI (Vectashield®), or subjected to immunofluorescence as described below.

#### 5.2.5.8 Indirect immunofluorescence

HeLa cells were seeded to 60% confluence on coverslips 24 h prior to transfection. Next day, cells were transfected with the indicated siRNAs or plasmids, and grown for 48 h. Before harvesting, cells were subjected to stress treatment (0.5 mM arsenite, 2 mM $H_2O_2$, or 0.6 M sorbitol for 1 h, or temperature shift to 43 °C for 2 h). Cells were then either harvested immediately or allowed to recover for the specified time under normal growth conditions before harvesting. Cells were washed twice with cold PBS for 5 min each, and coverslips were collected. Cells were fixed using 3.7% formaldehyde in 1x PBS for 10 min at RT. Cells were washed again with cold 1x PBS for 5 min, and then permeabilized with 0.2% Triton X-100 and 1% BSA in 1x PBS for 30 min at 4 °C. Cells were then incubated with primary antibody overnight at 4 °C. Cells were washed two times with cold 1x PBS for 5 min, and then incubated with the secondary antibody for 2-3 h at RT. Cells were washed with cold 1x PBS for 5 min, and a last washing step was

performed with dd$H_2O$. Coverslips were mounted for microscopy with mounting medium containing DAPI (Vectashield®) and sealed with nail polish.

#### 5.2.5.9 Fluorescence microscopy and image processing

Immunofluorescence microscopy of HeLa cells was performed on either a Zeiss Axiovert 200M fluorescence microscope (see section 4.2.4.8), or on a Leica TCS SP2 confocal microscope. For confocal microscopy, an acusto-optical beam splitter was used with a 63x/1.4 oil immersion objective. In order to achieve a higher resolution, 2x digital zooming was applied. Z stacks (4 µm depth, 0.5 µm slices) were acquired using the following laser sources for excitation: Ar laser (488 nm); HeNe laser (561 nm, 633 nm), Diode UV laser (405 nm).

Images were processed using ImageJ (https://imagej.nih.gov/ij/), Fiji software (http://fiji.sc), and Photoshop (Adobe Photosystems). SG number analysis was performed using the macro shown below in Fiji. The total number of analyzed cells was determined by manually counting cells in the bright field channel using the Fiji cell counter plugin. Aberrant SGs positive for TIA-1 and DRiPs (Fig. 41 and 43) were counted by running the JACoP plugin in Fiji. Generation of graphs and statistical analysis were performed using Excel (Microsoft Corporation). Macro used for particle counting:

```
run("8-bit"); //for particle counting
run("Median...", "radius=2");
run("Subtract Background...", "rolling=25");
run("Enhance Contrast...", "saturated=0 normalize");
run("Unsharp Mask...", "radius=0 mask=0.60");
//run("Brightness/Contrast...");
run("Auto Threshold", "method=RenyiEntropy white");
run("Watershed");
run("Set Measurements...", "area mean standard modal min centroid center
perimeter bounding fit shape feret's integrated median skewness kurtosis
area_fraction stack display redirect=None decimal=3");
run("Analyze Particles...", "size=2-300 pixel show=Outlines exclude summarize
add"); //to count particles
```

# 6 References

Akutsu, M., Dikic, I., and Bremm, A. (2016). Ubiquitin chain diversity at a glance. J Cell Sci *129*, 875-880.

Alberti, S., Mateju, D., Mediani, L., and Carra, S. (2017). Granulostasis: Protein Quality Control of RNP Granules. Front Mol Neurosci *10*, 84.

Amaravadi, R., Kimmelman, A.C., and White, E. (2016). Recent insights into the function of autophagy in cancer. Genes Dev *30*, 1913-1930.

Amerik, A.Y., and Hochstrasser, M. (2004). Mechanism and function of deubiquitinating enzymes. Biochim Biophys Acta *1695*, 189-207.

Anderson, P., Kedersha, N., and Ivanov, P. (2015). Stress granules, P-bodies and cancer. Biochm Biophys Acta *1849*, 861-870

Antonioli, M., Di Rienzo, M., Piacentini, M., and Fimia, G.M. (2016). Emerging mechanisms in initiating and terminating autophagy. Trends Biochem Sci *42*, 28-41.

Balchin, D., Hayer-Hartl, M., and Hartl, F.U. (2016). In vivo aspects of protein folding and quality control. Science *353*, aac4354.

Bochtler, M., Ditzel, L., Groll, M., Hartmann, C., and Huber, R. (1999). The proteasome. Annu Rev Biophys Biomol Struct *28*, 295-317.

Bohm, S. (2011). PhD thesis, Ludwig-Maximilians-Universität München, 2011.

Bohm, S., Lamberti, G., Fernandez-Saiz, V., Stapf, C., and Buchberger, A. (2011). Cellular functions of Ufd2 and Ufd3 in proteasomal protein degradation depend on Cdc48 binding. Mol Cell Biol *31*, 1528–1539

Braun, S., Matuschewski, K., Rape, M., Thoms, S., and Jentsch, S. (2002). Role of the ubiquitin-selective CDC48(UFD1/NPL4 )chaperone (segregase) in ERAD of OLE1 and other substrates. EMBO J *21*, 615-621.

Buchan, J.R. (2014). mRNP granules: Assembly, function, and connections with disease. RNA Biology *11*, 1019-1030.

Buchan, J.R., Kolaitis, R.M., Taylor, J.P., and Parker, R. (2013). Eukaryotic stress granules are cleared by autophagy and Cdc48/VCP function. Cell *153*, 1461-1474.

Buchberger A (2010). Control of ubiquitin conjugation by Cdc48 and its cofactors. Subcell Biochem *54*, 17-30.

Buchberger, A. (2006). Cdc48 (p97) and its cofactors - protein degradation: cell biology of the ubiquitin proteasome system, A.C. R. John Mayer, Martin Rechsteiner, ed. (Weinheim, Wiley-VCH ).

Buchberger, A. (2013). Roles of Cdc48 in regulated protein degradation in yeast. Subcell Biochem *66*, 195-222.

Buchberger, A., Schindelin, H., and Hänzelmann, P. (2015) Control of p97 function by cofactor binding. FEBS Lett *589,* 2578-2589.

Ciechanover, A., Heller, H., Katz-Etzion, R., and Hershko, A. (1981). Activation of the heat-stable polypeptide of the ATP-dependent proteolytic system. Proc Natl Acad Sci U S A *78*, 761-765.

Collins, G.A., and Goldberg, A.L. (2017). The Logic of the 26S Proteasome. Cell *169*, 792-806.

Cushman, M., Johnson, B.S., King, O.D., Gitler, A.D., and Shorter, J. (2010). Prion-like disorders: blurring the divide between transmissibility and infectivity. J. Cell Sci *123*, 1191–1201.

Deretic, V., Saitoh, T., and Akira, S. (2013). Autophagy in infection, inflammation and immunity. Nat Rev Immunol *13*, 722-737.

Deveraux, Q., Ustrell, V., Pickart, C., and Rechsteiner, M. (1994). A 26S protease subunit that binds ubiquitin conjugates. J Biol Chem *269*, 7059-7061.

Dobson, C.M. (2003). Protein folding and misfolding. Nature *426*, 884-890.

Elsasser, S., Gali, R.R., Schwickart, M., Larsen, C.N., Leggett, D.S., Muller, B., Feng, M.T., Tubing, F., Dittmar, G.A., and Finley, D. (2002). Proteasome subunit Rpn1 binds ubiquitin-like protein domains. Nat Cell Biol *4*, 725-730.

Finley, D., Ozkaynak, E., and Varshavsky, A. (1987). The yeast polyubiquitin gene is essential for resistance to high temperatures, starvation, and other stresses. Cell *48*, 1035-1046.

Galluzzi, L., Baehrecke, E.H., Ballabio, A., Boya, P., Bravo-San Pedro, J.M., Cecconi, F., et al. (2017). Molecular definitions of autophagy and related processes. EMBO J *36*, 1811-1836.

Ganassi, M., Mateju, D., Bigi, I., Mediani, L., Poser, I., Lee, H.O., Seguin, S.J., Morelli, F.F., Vinet, J., Leo, G., et al. (2016). A Surveillance Function of the HSPB8-BAG3-HSP70 Chaperone Complex Ensures Stress Granule Integrity and Dynamism. Mol Cell *63*, 796-810.

Gietz, R.D., and Sugino, A. (1988). New yeast-Escherichia coli shuttle vectors constructed with in vitro mutagenized yeast genes lacking six-base pair restriction sites. Gene *74*, 527-534.

Gilks, N., Kedersha, N., Ayodele, M., Shen, L., Stoecklin, G., and Dember, L.M. (2004). Stress granule assembly is mediated by prion-like aggregation of TIA-1. Mol Biol Cell *15*, 5383–5398.

Glinka, T., Alter, J., Braunstein, I., Tzach, L., Wei Sheng, C., Geifman, S., Edelmann, M.J., Kessler, B.M., and Stanhill, A. (2014). Signal-peptide-mediated translocation is regulated by a p97-AIRAPL complex. Biochem J *457*, 253-261.

Gregory, R.C., Taniguchi, T., and D'Andrea, A.D. (2003). Regulation of the Fanconi anemia pathway by monoubiquitination. Semin Cancer Biol *13*, 77-82.

Groll, M., and Huber, R. (2003). Substrate access and processing by the 20S proteasome core particle. The international journal of biochemistry & cell biology *35*, 606-616.

Groll, M., Bajorek, M., Kohler, A., Moroder, L., Rubin, D.M., Huber, R., Glickman, M.H., and Finley, D. (2000). A gated channel into the proteasome core particle. Nat Struct Biol *7*, 1062-1067.

Groll, M., Ditzel, L., Lowe, J., Stock, D., Bochtler, M., Bartunik, H.D., and Huber, R. (1997). Structure of 20S proteasome from yeast at 2.4 A resolution. Nature *386*, 463-471.

Guerra-Moreno, A., Isasa, M., Bhanu, M.K., Waterman, D.P., Eapen, V.V., Gygi, S.P., and Hanna, J. (2015). Proteomic Analysis Identifies Ribosome Reduction as an Effective Proteotoxic Stress Response. J Biol Chem *290*, 29695-29706.

Haas, A.L., Warms, J.V., Hershko, A., and Rose, I.A. (1982). Ubiquitinactivating enzyme. Mechanism and role in protein-ubiquitin conjugation. J Biol Chem *257*, 2543-2548.

Hanna, J., and Finley, D. (2007). A proteasome for all occasions. FEBS Lett *581*, 2854-2861.

Hanna, J., Waterman, D., Isasa, M., Elsasser, S., Shi, Y., Gygi, S., and Finley, D. (2014). Cuz1/Ynl155w, a zinc-dependent ubiquitin-binding protein, protects cells from metalloid-induced proteotoxicity. J Biol Chem *289*, 1876-1885.

Hendrick, J.P., and Hartl, F.U. (1995). The role of molecular chaperones in protein folding. FASEB J *9*, 1559-1569.

Hershko, A., and Ciechanover, A. (1998). The ubiquitin system. Annual review of biochemistry *67*, 425-479.

Hofmann, K. (2009). Ubiquitin-binding domains and their role in the DNA damage response. DNA Repair (Amst) *8*, 544-556.

Huang, X., Luan, B., Wu, J., and Shi, Y. (2016). An atomic structure of the human 26S proteasome. Nat Struct Mol Biol *23*, 778-785.

Hughes, M.F. (2002). Arsenic toxicity and potential mechanisms of action. Toxicol Lett *133*, 1-16.

Husnjak, K., Elsasser, S., Zhang, N., Chen, X., Randles, L., Shi, Y., Hofmann, K., Walters, K. J., Finley, D., and Dikic, I. (2008). Proteasome subunit Rpn13 is a novel ubiquitin receptor. Nature *453*, 481-488.

Isakov, E., and Stanhill, A. (2011). Stalled proteasomes are directly relieved by P97 recruitment. J Biol Chem *286*, 30274-30283.

Jacobson, T., Navarrete, C., Sharma, S.K., Sideri, T.C., Ibstedt, S., Priya, S., Grant, C.M., Christen, P., Goloubinoff, P., and Tamas, M.J. (2012). Arsenite interferes with protein folding and triggers formation of protein aggregates in yeast. J Cell Sci *125*, 5073-5083.

Jain, S., Wheeler, J.R., Walters, R.W., Agrawal, A., Barsic, A., and Parker, R. (2016). ATPase-modulated stress granules contain a diverse proteome and substructure. Cell *164*, 487-498.

James, P., Halladay, J., and Craig, E.A. (1996). Genomic libraries and a host strain designed for highly efficient two-hybrid selection in yeast. Genetics *144*, 1425-1436.

Jentsch, S., and Rumpf, S. (2007). Cdc48 (p97): a "molecular gearbox" in the ubiquitin pathway? Trends Biochem Sci *32*, 6-11.

Ju, J.S., Fuentealba, R.A., Miller, S.E., Jackson, E., Piwnica-Worms, D., Baloh, R.H., and Weihl, C.C. (2009). Valosin-containing protein (VCP) is required for autophagy and is disrupted in VCP disease. J Cell Biol *187*, 875-888.

Kabeya, Y., Mizushima, N., Ueno, T., Yamamoto, A., Kirisako, T., Noda, T., Kominami, E., Ohsumi, Y., and Yoshimori, T. (2000). LC3, a mammalian homologue of yeast Apg8p, is localized in autophagosome membranes after processing. EMBO J *19*, 5720-5728.

Kedersha, N., Cho, M.R., Li, W., Yacono, P.W., Chen, S., Gilks, N., Golan, D.E., and Anderson, P. (2000). Dynamic shuttling of TIA-1 accompanies the recruitment of mRNA to mammalian stress granules. J Cell Biol *151*,1257-1268.

Kedersha, N.L., Gupta, M., Li, W., Miller, I., and Anderson, P. (1999). RNA-binding proteins TIA-1 and TIAR link the phosphorylation of eIF-2 alpha to the assembly of mammalian stress granules. J Cell Biol *147*, 1431-1442.

Khairul, I., Wang, Q.Q., Jiang, Y.H., Wang, C., and Naranmandura, H. (2017). Metabolism, toxicity and anticancer activities of arsenic compounds. Oncotarget *8*, 23905-23926.

Kirkpatrick, D.S., Dale, K.V., Catania, J.M., and Gandolfi, A.J. (2003). Low-level arsenite causes accumulation of ubiquitinated proteins in rabbit renal cortical slices and HEK293 cells. Toxicol Appl Pharmacol *186*, 101-109.

Kitajima, Y., Tashiro, Y., Suzuki, N., Warita, H., et al. (2014). Proteasome dysfunction induces muscle growth defects and protein aggregation. J Cell Sci *127*, 5204-5217.

Komader, D. (2009). The emerging complexity of protein ubiquitination. Biochem Soc Trans *37*, 937-953.

Komander, D., and Rape, M. (2012). The ubiquitin code. Annu Rev Biochem *81*, 203-229.

Labbadia, J., and Morimoto, R.I. (2015). The biology of proteostasis in aging and disease. Annu Rev Biochem *84*, 435-464.

Lamark, T., Kirkin, V., Dikic, I., and Johansen, T. (2009). NBR1 and p62 as cargo receptors for selective autophagy of ubiquitinated targets. Cell Cycle *8*, 1986-1990.

Lander, G.C., Estrin, E., Matyskiela, M.E., Bashore, C., Nogales, E., and Martin, A. (2012). Complete subunit architecture of the proteasome regulatory particle. Nature *482*, 186-191.

Lasker, K., Forster, F., Bohn, S., Walzthoeni, T., Villa, E., Unverdorben, P., Beck, F., Aebersold, R., Sali, A., and Baumeister, W. (2012). Molecular architecture of the 26S proteasome holocomplex determined by an integrative approach. Proc Natl Acad Sci U S A *109*, 1380-1387.

Livnat-Levanon, N., Kevei, É., Kleifeld, O., Krutauz, D., Segref, A., Rinaldi, T., Erpapazoglou, Z., Cohen, M., Reis, N., Hoppe, T., and Glickman, M.H. (2014). Reversible 26S Proteasome Disassembly upon Mitochondrial Stress. Cell Rep *7*, 1371-1380.

Long, J., Gallagher, T.R., Cavey, J.R., Sheppard, P.W., Ralston, S.H., Layfield, R., and Searle, M.S. (2008). Ubiquitin recognition by the ubiquitin-associated domain of p62 involves a novel conformational switch. J Biol Chem *283*, 5427-5440.

Mateju, D., Franzmann, T.M., Patel, A., Kopach, A., Boczek, E.E., Maharana, S., Lee, H.O., Carra, S., Hyman, A.A., and Alberti, S. (2017). An aberrant phase transition of stress granules triggered by misfolded protein and prevented by chaperone function. EMBO J *36*, 1669-1687.

Mazroui, R., Di Marco, S., Kaufman, R.J., and Gallouzi, I.E. (2007). Inhibition of the ubiquitin-proteasome system induces stress granule formation. Mol Biol Cell *18*, 2603-2618.

Mazroui, R., Huot, M.E., Tremblay, S., Filion, C., Labelle, Y., and Khandjian, E.W. (2002). Trapping of messenger RNA by Fragile X Mental Retardation protein into cytoplasmic granules induces translation repression. Hum Mol Genet. *11*, 3007-3017.

Menzies, F.M., Fleming, A., and Rubinsztein, D.C. (2015). Compromised autophagy and neurodegenerative diseases. Nat Rev Neurosci *16*, 345-357.

Meusser, B., Hirsch, C., Jarosch, E., and Sommer, T. (2005). ERAD: the long road to destruction. Nat Cell Biol *7*, 766-772.

Meyer, H., Bug, M., and Bremer, S. (2012). Emerging functions of the VCP/p97 AAA-ATPase in the ubiquitin system. Nat Cell Biol *14*, 117-123.

Mizushima, N., Yoshimori, T., and Ohsumi, Y. (2011). The role of Atg proteins in autophagosome formation. Annu Rev Cell Dev Biol *27*, 107-132.

Nalbandian, A., Donkervoort, S., Dec, E., Badadani, M., Katheria, V., Rana, P., Nguyen, C., Mukherjee, J., Caiozzo, V., Martin, B.*, et al.* (2011). The multiple faces of valosin-containing protein-associated diseases: inclusion body myopathy with Paget's disease of bone, frontotemporal dementia, and amyotrophic lateral sclerosis. Journal of molecular neuroscience : MN *45*, 522-531.

Nedelsky, N. B., Todd, P. K., and Taylor, J. P. (2008) Autophagy and the ubiquitin-proteasome system: Collaborators in neuroprotection. Biochim Biophys Acta *1782*, 691-699.

Noda, N.N., and Inagaki, F. (2015). Mechanisms of autophagy. Annu Rev Biophys *44*, 101-122.

Panas, M.D., Ivanov, P., and Anderson, P. (2016). Mechanistic insights into mammalian stress granule dynamics. J Cell Biol *215*, 313-323.

Pickart, C.M. (2001). Mechanisms underlying ubiquitination. Annu Rev Biochem *70*, 503-533.

Pickart, C.M., and Eddins, M.J. (2004). Ubiquitin: structures, functions, mechanisms. Biochim Biophys Acta *1695*, 55-72.

Pickart, C.M., and Fushman, D. (2004). Polyubiquitin chains: polymeric protein signals. Curr Opin Chem Biol *8*, 610-616.

Protter, D.S., and Parker, R. (2016). Principles and Properties of Stress Granules. Trends Cell Biol *26*, 668-679.

Ramadan, K., Bruderer, R., Spiga, F.M., Popp, O., Baur, T., Gotta, M., and Meyer, H.H. (2007). Cdc48/p97 promotes reformation of the nucleus by extracting the kinase Aurora B from chromatin. Nature *450*, 1258-1262.

Ramaswami, M., Taylor, J.P., and Parker, R. (2013). Altered ribostasis: RNA-protein granules in degenerative disorders. Cell *154*, 727-736.

Rodriguez-Ortiz, C.J., Flores, J.C., Valenzuela, J.A., Rodriguez, G.J., Zumkehr, J., Tran, D.N., Kimonis, V.E., and Kitazawa, M. (2016). The myoblast C2C12 transfected with mutant valosin-containing protein exhibits delayed stress granule resolution on oxidative stress. Am J Pathol *186*, 1623-1634.

Rosenzweig, R., Bronner, V., Zhang, D., Fushman, D., and Glickman, M.H. (2012). Rpn1 and Rpn2 coordinate ubiquitin processing factors at proteasome. J Biol Chem *287*, 14659-14671.

Rumpf, S., and Jentsch, S. (2006). Functional division of substrate processing cofactors of the ubiquitin-selective Cdc48 chaperone. Mol Cell *21*, 261-269.

Rutkowski, D.T., and Kaufman, R.J. (2003). All roads lead to ATF4. Dev Cell *4*, 442-444.

Sa-Moura, B., Funakoshi, M., Tomko, R.J., Jr., Dohmen, R.J., Wu, Z., Peng, J., and Hochstrasser, M. (2013). A conserved protein with AN1 zinc finger and ubiquitin-like domains modulates Cdc48 (p97) function in the ubiquitin-proteasome pathway. J Biol Chem *288*, 33682-33696.

Schuberth, C., and Buchberger, A. (2008). UBX domain proteins: major regulators of the AAA ATPase Cdc48/p97. Cell Mol Life Sci *65*, 2360-2371.

Schweitzer, A., Aufderheide, A., Rudack, T., Beck, F., Pfeifer, G., Plitzko, J. M., Sakata, E., Schulten, K., Förster, F., and Baumeister, W. (2016). Structure of the human 26S proteasome at a resolution of 3.9 Å. Proc Natl Acad Sci U S A *113,* 7816-7821.

Seguin, S.J., Morelli, F.F., Vinet, J., Amore, D., De Biasi, S., Poletti, A., Rubinsztein, D.C., and Carra, S. (2014). Inhibition of autophagy, lysosome and VCP function impairs stress granule assembly. Cell Death Differ *21*, 1838-1851.

Seibenhener, M.L., Babu, J.R., Geetha, T., Wong, H.C., Krishna, N.R., and Wooten, M.W. (2004). Sequestosome 1/p62 Is a Polyubiquitin Chain Binding Protein Involved in Ubiquitin Proteasome Degradation. Mol Cell Biol *24*, 8055-8068.

Shirakabe, A., Ikeda, Y., Sciarretta, S., Zablocki, D.K., and Sadoshima, J. (2016). Aging and autophagy in the heart. Circ Res *118*, 1563-1576.

Smith, D.M., Chang, S.C., Park, S., Finley, D., Cheng, Y., and Goldberg, A.L. (2007). Docking of the proteasomal ATPases' carboxyl termini in the 20S proteasome's alpha ring opens the gate for substrate entry. Mol Cell *27*, 731-744.

Spence, J., Sadis, S., Haas, A.L., and Finley, D. (1995). A ubiquitin mutant with specific defects in DNA repair and multiubiquitination. Mol Cell Biol *15*, 1265-1273.

Stanhill, A., Haynes, C.M., Zhang, Y., Min, G., Steele, M.C., Kalinina, J., Martinez, E., Pickart, C.M., Kong, X.P., and Ron, D. (2006). An arsenite-inducible 19S regulatory particle-associated protein adapts proteasomes to proteotoxicity. Mol Cell *23*, 875-885.

Stolz, A., Ernst, A., and Dikic, I. (2014). Cargo recognition and trafficking in selective autophagy. Nat Cell Biol *16*, 495-501.

Stolz, A., Hilt, W., Buchberger, A., and Wolf, D.H. (2011). Cdc48: a power machine in protein degradation. Trends Biochem Sci *36*, 515–523.

Sun, Z.J., Bhanu, M.K., Allan, M.G., Arthanari, H., Wagner, G., and Hanna, J. (2016). Solution Structure of the Cuz1 AN1 Zinc Finger Domain: An Exposed LDFLP Motif Defines a Subfamily of AN1 Proteins. PLoS One *11*, e0163660.

Suraweera, A., Münch, C., Hanssum, A., and Bertolotti, A. (2012). Failure of Amino Acid Homeostasis Causes Cell Death following Proteasome Inhibition. Mol Cell *48*, 242–253.

Tamas, M.J., Sharma, S.K., Ibstedt, S., Jacobson, T., and Christen, P. (2014). Heavy metals and metalloids as a cause for protein misfolding and aggregation. Biomolecules *4*, 252-267.

Tan, J.M., Wong, E.S., Dawson, V.L., Dawson, T.M., and Lim K.L. (2007). Lysine 63-linked polyubiquitin potentially partners with p62 to promote the clearance of protein inclusions by autophagy. Autophagy *4*, 251-253.

Tanaka, K. (2009). The proteasome: overview of structure and functions. Proceedings of the Japan Academy. Series B, Physical and biological sciences *85*, 12-36.

Taylor, J.P., Brown, R.H., and Cleveland, D.W. (2016). Decoding ALS: from genes to mechanism. Nature *539*, 197-206.

Thrower, J.S., Hoffman, L., Rechsteiner, M., and Pickart, C.M. (2000). Recognition of the polyubiquitin proteolytic signal. EMBO J *19*, 94-102.

Tillotson, J., Zerio, C.J., Harder, B., Ambrose, A.J., Jung, K.S., Kang, M., Zhang, D.D., and Chapman, E. (2017). Arsenic Compromises Both p97 and Proteasome Functions. Chem Res Toxicol *30*, 1508-1514.

Tomko, R.J. Jr., Funakoshi, M., Schneider, K., Wang, J., and Hochstrasser, M. (2010). Heterohexameric ring arrangement of the eukaryotic proteasomal ATPases: implications for proteasome structure and assembly. Mol Cell *38*, 393-403.

Tourriere, H., Chebli, K., Zekri, L., Courselaud, B., Blanchard, J.M., Bertrand, E., and Tazi, J. (2003). The RasGAP-associated endoribonuclease G3BP assembles stress granules. J Cell Biol *160*, 823-831.

Tresse, E., Salomons, F.A., Vesa, J., Bott, L.C., Kimonis, V., Yao, T.P., Dantuma, N.P., and Taylor, J.P. (2010). VCP/p97 is essential for maturation of ubiquitin-containing autophagosomes and this function is impaired by mutations that cause IBMPFD. Autophagy *6*, 217-227.

Verma, R., Aravind, L., Oania, R., McDonald, W.H., Yates, J.R., Koonin, E.V., and Deshaies, R.J. (2002). Role of Rpn11 metalloprotease in deubiquitination and degradation by the 26S proteasome. Science *298*, 611-615.

Verma, R., Oania, R., Fang, R., Smith, G.T., and Deshaies, R.J. (2011). Cdc48/p97 mediates UV dependent turnover of RNA Pol II. Mol Cell *41*, 82-92.

Verma, R., Oania, R.S., Kolawa, N.J., and Deshaies, R.J. (2013). Cdc48/p97 promotes degradation of aberrant nascent polypeptides bound to the ribosome. eLife *2*: e00308

Wang, P., Chang, K., Lin, Y., Kuo, T., Wang, G. (2018). Ubiquitination of MBNL1 is required for its cytoplasmic localization and function in promoting neurite outgrowth. Cell Rep *22*, 2294-2306.

Waxman, S., and Anderson, K.C. (2001) History of the development of arsenic derivatives in cancer therapy. Oncologist *6*, 3-10.

Wek, R.C., Jiang, H.Y., and Anthony, T.G. (2006). Coping with stress: eIF2 kinases and translational control. Biochem Soc Trans *34*, 7–11.

Wheeler, J.R., Matheny, T., Jain, S., Abrisch, R., and Parker, R. (2016). Distinct stages in stress granule assembly and disassembly. eLife *5*, 1-25.

Wild, P., McEwan, D.G., and Dikic, I. (2014). The LC3 interactome at a glance. J Cell Sci *127*, 3-9.

Wooten, M.W., Geetha, T., Babu, J.R., Seibenhener, M.L., Peng, J., Cox, N., Diaz-Meco, M.T., and Moscat J. (2008). Essential role of sequestosome 1/p62 in regulating accumulation of Lys63-ubiquitinated proteins. J Biol Chem *283*, 6783-6789.

Xu, P., Duong, D.M., Seyfried, N.T., Cheng, D., Xie, Y., Robert, J., Rush, J., Hochstrasser, M., Finley, D., and Peng, J. (2009). Quantitative proteomics reveals the function of unconventional ubiquitin chains in proteasomal degradation. Cell *137*, 133-145.

Xu, S., Peng, G., Wang, Y., Fang, S., and Karbowski, M. (2011). The AAA-ATPase p97 is essential for outer mitochondrial membrane protein turnover. Mol Biol Cell *22*, 291-300.

Xue, L., Blythe, E.E., Freiberger, E.C., Mamrosh, J.L., Hebert, A.S., Reitsma, J.M., Hess, S., Coon, J.J., and Deshaies, R.J. (2016). Valosin-containing protein (VCP)-Adaptor Interactions are Exceptionally Dynamic and Subject to Differential Modulation by a VCP Inhibitor. Molecular & cellular proteomics : MCP *15*, 2970-2986.

Yamamoto, S., Tomita, Y., Hoshida, Y., Iizuka, N., Monden, M., Yamamoto, S., Iuchi, K., and Aozasa, K. (2004). Expression level of valosin-containing protein (p97) is correlated with progression and prognosis of non-small-cell lung carcinoma. Ann Surg Oncol *11*, 697-704.

Yamamoto, S., Tomita, Y., Uruno, T., Hoshida, Y., Qiu, Y., Iizuka, N., Nakamichi, I., Miyauchi, A., and Aozasa, K. (2005). Increased expression of valosin-containing protein (p97) is correlated with disease recurrence in follicular thyroid cancer. Ann Surg Oncol *12*, 925-934.

Yamasaki, S., and Anderson, P. (2008). Reprogramming mRNA translation during stress. Curr Opin Cell Biol *20*, 222-226.

Yao, T., and Cohen, R.E. (2002). A cryptic protease couples deubiquitination and degradation by the proteasome. Nature *419*, 403-407.

Yeung, H.O., Kloppsteck, P., Niwa, H., Isaacson, R.L., Matthews, S., Zhang, X., and Freemont, P.S. (2008). Insights into adaptor binding to the AAA protein p97. Biochem Soc Trans *36*, 62–67

Yewdell, J.W. (2011). DRiPs solidify: progress in understanding endogenous MHC class I antigen processing. Trends Immunol *32*, 548-558.

Yun, C., Stanhill, A., Yang, Y., Zhang, Y., Haynes, C. M., Xu, C., Neubert, T. A., Mor, A., Philips, M.R., and Ron, D. (2008). Proteasomal adaptation to environmental stress links resistance to proteotoxicity with longevity in Caenorhabditis elegans. Proc Natl Acad Sci USA *105*, 7094-7099.

Zhong, Z., Sanchez-Lopez, E., and Karin, M. (2016). Autophagy, inflammation, and immunity: a troika governing cancer and its treatment. Cell *166*, 288-298.

**Publication list**

**Turakhiya, A.**, Meyer, S.R., Marincola, G., Böhm, S., Vanselow, J., Schlosser, A., Hofmann, K., and Buchberger, A. (2018). ZFAND1 recruits p97 and the 26S proteasome to promote the clearance of arsenite-induced stress granules. Mol Cell (*in press*)

Saleh, A.A., Gune, U.S., Chaudhary, R.K., **Turakhiya, A.P.**, and Roy, I. (2014). Roles of Hsp104 and trehalose in solubilisation of mutant huntingtin in heat shocked *Saccharomyces cerevisiae* cells. Biochim Biophys Acta *1843*, 746-757

**Curriculum Vitae**